

NASA TECHNICAL NOTE



NASA TN D-5364

c. 1

NASA TN D-5364

LOAN COPY: RETURN  
AFWL (WLIL-2)  
KIRTLAND AFB, N M



TECH LIBRARY KAFB, NM

WIND-TUNNEL INVESTIGATION OF AN  
STOL AIRCRAFT CONFIGURATION EQUIPPED  
WITH AN EXTERNAL-FLOW JET FLAP

*by Lysle P. Parlett and James P. Shivers*

*Langley Research Center*

*Langley Station, Hampton, Va.*



WIND-TUNNEL INVESTIGATION OF AN STOL AIRCRAFT CONFIGURATION  
EQUIPPED WITH AN EXTERNAL-FLOW JET FLAP

By Lysle P. Parlett and James P. Shivers

Langley Research Center  
Langley Station, Hampton, Va.

NATIONAL AERONAUTICS AND SPACE ADMINISTRATION

---

*For sale by the Clearinghouse for Federal Scientific and Technical Information  
Springfield, Virginia 22151 - CFSTI price \$3.00*

# WIND-TUNNEL INVESTIGATION OF AN STOL AIRCRAFT CONFIGURATION EQUIPPED WITH AN EXTERNAL-FLOW JET FLAP

By Lysle P. Parlett and James P. Shivers  
Langley Research Center

## SUMMARY

The present investigation was performed to provide information on the static longitudinal and lateral characteristics of a proposed short take-off and landing (STOL) transport configuration utilizing the jet-flap principle. Longitudinal tests were conducted at engine gross-thrust coefficients of from 0 to 3.4 through a range of angle of attack which included the stall; and lateral tests were made, both power-off and power-on, through a sideslip range of  $\pm 30^\circ$  at angles of attack of  $0^\circ$  and  $10^\circ$ .

Untrimmed lift coefficients up to 7.8 were attained at a gross-thrust coefficient of 2.83 in the tail-off condition. With the tail on, nearly all high-lift conditions were characterized by a marked longitudinal instability (or pitch-up tendency) which began at an angle of attack of  $7^\circ$ . The instability was apparently caused by the tip vortices which, under the influence of the highly loaded center section of the wing, were drawn into the region of the horizontal tail. The tail-on configuration was directionally stable and had positive dihedral effect at all flap and power settings tested; and in the take-off and landing conditions increasing power increased directional stability and decreased dihedral effect. With one outboard engine not operating, the model could be trimmed laterally and directionally up to lift coefficients of 4.2 in the take-off condition and 5.7 in the landing condition. Above these lift coefficients the model could not be trimmed in roll, but trim in yaw could still be attained.

## INTRODUCTION

The external-flow jet-flap principle is incorporated in a recently proposed design for a medium-size four-engine jet transport intended to have short take-off and landing (STOL) capabilities. Previous investigations (refs. 1, 2, and 3) have demonstrated that an external-flow jet flap can produce the high lift coefficients required for short-field operation, but that the high lift coefficients may be accompanied by serious trim and stability problems. These problems are attributed primarily to downwash characteristics and unsymmetrical span loading of powered lift which would vary with configuration. In order to broaden the knowledge in the jet-flap field by testing a configuration significantly

different from those of past investigations, the NASA undertook to test a model of the proposed STOL transport. The wing of this configuration is more highly tapered and the engines are located relatively closer to the fuselage than in the previous investigations. The tests provided general aerodynamic data for the take-off, cruise, and landing conditions, with emphasis on trim and stability studies in the high-power, high-lift conditions. Longitudinal and lateral forces and moments were measured at angles of attack up to  $28^\circ$ , at sideslip angles up to  $30^\circ$ , and at engine gross-thrust coefficients up to 3.4. In terms of trim flight conditions for the proposed full-scale aircraft represented by the model, a gross-thrust coefficient of 3.4 would result in a thrust-weight ratio of approximately 0.6.

### SYMBOLS

A sketch of the axis system used in the investigation is presented in figure 1. Longitudinal forces and moments are referred to the wind-axis system; lateral and directional forces and moments are referred to the body-axis system.

b	wing span, ft (m)
$C_D$	drag coefficient, $D/qS$
$C_L$	lift coefficient, $L/qS$
$C_{L,0}$	lift coefficient, power off
$C_{L,\Gamma}$	jet-induced circulation lift coefficient
$C_l$	rolling-moment coefficient, $M_X/qSb$
$C_{l\beta} = \frac{\partial C_l}{\partial \beta}$	
$C_m$	pitching-moment coefficient, $M_Y/qS\bar{c}$
$C_n$	yawing-moment coefficient, $M_Z/qSb$
$C_{n\beta} = \frac{\partial C_n}{\partial \beta}$	
$C_Y$	side-force coefficient, $F_Y/qS$
$C_{Y\beta} = \frac{\partial C_Y}{\partial \beta}$	
$C_\mu$	engine gross-thrust coefficient, $\dot{m}V_E/qS$
c	local wing chord, ft (m)

$\bar{c}$	length of mean aerodynamic chord, ft (m)
D	drag, lb (N)
$F_A$	axial force, lb (N)
$F_N$	normal force, lb (N)
$F_Y$	side force, lb (N)
$i_t$	incidence of horizontal tail, deg
L	lift, lb (N)
$M_X$	rolling moment, ft-lb (N-m)
$M_Y$	pitching moment (referred to $0.25\bar{c}$ ), ft-lb (N-m)
$M_Z$	yawing moment, ft-lb (N-m)
$\dot{m}$	engine mass flow rate, slugs/sec (kg/sec)
q	free-stream dynamic pressure, lb/ft <sup>2</sup> (N/m <sup>2</sup> )
S	wing area, ft <sup>2</sup> (m <sup>2</sup> )
T	thrust, lb (N)
$V_E$	engine exit velocity, ft/sec (m/sec)
X, Y, Z	model body axes
$\alpha$	angle of attack, deg
$\beta$	angle of sideslip, deg
$\delta_{aux}$	deflection of auxiliary flap, deg
$\delta_f$	flap deflection, deg
$\delta_j$	jet deflection, deg

$\delta_r$	rudder deflection, deg
$\delta_s$	spoiler deflection, deg
$\delta_v$	vane deflection, deg
$\epsilon$	downwash angle, deg
$\eta$	flap turning efficiency, $\frac{\sqrt{F_A^2 + F_N^2}}{T}$

Designations for flap settings are given in figure 2(b).

### MODEL AND APPARATUS

The investigation was conducted on the four-engine high-wing jet transport model illustrated by the three-view drawing of figure 2(a). A typical section through the flap system and the relationship of the flaps to the engines are shown in figure 2(b). The leading-edge slat shown in figure 2(b) was extended for all test conditions. The flap combinations are defined in the table of figure 2(b) and a plan view of the wing semispan is presented in figure 2(c). Photographs of the model are presented in figure 3, and dimensional characteristics are listed in table I.

The engines were of the ejector type (in which thrust resulting from gas flow through primary nozzles is augmented by a secondary flow of ambient air induced by the primary flow) and had the same external geometry as a current turbofan engine. Flow of the primary gas (compressed nitrogen) to the section of the engine simulating the turbine was controlled independently of primary flow to the fan simulator so that the desired thrust was obtained at the desired bypass ratio (8 to 1). For some of the tests, thrust deflector plates were installed on the outboard fan simulators as shown in figure 2(b).

It may be noted that the use of these ejector engines did not allow inlet and exit mass flow rates to be simulated correctly at the same time, but for the present tests the exit mass flow was considered to be the more important of the two.

The model was mounted on a six-component strain-gage balance and was strut-supported in the test section of the Langley full-scale tunnel. This tunnel has an open-throat test section of 30 by 60 feet (9.14 by 18.29 meters), which allows models of the present size (8-foot (2.5-m) span) to be tested at high lift coefficients without introducing significant tunnel wall effects.

## TESTS AND PROCEDURES

In preparation for the present tests, single-engine calibrations were made to determine net thrust and mass flow rates as functions of nitrogen drive pressure in the static condition and at the test free-stream airspeed at zero angle of attack. The tests were then run by setting the drive pressures for the fan and turbine simulators, respectively, to the desired values and holding these pressures constant through the ranges of angle of attack or sideslip.

Jet deflection angles and flap turning efficiencies were determined from measurements of the normal and axial forces made in the static thrust condition with flaps deflected. The static thrust used in computing turning efficiency was taken directly from the single-engine calibrations at the appropriate drive pressures.

During the wind-on tests various changes were made to the flap geometry or to control-surface deflections; each condition was usually tested at values of  $C_{\mu}$  of 0 to 3.4 through a range of angle of attack of  $-4^{\circ}$  to  $28^{\circ}$ . All tail-off tests were made with both the horizontal and vertical tails removed. Sideslip runs were made over a range of angles of sideslip from  $-30^{\circ}$  to  $30^{\circ}$ . Nearly all wind-on tests were made at a free-stream dynamic pressure of  $11 \text{ lb/ft}^2$  ( $527 \text{ N/m}^2$ ), which corresponds to a velocity of  $97 \text{ ft/sec}$  ( $29.6 \text{ m/sec}$ ). The Reynolds number was approximately  $0.8 \times 10^6$  based on the mean aerodynamic chord of the wing.

No wind-tunnel jet boundary corrections were applied to the data because such corrections were computed for a somewhat larger high-lift model during a previous investigation (ref. 3) and were found to be negligible.

## PRESENTATION OF DATA

The test data are presented in the following figures. The four main headings correspond to those in the Discussion section.

	Figure
<b>Lift Characteristics</b>	
Longitudinal characteristics, tail off . . . . .	4-7
Longitudinal basic data, tail off, auxiliary flaps deflected . . . . .	8
Summary of auxiliary-flap performance . . . . .	9
Analysis of jet-flap effectiveness . . . . .	10-12
<b>Longitudinal Stability and Trim, Symmetric Thrust</b>	
Longitudinal characteristics, tail on, basic configurations . . . . .	13-16
Photographs of smoke flow showing vortex system . . . . .	17

	Figure
Longitudinal characteristics, tail on, configurations intended to remedy longitudinal instability . . . . .	18-23
Horizontal-tail effectiveness . . . . .	24
<b>Lateral Characteristics, Symmetric Thrust</b>	
Lateral characteristics, tail off . . . . .	25-27
Lateral characteristics, tail on, basic configurations . . . . .	28-31
Lateral characteristics, tail on, controls deflected . . . . .	32-35
<b>Lateral and Longitudinal Characteristics, Asymmetric Thrust</b>	
Lateral characteristics, tail on, asymmetric thrust and control . . . . .	36-38
Lateral trim capability, one engine out . . . . .	39
Longitudinal characteristics, asymmetric thrust and control . . . . .	40-45
Effect of thrust distribution on lift . . . . .	46

## DISCUSSION

### Lift Characteristics

Basic longitudinal data for the model in the tail-off condition at flap deflections representing the cruise, take-off (two deflections), and landing configurations are presented in figures 4 to 7. The leading-edge slat was extended for all test conditions. The data show that the stall angle and maximum lift coefficient increased with increasing thrust coefficient, and that as flap deflection increased, the effects of thrust on the lift characteristics became more pronounced. The landing flap deflection (fig. 7) produced lift coefficients up to 7.8 (untrimmed) at a gross-thrust coefficient of 2.83. As would be expected, high lift coefficients are accompanied by large nose-down moments because of the rearward location of the flap loads.

With the basic landing flap setting LDG, which produced the highest lift coefficients, auxiliary flaps were investigated as a means of providing glidepath control during a landing approach. Data which show the longitudinal characteristics with various auxiliary-flap deflections in the approach condition are presented in figure 8 and are summarized in figure 9. Figure 9 shows that with the basic landing flap setting LDG, increases in thrust can produce increases in drag. These drag increases reflect the large induced drag which accompanies the induced lift at high flap settings in a high-lift system, and suggest that the auxiliary flap might be an impractical device for glidepath control, at least, in the usual sense, with large main-flap deflections. If the flap deflection for landing were lower, it is possible that the auxiliary flap would appear in a more favorable light as a glidepath control system.

The effectiveness of a jet-flap system is usually analyzed in terms of  $C_{L,\Gamma}$ , the jet-induced circulation lift coefficient. The quantity  $C_{L,\Gamma}$  is significant because it

represents a lift component not solely attributable either to the upward component of the deflected engine thrust or to the power-off lift of the wing, and is therefore an indication of the ability of the integrated engine-wing-flap system to utilize engine power to produce additional increments of lift coefficient. A typical resolution of total lift coefficient into its three components is shown for a  $60^\circ$  flap setting in figure 10. The  $C_L$  at  $C_\mu = 0$  represents the circulation lift normally developed by the wing and flap system in a moving airstream in the power-off condition. In the powered condition, the engine slipstream impinges on the flap system and is thereby deflected downward through the angle  $\delta_j$ ; and the term  $C_\mu \sin(\delta_j + \alpha)\eta$  represents the lift contribution due to this redirection of engine gross thrust. The flow of the engine slipstream through the flap system and downward from the trailing edge as a jet sheet not only produces the force represented by  $C_\mu \sin(\delta_j + \alpha)\eta$ , but also induces a flow which augments the circulation over the wing. This increased circulation gives rise to the third lift component, the jet-induced added circulation lift  $C_{L,\Gamma}$ .

With  $C_{L,\Gamma}$  as the basis for comparison, the effectiveness of the engine-wing-flap system of the present model is compared to that of the model of reference 2 in figure 11. The comparison is not exact because the data for reference 2 are for a jet deflection angle of  $60^\circ$ , whereas the most nearly comparable jet deflection in the present investigation was  $65^\circ$ . It is believed, however, that this slight discrepancy does not materially affect the comparison. The  $C_{L,\Gamma}$  values produced by the model of reference 2 do not necessarily represent the ideal, but they have been considered generally representative of those to be expected from an efficient external-flow jet-flap system. Figure 11 shows that the jet-induced circulation lift for the present model compares unfavorably with that of the model of reference 2 throughout the range of  $C_\mu$  for which both models were tested. Analysis of the probable effects of geometric differences between the models seems to indicate that it is important to have the engine efflux flattened and spread more widely across the span than is the case for the present model.

Because the jet-induced lift is highly dependent on the direction and velocity of the engine slipstream as it leaves the flap system, it appears that for best jet-flap performance the flap system should be capable of turning the slipstream efficiently through large angles. The slipstream angle  $\delta_j$  and the static turning efficiency  $\eta$  for the present model are shown in figure 12, which is a plot of the ratio of normal force to thrust  $F_N/T$  against the ratio of net axial force to thrust  $F_A/T$ . Figure 12 shows that at turning angles near  $60^\circ$  the turning efficiency was approximately 0.7, which is low enough to be at least partially responsible for the relatively low values of  $C_{L,\Gamma}$ .

#### Longitudinal Stability and Trim, Symmetric Thrust

The longitudinal stability and trim characteristics of the model with the tail on are plotted against angle of attack for various thrust levels and flap settings in figures 13

to 16. Some of the tests on which this group of figures is based were performed with the landing-gear pod on, and some with the pod off; figure 13 is presented first to establish that the pod had virtually no effect on longitudinal characteristics, and that data for other configuration variations may therefore be compared regardless of the presence or absence of the pod.

Longitudinal characteristics for the cruise condition (although with leading-edge slat extended) are presented in figure 14. The most noteworthy characteristic shown by figure 14 is the longitudinal instability which develops under power-on conditions at an angle of attack of approximately  $7^\circ$ . Figures 15 and 16, presenting data for the take-off and landing flap settings, respectively, also show instability developing at an angle of attack of  $7^\circ$ , and this instability becomes progressively worse with increasing angle of attack until near the stall the model was more unstable than it was with the tail off. This destabilizing effect of the tail indicates that the tail was operating in a downwash field which increased in intensity at a rate greater than that at which the angle of attack increased, with the result that the downwash factor  $1 - \frac{d\epsilon}{d\alpha}$  was negative. A brief smoke-flow study (sample photographs are presented in fig. 17) showed that the tail was indeed immersed in a downwash field that for the present model may have been particularly powerful because of the high concentration of lift on the inboard sections of the wing, which caused a large and powerful tip vortex to be located far inboard in the region of the horizontal tail. The model of reference 2 did not have such a pronounced instability as the present model; therefore, attempts were made to achieve a more nearly uniform spanwise lift distribution by means of thrust deflection and flap changes. Figure 18 presents the results of tests made with the thrust deflectors installed on the two outboard engines. The data of figure 18 show that the deflectors produce some slight increment in lift but that they do not improve the stability. Apparently the outboard engines are located so far inboard that increasing the spread of their efflux somewhat does not alter the spanwise lift distribution (or the downwash) sufficiently to relieve the vortex in the region of the horizontal tail.

The results of an additional modification, that of drooping the ailerons  $40^\circ$  to increase the lift on the outer part of the wing, are presented in figure 19. These data show that the combination of aileron droop and thrust deflection produce a noticeable, although insufficient, contribution toward stability.

Although the use of spoiler deflection is not normally associated with a take-off configuration, the effects of symmetrically deflecting the inboard section of the spoiler were investigated in the present case as a possible means of improving longitudinal stability by reducing lift on the inboard part of the wing, thereby making the lift distribution more uniform. Figure 20 shows, however, that inboard-spoiler deflections of  $10^\circ$  and  $60^\circ$  had negligible effects on lift and stability.

Early in the present test program the flap deflection ATO2 (see fig. 2(b)) was investigated as an alternate take-off flap setting. On the basis of test results, the ATO2 arrangement was discarded in favor of the take-off (TO) flap arrangement which has been the subject of the foregoing take-off discussion; figure 21 presents the ATO2 data, however, primarily as further evidence that inboard concentration of lift is the source of the present longitudinal stability problem. Figure 21(b) shows that the ATO2 flap deflection has a slightly higher maximum lift, but, at high lift, slightly more instability than the TO flap setting.

In the landing flap configuration, as in the take-off configuration, symmetric control deflection proved ineffective in relieving the longitudinal instability. Figures 22 and 23 show that in the landing configuration the longitudinal stability characteristics were virtually unchanged either by  $40^\circ$  of aileron droop or by  $60^\circ$  of symmetric spoiler deflection.

If it is assumed that the downwash caused by inboard concentration of lift is a major factor in the longitudinal instability, speculation may then be made on various means by which a more favorable downwash distribution might be obtained. One possible means would be to move the engines outboard. The engines are presently located fairly close inboard to minimize lateral out-of-trim moments in the engine-out condition; it may be, however, that in their present location their adverse effect on longitudinal stability would outweigh the lateral considerations. Another possible means of improving lift distribution might be to reduce the taper ratio. The present wing is highly tapered, with all of the power applied to inboard, long-chord areas; therefore, reducing the length of inboard chords while lengthening the outboard chords would probably spread lift outboard somewhat. Another possibility for making the spanwise lift distribution more uniform is the use of wing sweep, since sweep has the effect of inducing outward spanwise flow. If the engine slipstream is thereby induced to spread outboard, it is possible that the jet-flap effect would be extended to outboard areas which are not now developing high lift. In configurations such as the present one in which the engines are located fairly close inboard, sweeping the wing also has the advantage of causing a reduction in trim requirements by locating the flap load closer to the aerodynamic center. Another possibility for improving longitudinal stability might be to relocate the horizontal tail of the configuration. Smoke flow studies (fig. 17) showed that after leaving the wing tip, the tip vortices move toward the airplane center line as they move rearward, passing over the outboard areas of the horizontal tail. If the tail were moved forward, these vortices might pass far enough outboard of the horizontal tail to avoid the present downwash effect. Such a result is suggested by the fact that the model of reference 2, which had a shorter tail length and lower tail height, had much better longitudinal stability than the present model.

Figure 24 presents the effect of varying the incidence of the horizontal tail, and shows that the tail, which has an area of 0.37 of the wing area, is capable of trimming the large nose-down moments produced by the wing and flap at high-lift conditions.

#### Lateral Characteristics, Symmetric Thrust

Tail off.- The tail-off static lateral and directional characteristics of the model are presented in figures 25 to 27 for the cruise, take-off, and landing configurations at three thrust levels and at angles of attack of  $0^\circ$  and  $10^\circ$ . As might be expected, the model with the tail off is directionally unstable in all flight conditions, and it is to be noted that the instability increases with increasing thrust. The data of figures 26 and 27 also show that in the take-off and landing configurations the dihedral effect ( $-C_{l\beta}$ ) goes from positive to negative as thrust is applied.

Tail on.- Figure 28 presents lateral and directional data for the tail-on configuration in the cruise condition. In this condition the model is laterally and directionally stable, and the stability characteristics are not noticeably affected by changes in thrust.

The lateral and directional characteristics of the configuration with flaps deflected to take-off and landing settings are presented in figures 29 to 31. The data show that the model is laterally and directionally stable in the power-off condition, but that in some cases power effects are pronounced. The application of power to the basic take-off configuration (fig. 29) produces a marked increase in directional stability, which contrasts with the destabilizing effect it produced in the tail-off condition. In the basic take-off and in the landing configurations, increasing power caused reduction in the dihedral effect. Theory and experience would lead to the expectation that increased power (with consequently increased lift) would produce increased dihedral effect; the reduction in the present case may have been due to asymmetric exposure of the horizontal tail to the wing tip vortices in sideslip conditions. With the landing flap setting LDG, but with inboard spoilers deflected  $60^\circ$  (fig. 32), the model was also laterally and directionally stable.

The control moments produced by asymmetric deflection of various control surfaces are presented in figures 33 to 35. Deflection of the inboard spoiler  $10^\circ$  (fig. 33(a), flap setting TO) produces virtually no moments; deflection of the outboard spoiler  $30^\circ$  (fig. 34(b), flap setting LDG) produces large rolling moments accompanied by small favorable yawing moments. Rudder effectiveness (fig. 35, flap setting TO) is, as would be expected, unaffected by engine thrust.

#### Lateral and Longitudinal Characteristics, Asymmetric Thrust

Under conditions of asymmetric thrust, the lateral characteristics of a configuration are usually the primary concern and will consequently be discussed in this section prior to the longitudinal characteristics.

Lateral and directional characteristics of the basic take-off configuration for the condition of left outboard engine not operating are plotted against angle of attack and against angle of sideslip in figures 36(a) and 36(b), respectively. As would be expected of a powered-lift configuration, out-of-trim yawing and rolling moments are large and increase with increasing thrust or angle of attack. The slopes of the curves in figure 36(b) show that the configuration is laterally and directionally stable with one outboard engine out; the change in slope of the  $C_l$  curve at  $\beta = 15^\circ$  may be further evidence that the wing tip vortex acting on the horizontal tail has a noticeable influence on dihedral effect. Figure 37 presents lateral and directional characteristics for the basic take-off configuration with left outboard engine not operating and with the ailerons, spoiler, and rudder deflected in the direction to restore trim. Figure 37(a) shows that trim in yaw was produced throughout the angle-of-attack range, whereas trim in roll was not achieved at angles of attack greater than  $13^\circ$  ( $C_L = 4.2$ ). It should be noted that these data are for a spoiler deflection of  $30^\circ$ ; better roll trim capability could reasonably be expected if full spoiler deflection ( $60^\circ$ ) had been utilized.

The preceding discussion of the ability of the control surfaces to restore lateral trim after loss of thrust from one outboard engine was for the take-off configuration; for the landing configuration, an analysis of roll trim capability with an engine out is presented in figures 38 and 39. The engine-out curve of figure 39 (landing configuration, flap setting LDG) is plotted from the basic data of figure 38 and represents the rolling moments and lift coefficients which would exist if, after loss of all thrust from the left outboard engine (assuming all four engines were initially operating at a  $C_{\mu}$  of 0.50 per engine), the  $C_{\mu}$  of the remaining left-hand engine were increased to 0.71. The spoiler-deflected curve (plotted with sign reversed for comparison) is based on rolling-moment data presented in figure 34(b). These control power data were obtained under conditions of symmetric thrust, but they are considered to be applicable to the engine-out condition because in engine-out operation the spoiler would be deflected on that wing on which two engines were still operating. Lift coefficients for the spoiler-deflected curve are those of the engine-out curve decreased at each angle of attack by the amount resulting from spoiler deflection. Figure 39 shows that, under this engine-out condition, trim in roll could be maintained at lift coefficients up to 5.7. Capability for trim and maneuver at somewhat higher lift coefficients would be expected if more than  $30^\circ$  spoiler deflection were used and if ailerons were also employed.

The longitudinal characteristics of the configuration under the conditions of lateral asymmetry which have been discussed are presented in figures 40 to 45. Loss of one outboard engine in either the take-off or landing configurations (figs. 40 and 41, respectively) results in markedly worse longitudinal stability characteristics in addition to the expected loss in maximum lift. Spoiler deflection (figs. 42, 43, and 45) produces a slight loss of lift and, in cases where lift is spoiled over outboard areas (figs. 44 and 45), increases

longitudinal instability. Deflection of all lateral control surfaces (fig. 44) produces no particular longitudinal effects other than those which the preceding discussion has attributed to the spoiler. Figure 46 shows that for a given total  $C_{\mu}$ , the lift is independent of the thrust distribution. This fact means that there is no loss in lift for an engine-out condition as compared with a symmetric thrust condition, provided the same total  $C_{\mu}$  is maintained by increasing the thrust of the remaining operable engines. This characteristic has been observed in connection with other jet-flap configurations (ref. 3) and would certainly be expected of the present configuration, in which the outboard engines are very close to the inboard engines.

### SUMMARY OF RESULTS

A wind-tunnel investigation of the aerodynamic characteristics of a transport model with a tapered wing equipped with an external-flow jet flap has yielded the following results:

1. In the power-on condition the configuration had a marked longitudinal instability, or pitch-up tendency, at angles of attack above  $7^{\circ}$ . This instability became more severe as angle of attack or thrust was increased.
2. The instability was apparently caused by the wing tip vortices being drawn into the region of the horizontal tail by the high concentration of lift over the inboard areas of the wing. Configuration or thrust changes which increased inboard lift concentration (outboard-spoiler deflection, outboard engine inoperative) caused increased instability. Changes intended to produce more nearly uniform spanwise lift distribution (drooped ailerons, thrust deflectors on outboard engines, and inboard-spoiler deflection) produced only negligible improvements in stability.
3. In the powered-lift conditions, loss of thrust of one outboard engine produced large rolling and yawing moments. Deflection of lateral controls could maintain trim at lift coefficients up to 4.2 in the take-off configuration and 5.7 in the landing configuration.
4. The model with tail on was laterally and directionally stable under all power-on test conditions. Increases in thrust produced decreases in dihedral effect and increases in directional stability.
5. The static turning efficiency and the jet-induced circulation lift which it produced were low compared with those of previous investigations.

Langley Research Center,  
National Aeronautics and Space Administration,  
Langley Station, Hampton, Va., April 30, 1969,  
721-01-00-31-23.

## REFERENCES

1. Lowry, John G.; Riebe, John M.; and Campbell, John P.: The Jet-Augmented Flap. Preprint No. 715, S.M.F. Fund Paper, Inst. Aeronaut. Sci., Jan. 1957.
2. Campbell, John P.; and Johnson, Joseph L., Jr.: Wind-Tunnel Investigation of an External-Flow Jet-Augmented Slotted Flap Suitable for Application to Airplanes With Pod-Mounted Engines. NACA TN 3898, 1956.
3. Parlett, Lysle P.; Fink, Marvin P.; and Freeman, Delma C., Jr. (With appendix B by Marion O. McKinney and Joseph L. Johnson, Jr.): Wind-Tunnel Investigation of a Large Jet Transport Model Equipped With an External-Flow Jet Flap. NASA TN D-4928, 1968.

TABLE I.- DIMENSIONS OF MODEL

Fuselage:

Length . . . . .	9.156 ft ( 2.791 m)
Maximum height . . . . .	1.060 ft ( 0.323 m)
Maximum width (excluding landing-gear pods) . . . . .	1.00 ft ( 0.305 m)
Maximum cross-sectional area (including landing-gear pods) . .	1.588 ft <sup>2</sup> (0.148 m <sup>2</sup> )

Wing:

Area . . . . .	9.80 ft <sup>2</sup> (0.910 m <sup>2</sup> )
Span . . . . .	8.28 ft ( 2.53 m)
Root chord . . . . .	1.91 ft ( 0.582 m)
Tip chord . . . . .	0.46 ft ( 0.140 m)
Mean aerodynamic chord length . . . . .	1.34 ft ( 0.408 m)
Spanwise station of mean aerodynamic chord . . . . .	1.65 ft ( 0.503 m)
Aspect ratio . . . . .	7.0
Taper ratio . . . . .	0.242
Sweep of quarter-chord line . . . . .	8°
Wing twist . . . . .	3°
Incidence at root . . . . .	-0.9°
Dihedral . . . . .	2°50'

Trailing-edge flaps:

f<sub>1</sub>

Span . . . . .	0.11 to 0.43 wing semispan
Chord . . . . .	0.26 local wing chord

f<sub>2</sub>

Span . . . . .	0.43 to 0.75 wing semispan
Chord . . . . .	0.26 local wing chord

Auxiliary flap 1

Span . . . . .	0.11 to 0.43 wing semispan
Chord . . . . .	0.17 local wing chord

Auxiliary flap 2

Span . . . . .	0.43 to 0.75 wing semispan
Chord . . . . .	0.17 local wing chord

Aileron:

Span . . . . .	0.75 to 1.00 wing semispan
Chord . . . . .	0.40 local wing chord

Leading-edge slat:

Span . . . . .	0.11 to 1.00 wing semispan
Chord . . . . .	0.13 local wing chord

TABLE I.- DIMENSIONS OF MODEL - Concluded

Vane:

Span . . . . .	0.11 to 0.75 wing semispan
Chord . . . . .	0.16 local wing chord

Inboard spoiler:

Span . . . . .	0.18 to 0.43 wing semispan
Hinge line . . . . .	0.69 local wing chord
Trailing edge . . . . .	0.79 local wing chord

Outboard spoiler:

Span . . . . .	0.43 to 0.75 wing semispan
Hinge line location . . . . .	0.69 local wing chord
Trailing edge . . . . .	0.79 local wing chord

Horizontal tail:

Area . . . . .	3.65 ft <sup>2</sup> ( 0.339 m <sup>2</sup> )
Span . . . . .	4.27 ft ( 1.30 m)
Root chord (theoretical at fuselage centerline) . . . . .	1.27 ft ( 0.387 m)
Tip chord (theoretical) . . . . .	0.44 ft ( 0.134 m)
Tail length . . . . .	5.65 ft ( 1.72 m)
Aspect ratio . . . . .	5.0
Sweep of quarter-chord line . . . . .	16.1°

Elevator:

Area (aft of hinge line) . . . . .	0.86 ft <sup>2</sup> (0.0798 m <sup>2</sup> )
Hinge line location . . . . .	0.75 local chord

Vertical tail:

Area . . . . .	2.24 ft <sup>2</sup> ( 0.208 m <sup>2</sup> )
Span . . . . .	1.31 ft ( 0.399 m)
Root chord (top of fuselage) . . . . .	2.04 ft ( 0.622 m)
Tip chord (at horizontal tail) . . . . .	1.37 ft ( 0.418 m)
Aspect ratio . . . . .	0.77
Sweep of quarter-chord line . . . . .	45.5°
Tail length . . . . .	4.53 ft ( 1.38 m)

Rudder:

Area (aft of hinge line) . . . . .	0.62 ft <sup>2</sup> (0.0576 m <sup>2</sup> )
Span . . . . .	1.10 ft ( 0.335 m)
Hinge line location . . . . .	0.68 local chord

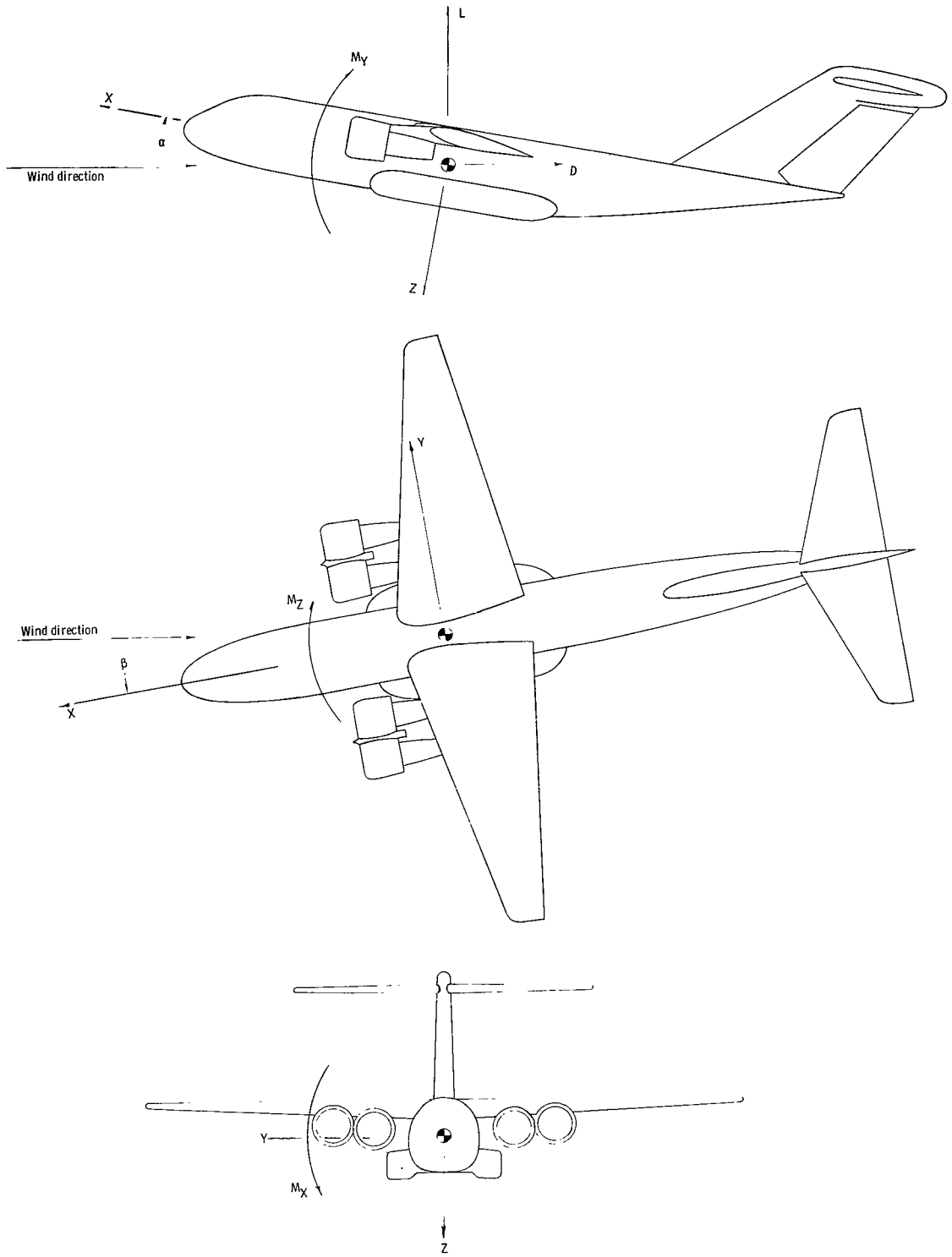
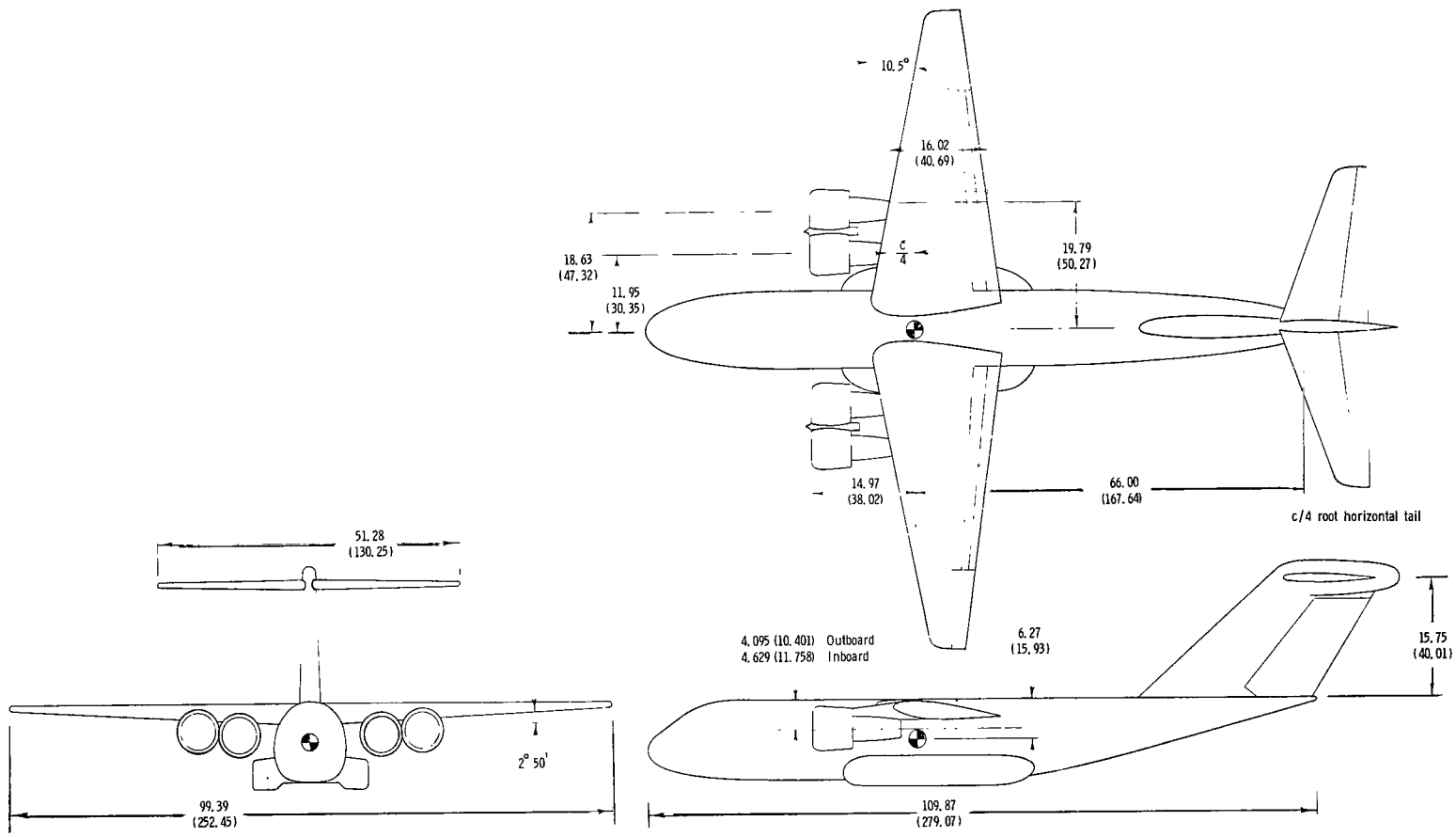
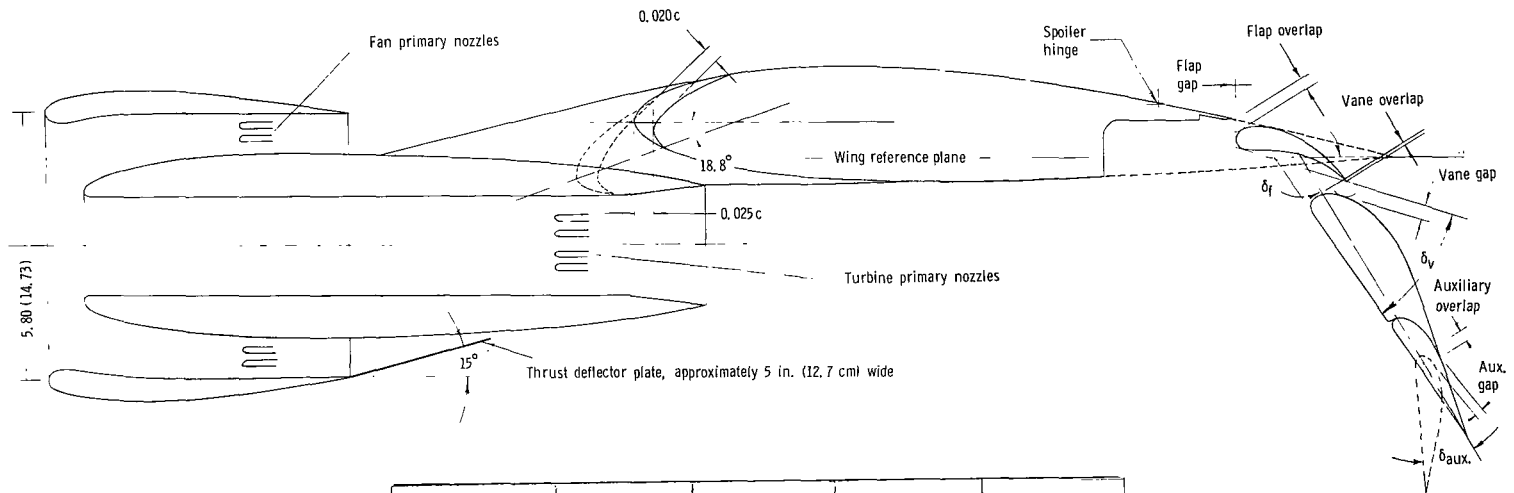


Figure 1.- Axis system used in presentation of data.



(a) Three-view drawing showing principal dimensions in inches (centimeters).

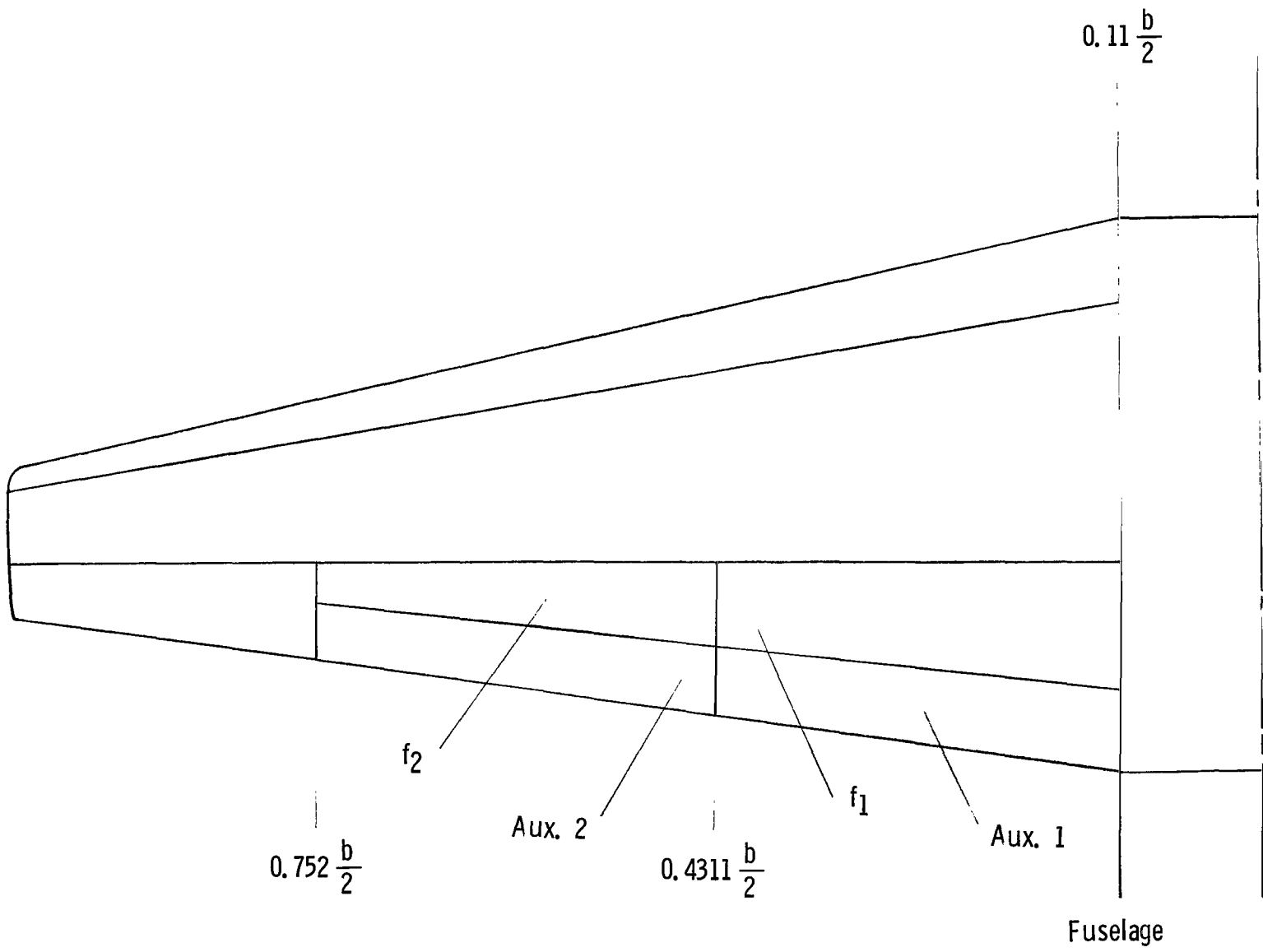
Figure 2.- Drawings of model.



Flap configuration		Inboard flaps, $f_1$			Outboard flaps, $f_2$			Auxiliary flap 1 and 2			Vane		
Symbol	Nominal	$\delta_f$	Overlap	Gap	$\delta_f$	Overlap	Gap	$\delta_{aux}$	Overlap	Gap	$\delta_v$	Overlap	Gap
CR	Cruise	0	-	-	0	-	-	0	-	-	-	-	-
TO	Take-off	30	11.5	0	60	0	1.4	0	0	0	42.5	0	2
ATO1	Alternate T.C	40	9.6	0	60	0	1.4	0	0	0	42.5	0	2
ATO2	Alternate T.C.	40	9.6	0	40	9.6	0	0	0	0	42.5	0	2
LDG	Landing	60	0	1.4	60	0	1.4	0	0	0	42.5	0	2
LA10	Landing	60	0	1.4	60	0	1.4	10	2	1	42.5	0	2
LA20	Landing	60	0	1.4	60	0	1.4	20	1	1	42.5	0	2
LA30	Landing	60	0	1.4	60	0	1.4	30	$\frac{1}{2}$	1	42.5	0	2

(b) Wing section and flap configuration schedule. Overlaps and gaps in percent local wing chord. Deflections in degrees.

Figure 2.- Continued.



(c) Wing planform showing flap segments.

Figure 2.- Concluded.



Figure 3.- Photographs of model installed in tunnel.

L-69-1395

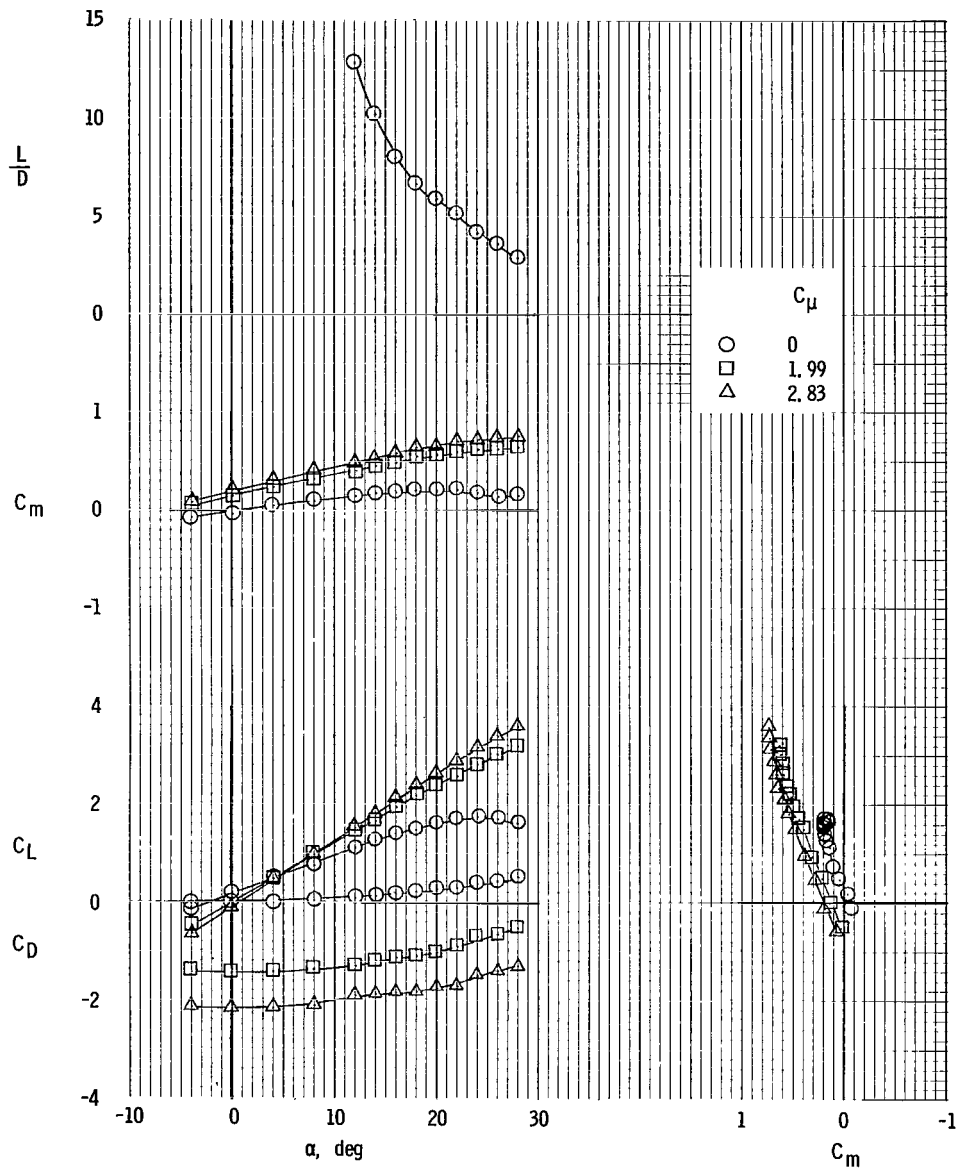


Figure 4.- Tail-off longitudinal data for cruise flap setting CR.

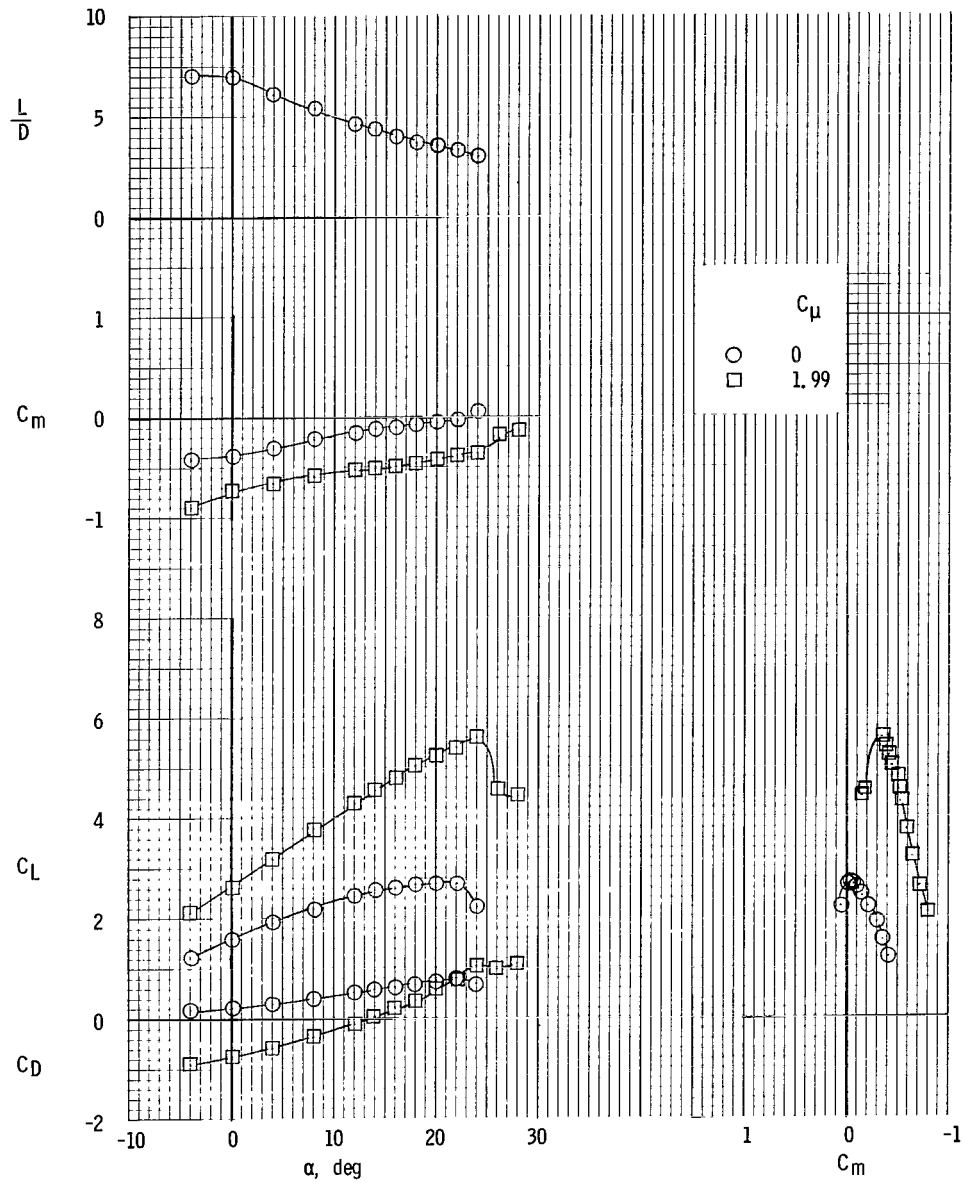


Figure 5.- Tail-off longitudinal data for take-off flap setting TO.

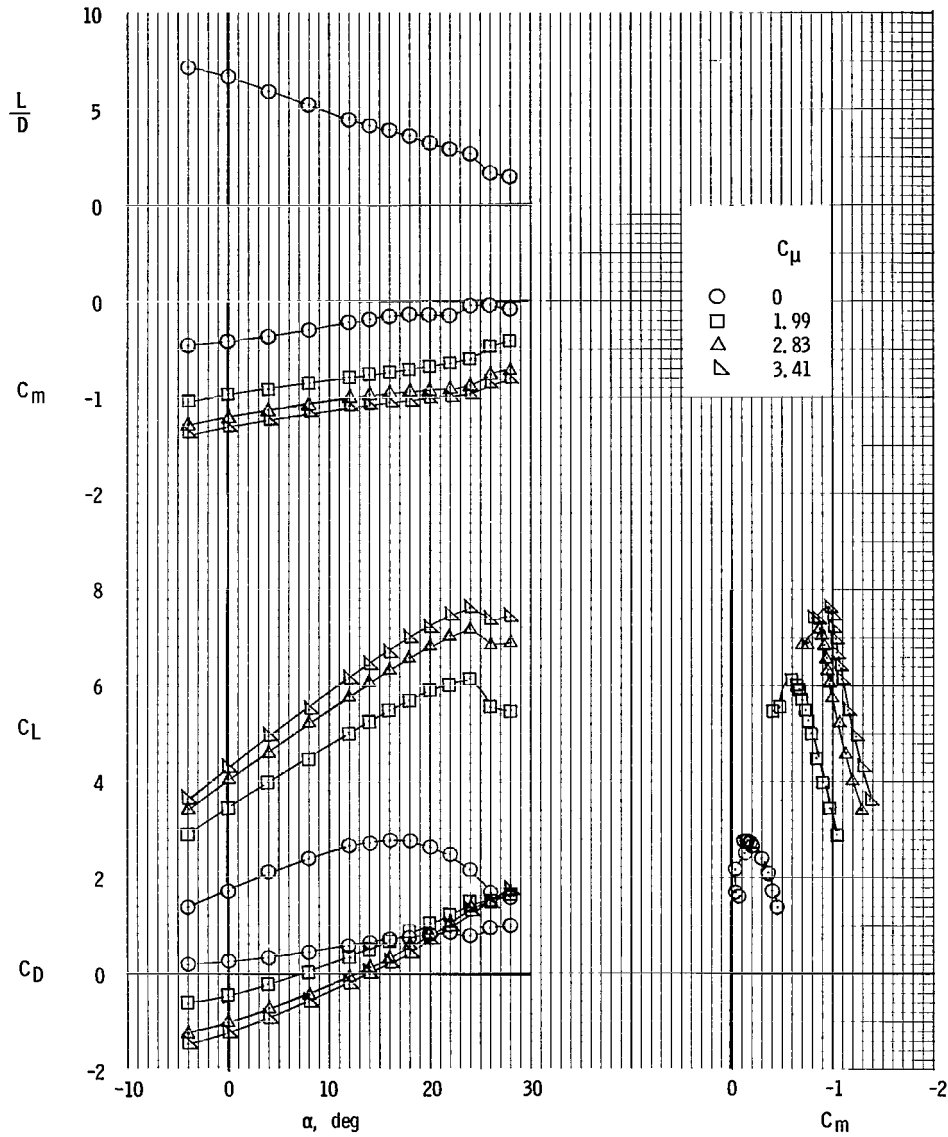


Figure 6.- Tail-off longitudinal data for an alternate take-off flap setting AT01.

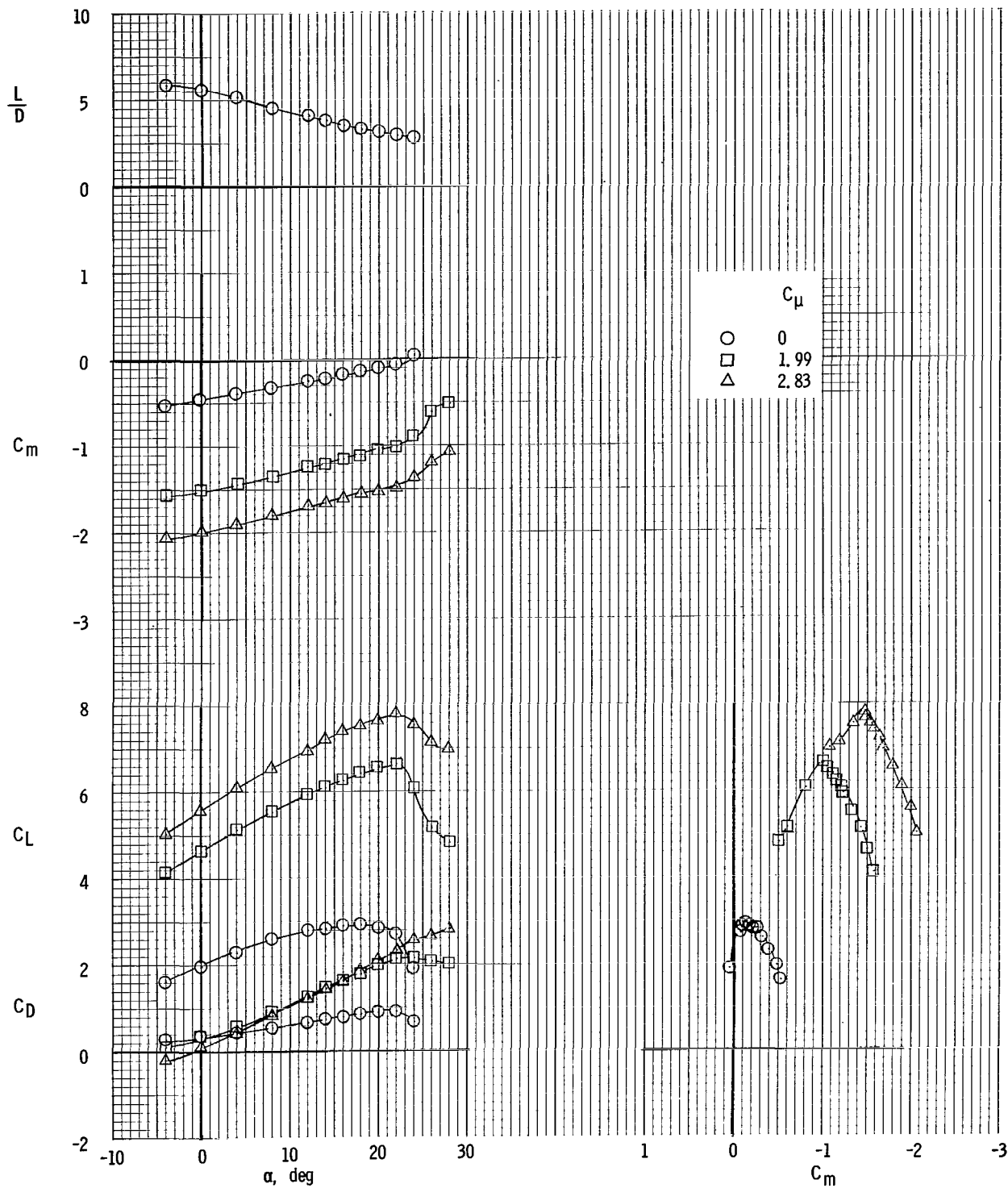
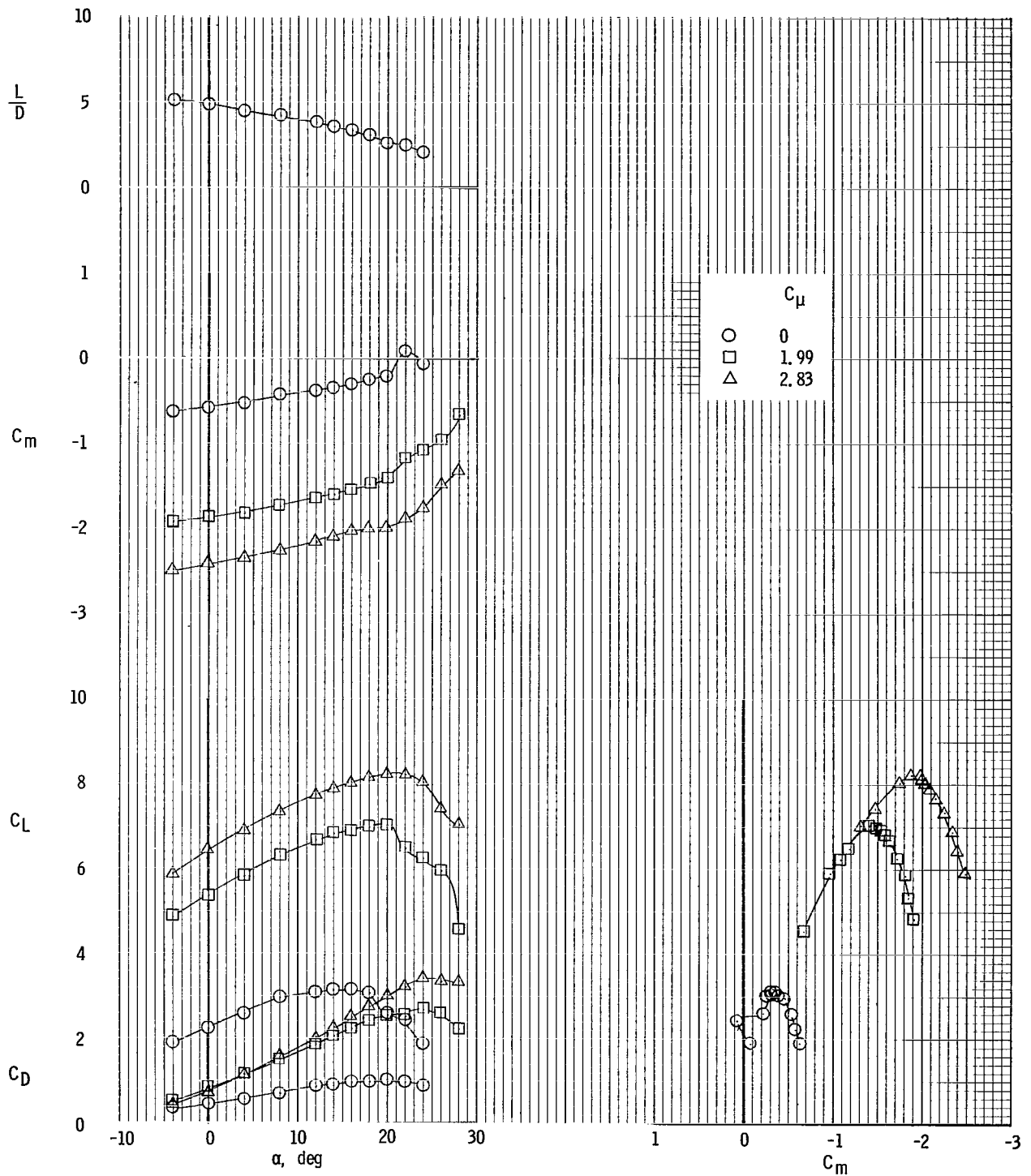
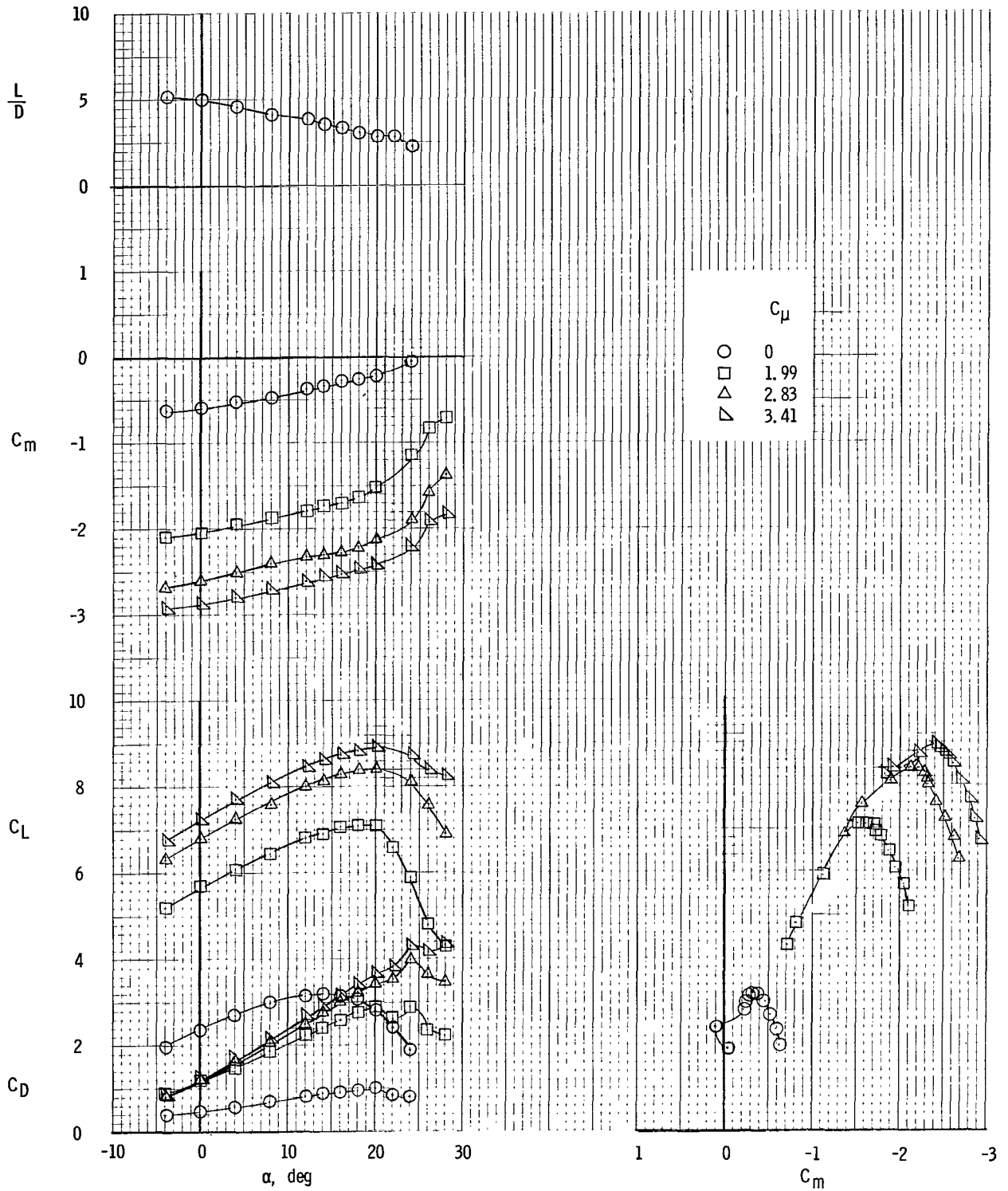


Figure 7.- Tail-off longitudinal data for landing flap setting LDG.



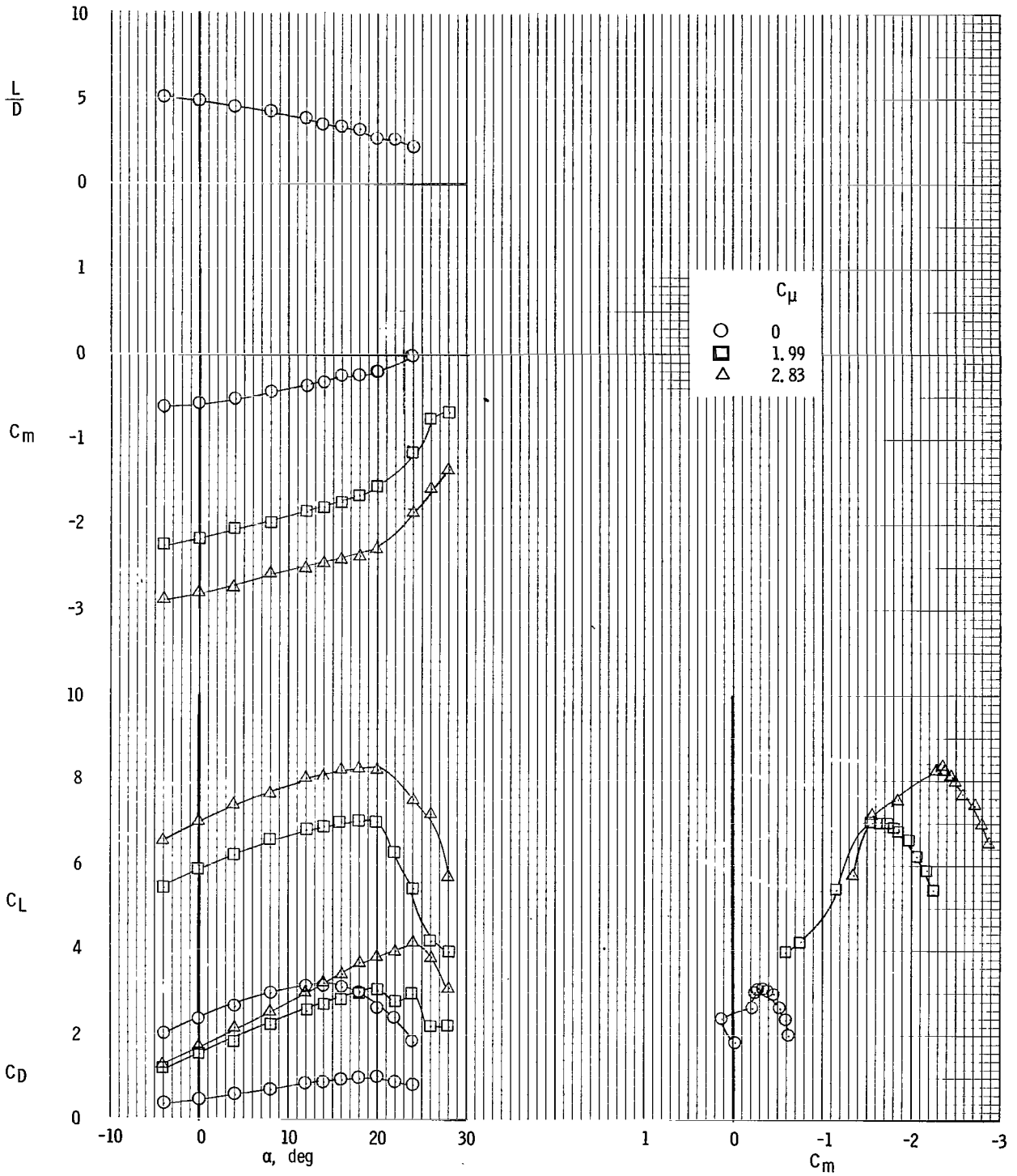
(a) Auxiliary flaps deflected  $10^\circ$ ; LA10.

Figure 8.- Longitudinal data for auxiliary flaps as glidepath control. Tail off.



(b) Auxiliary flaps deflected  $20^\circ$ ; LA20.

Figure 8.- Continued.



(c) Auxiliary flaps deflected 30°; LA30.

Figure 8.- Concluded.

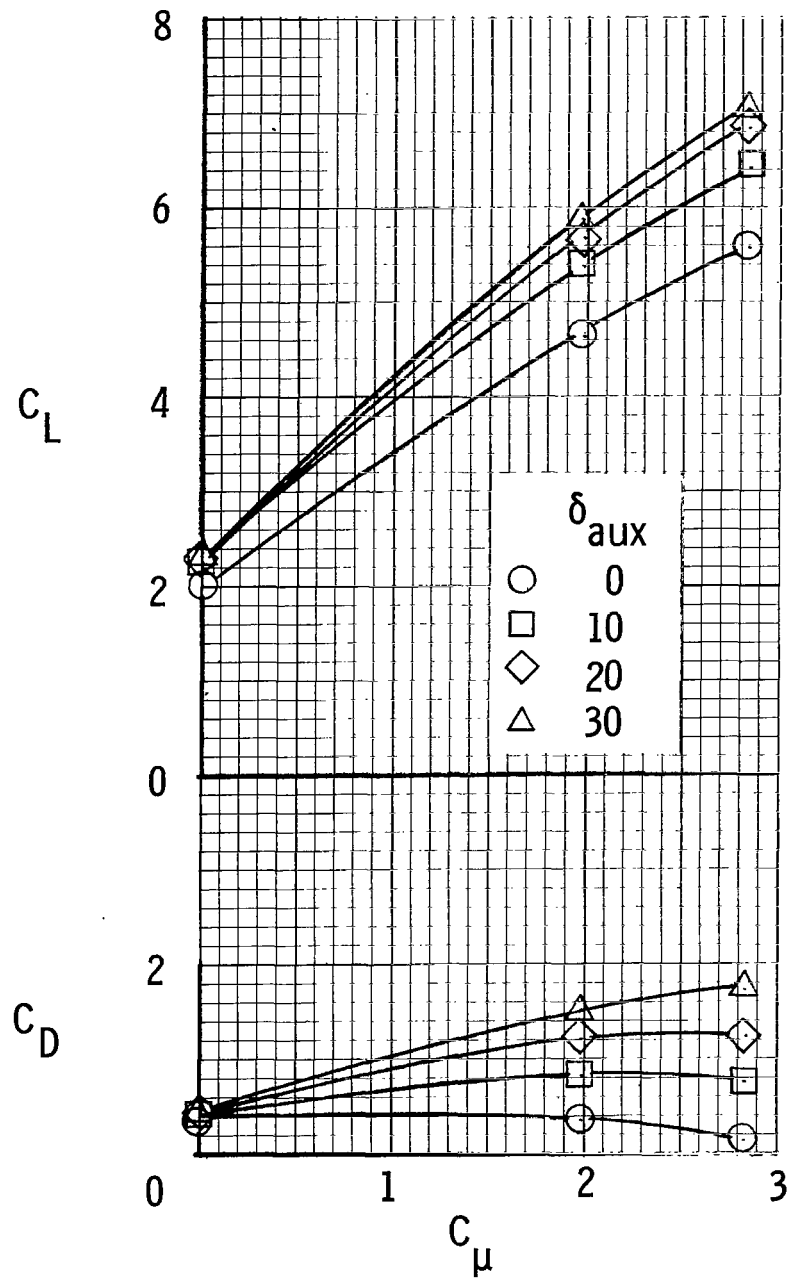


Figure 9.- Summary of auxiliary-flap performance. Landing flap settings;  $\alpha = 7.5^\circ$ .

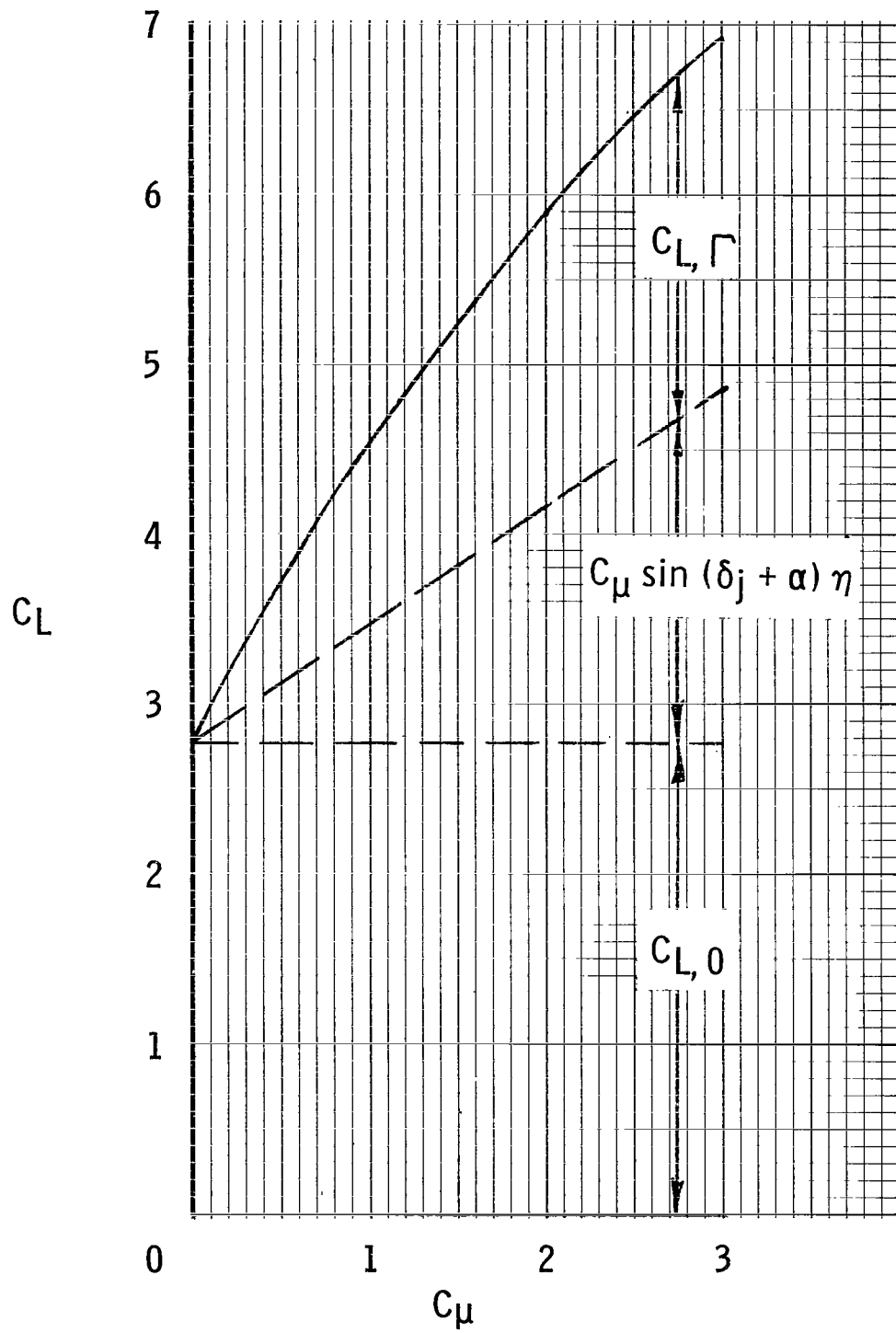


Figure 10.- Resolution of jet-flap lift into components. Tail off;  $\delta_f = 60^\circ$ ;  $\alpha = 10^\circ$ ; LDG.

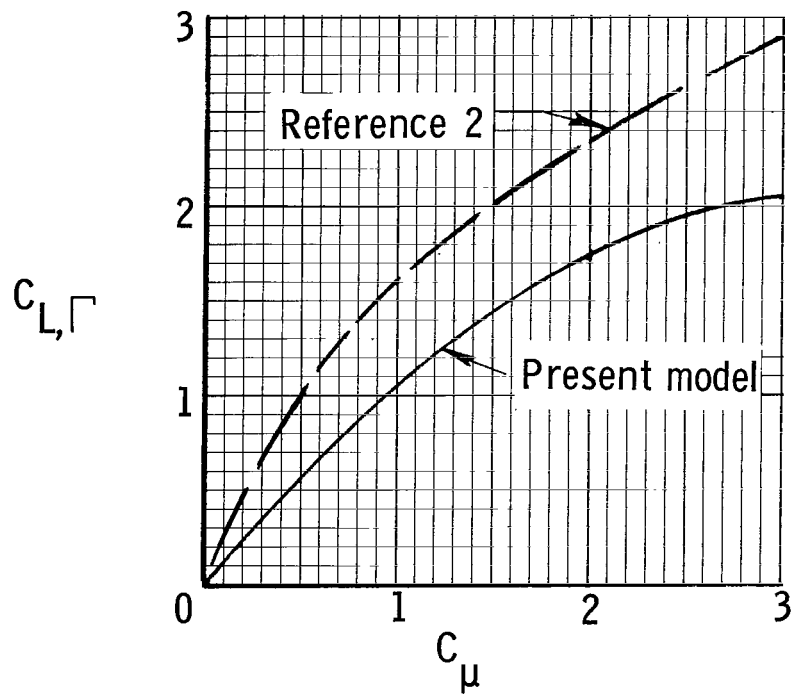


Figure 11.- Comparison of jet circulation lift produced by model of present investigation with that of reference 2. Landing flap setting LDG.

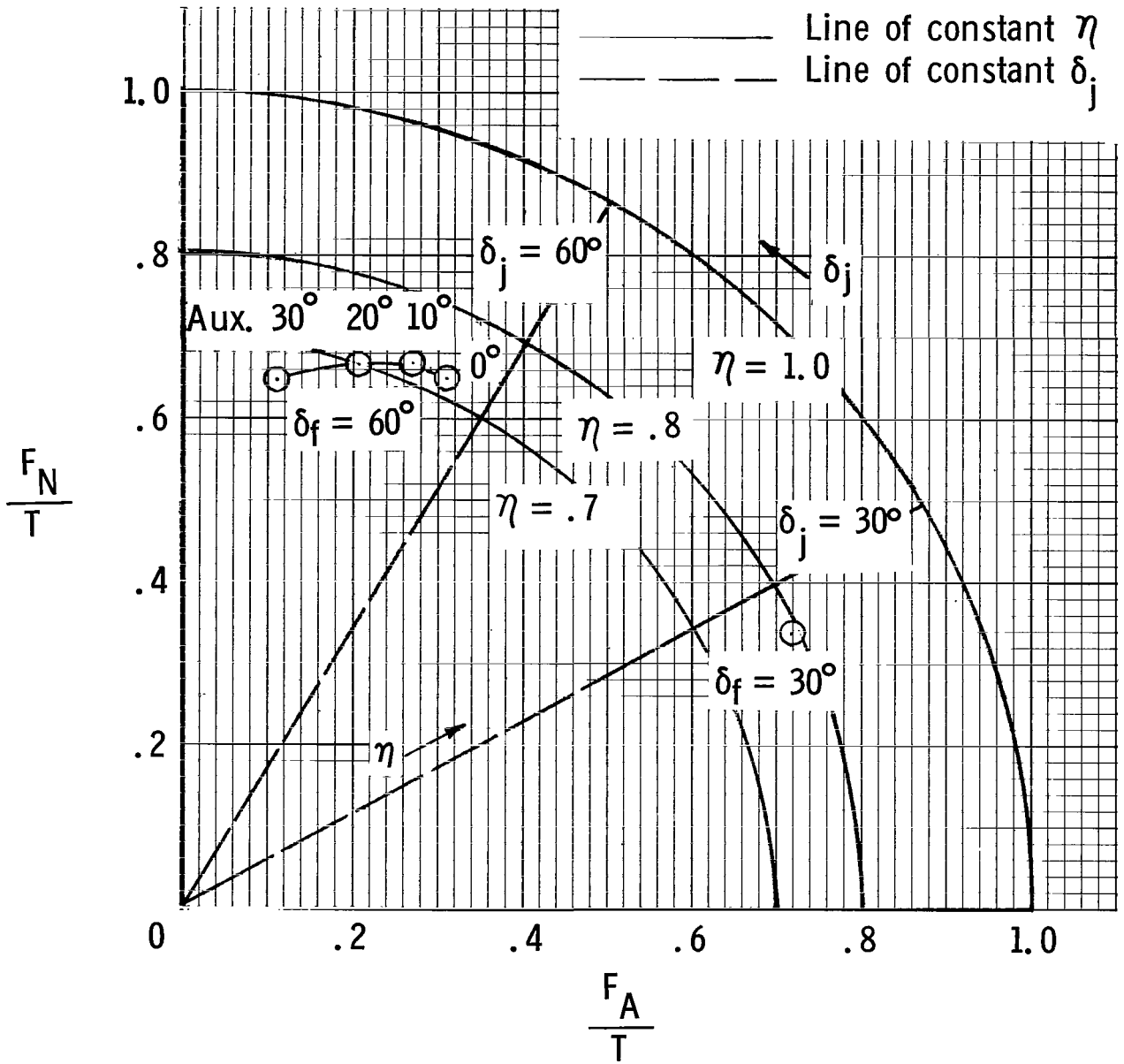


Figure 12.- Summary of turning efficiency and turning angle.

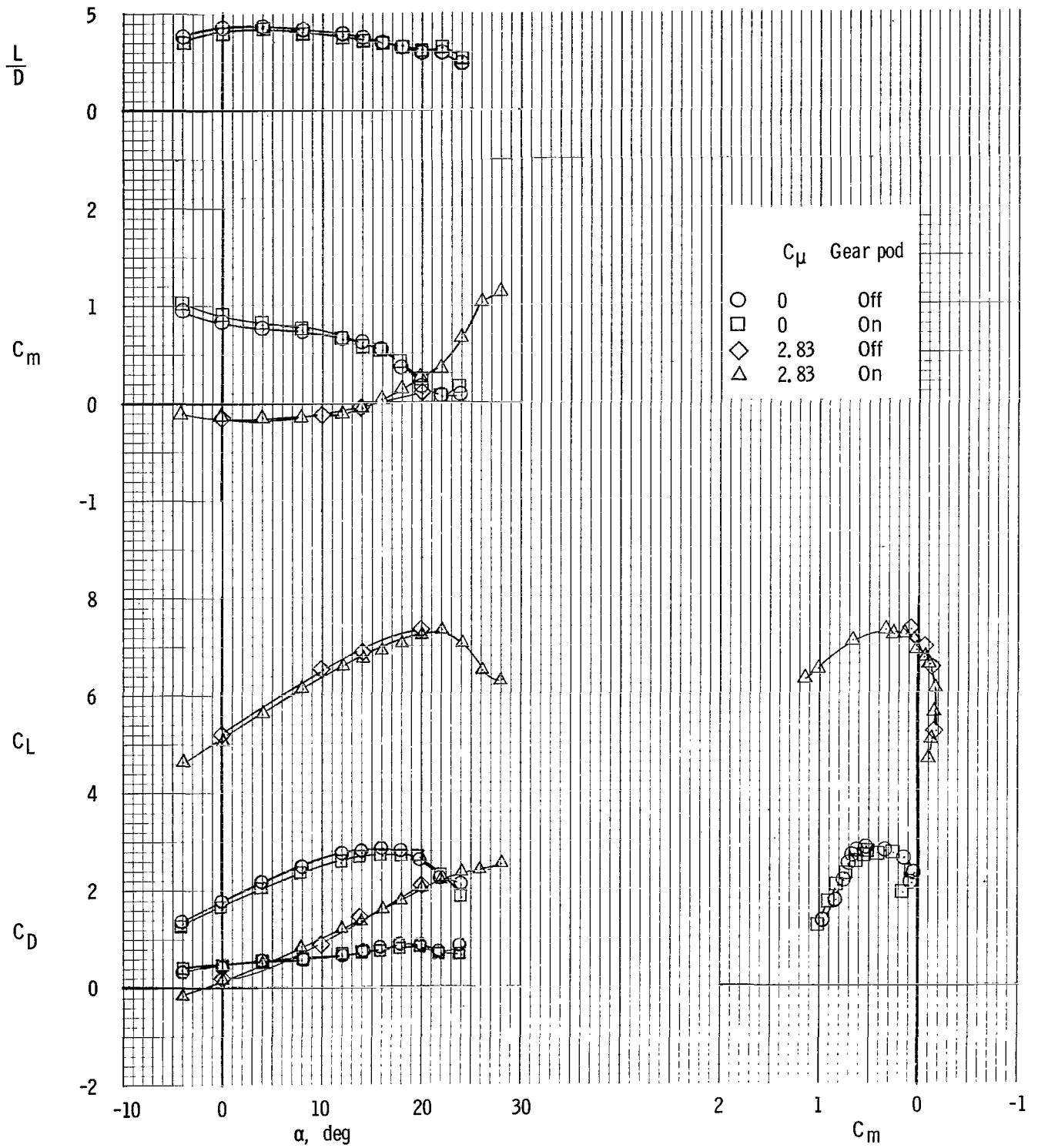


Figure 13.- Effect of landing-gear pod on longitudinal characteristics. Landing flap setting LDG; tail on.

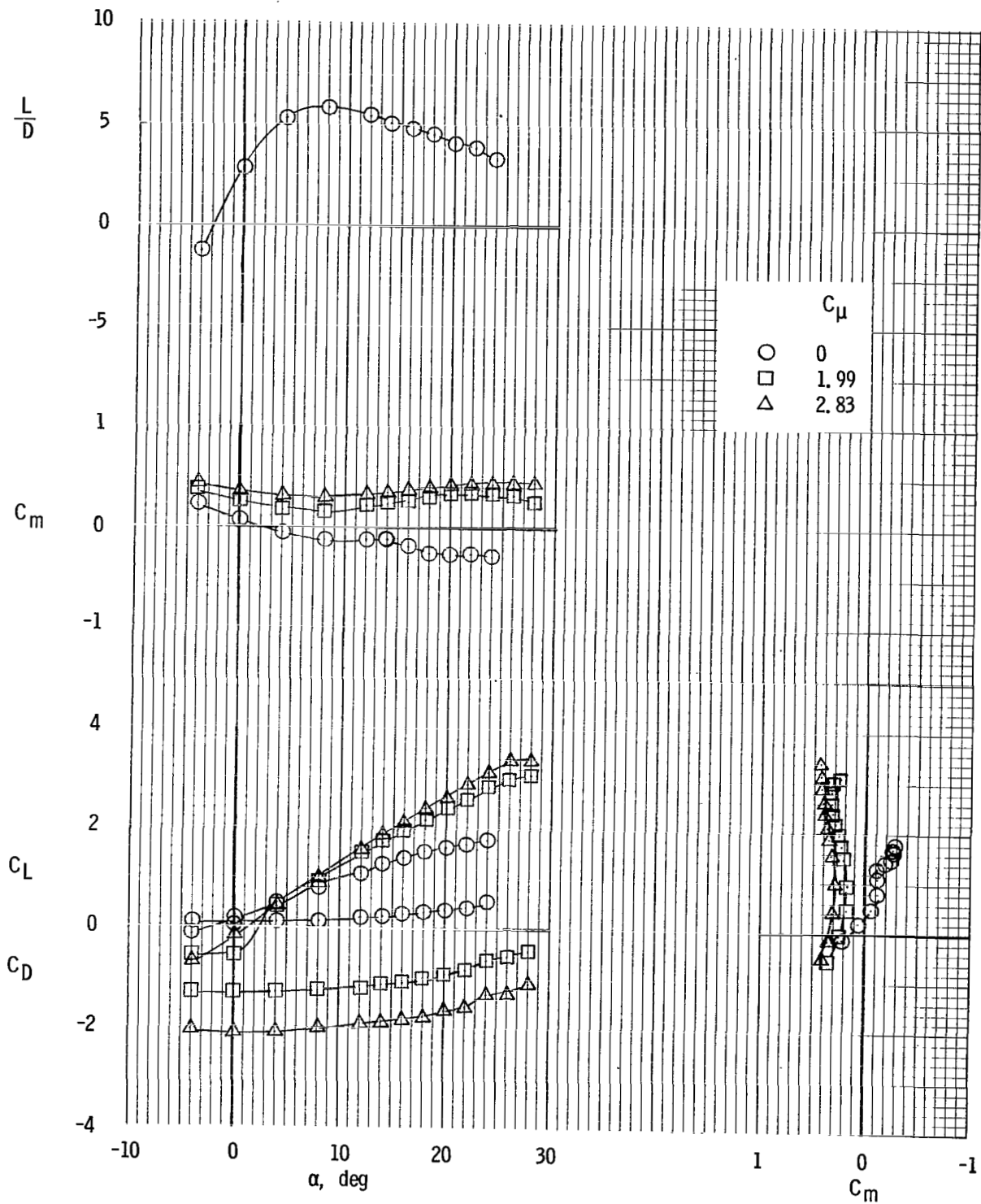


Figure 14.- Tail-on longitudinal data for cruise flap setting CR.

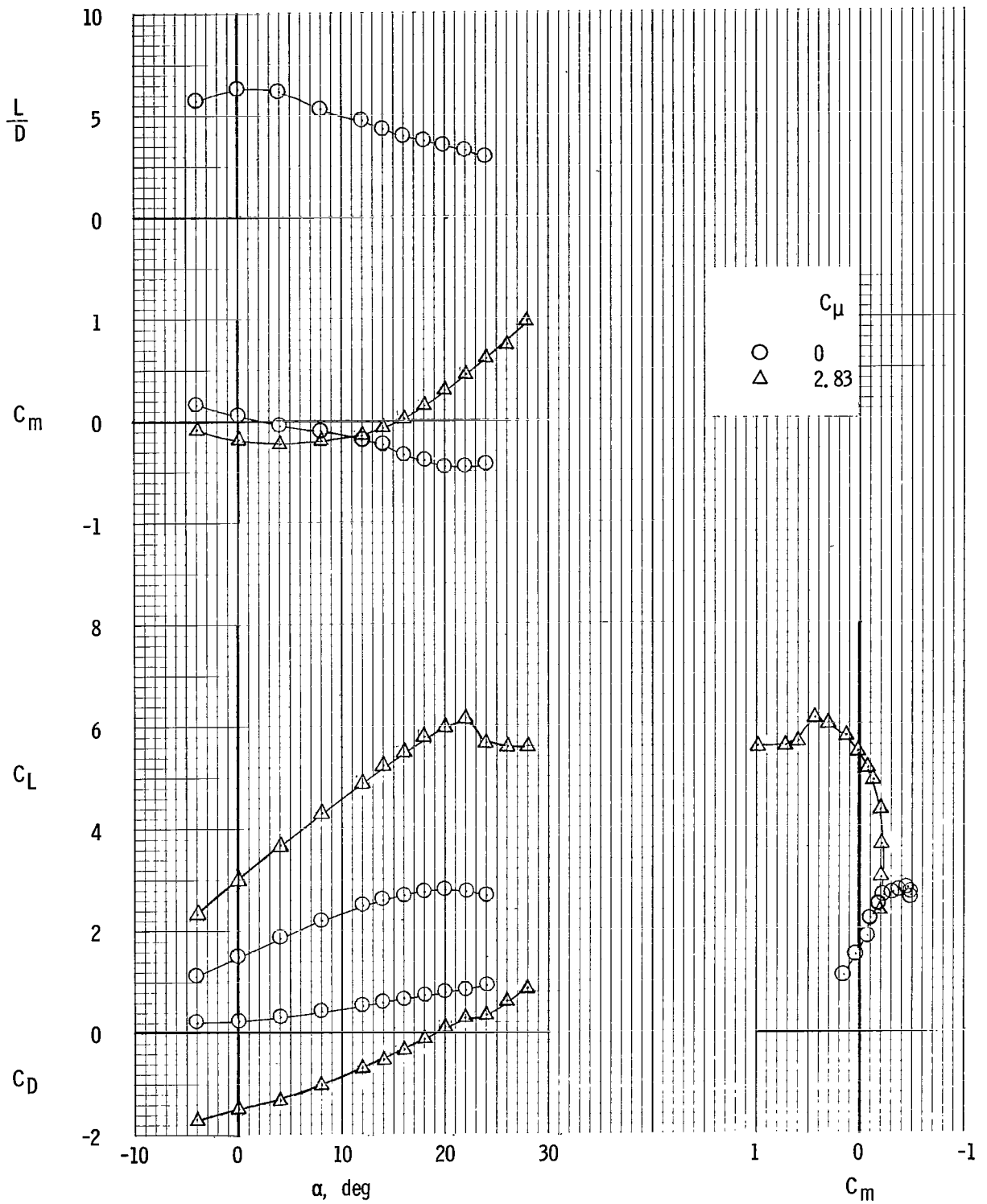


Figure 15.- Tail-on longitudinal data for take-off flap setting T0.

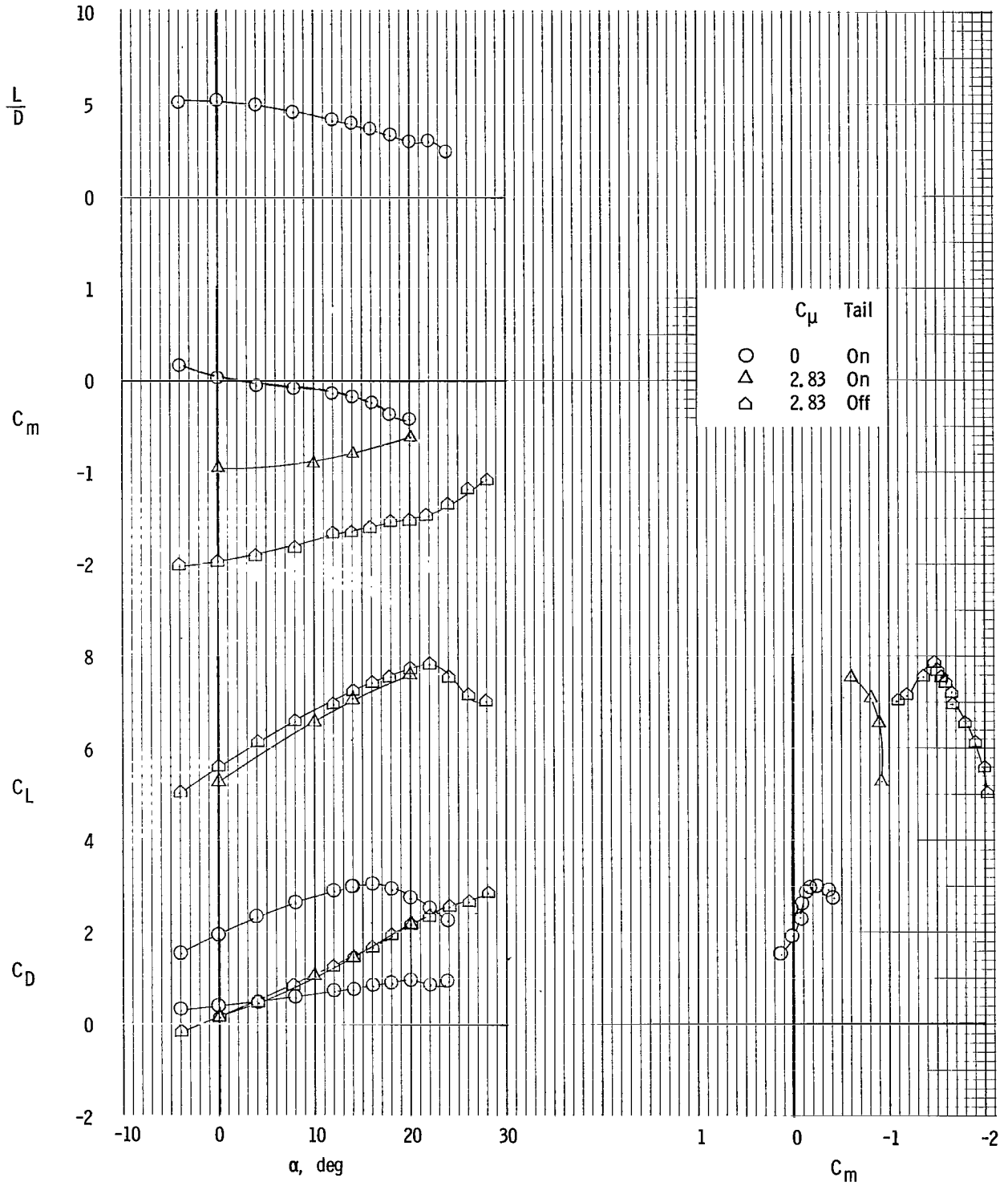
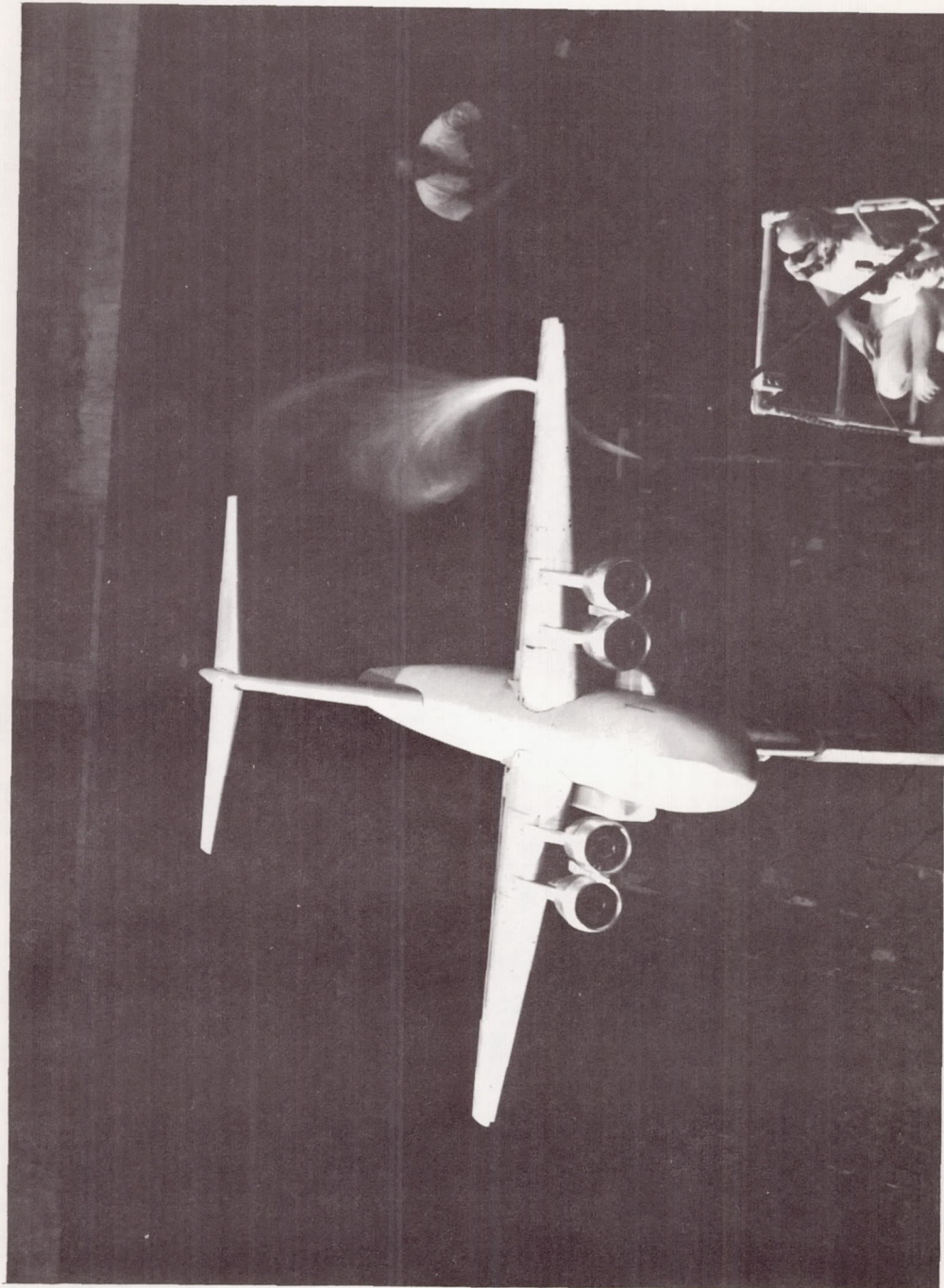


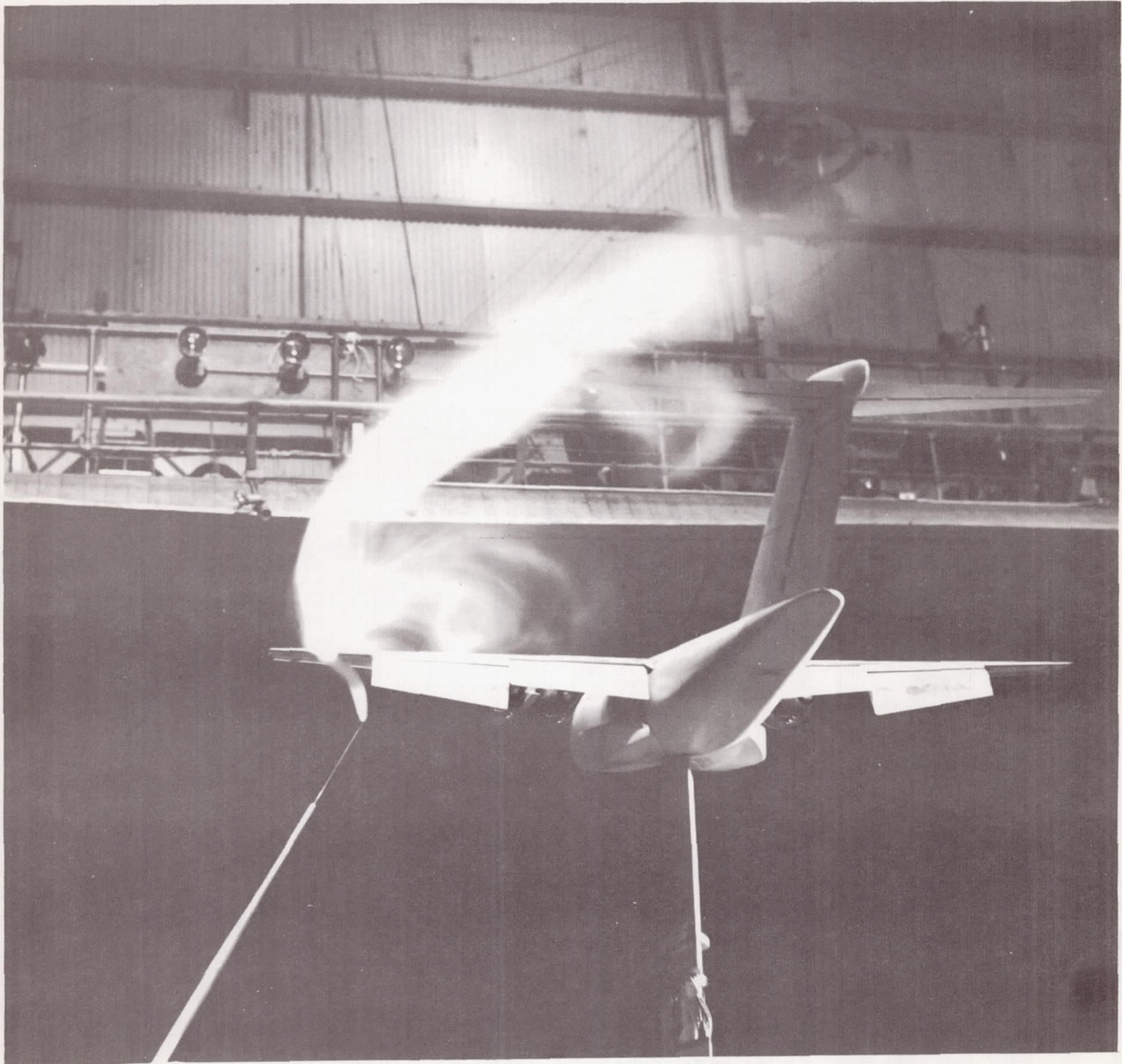
Figure 16.- Tail-on longitudinal data for landing flap setting LDG.



(a) Top view.

L-69-1396

Figure 17.- Smoke-flow study of model. Take-off flap deflection TO.



(b) Three-quarter rear view.

L-69-1397

Figure 17.- Concluded.

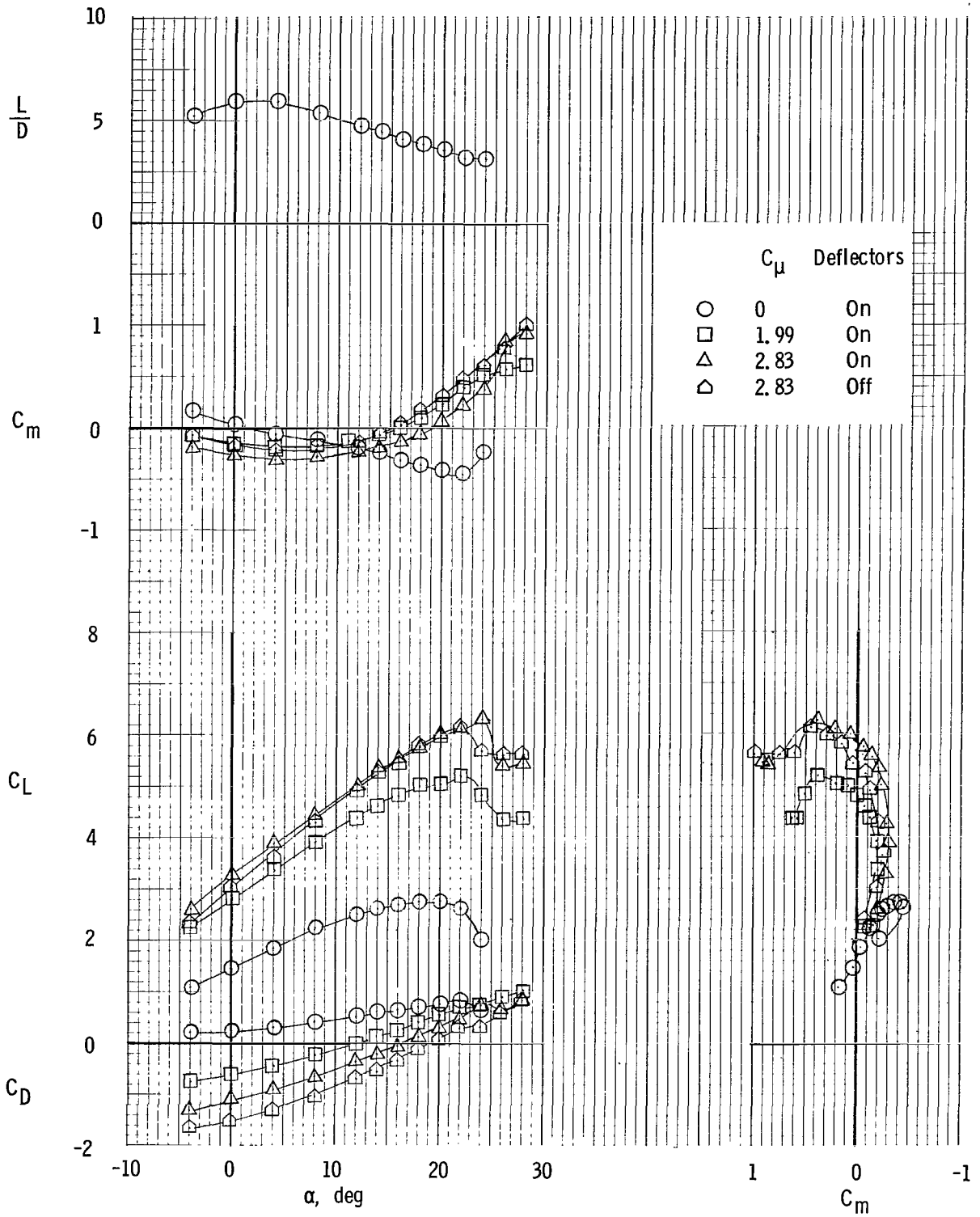


Figure 18.- Effect of thrust deflectors on longitudinal characteristics. Take-off flap setting T0; tail on.

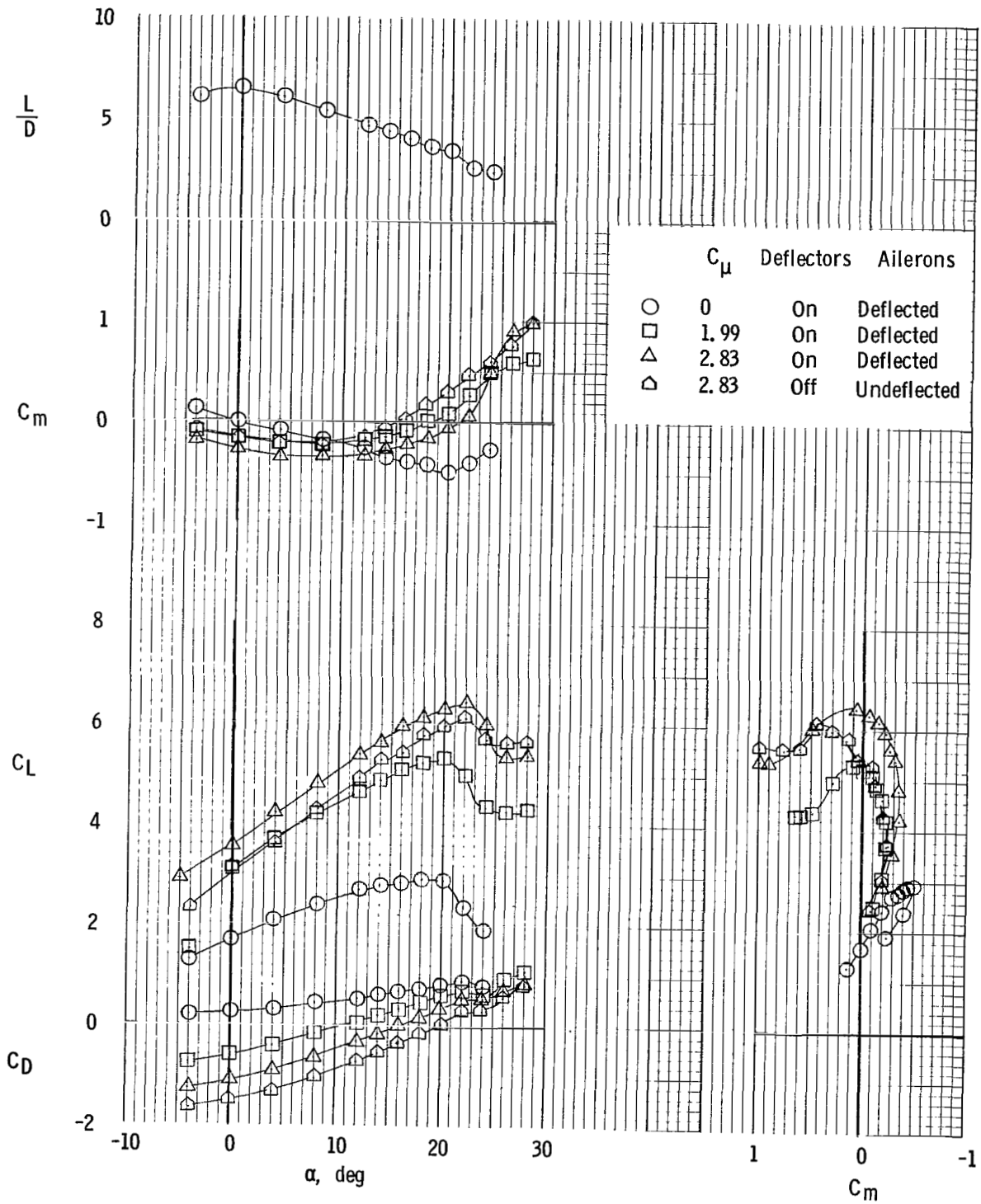
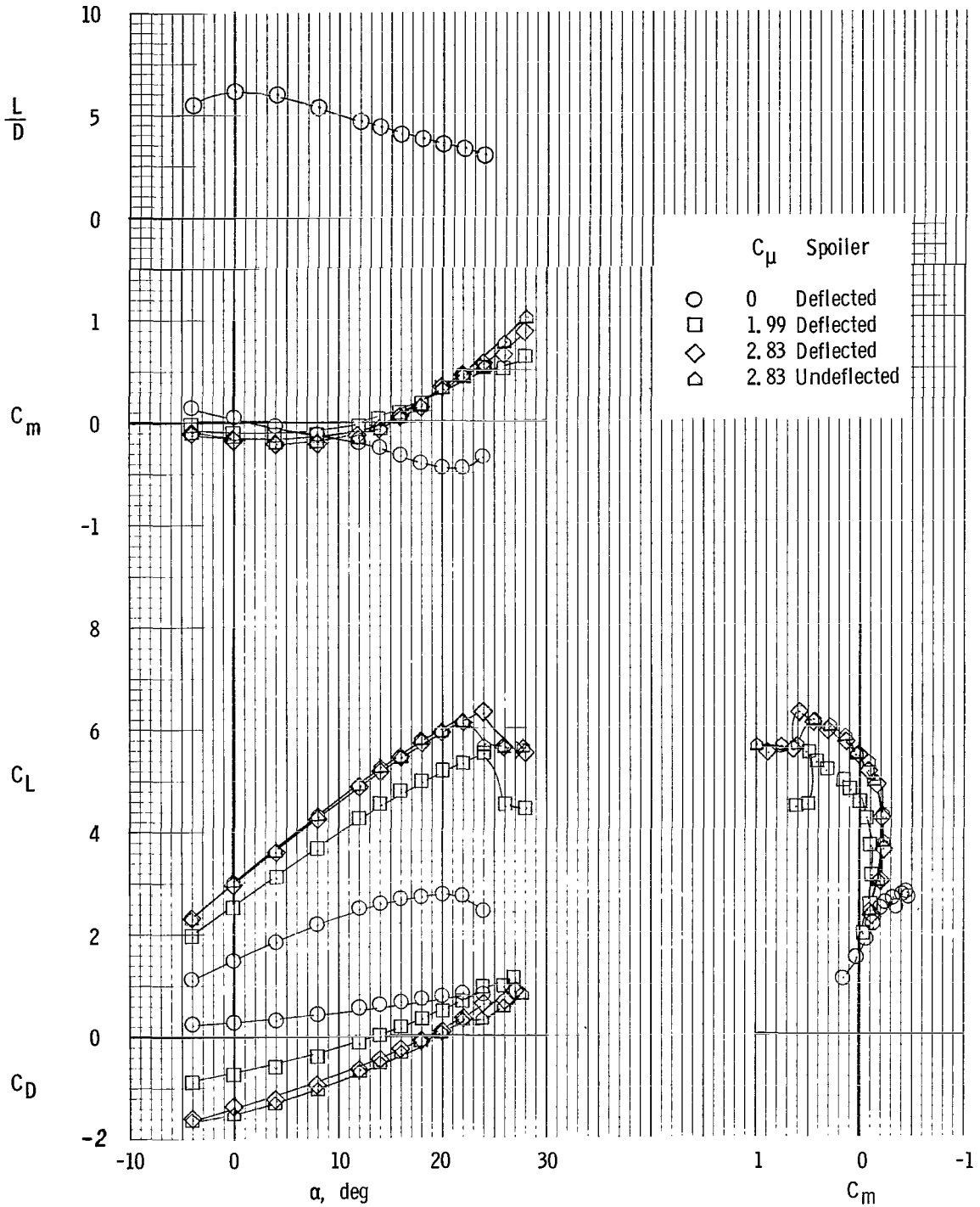
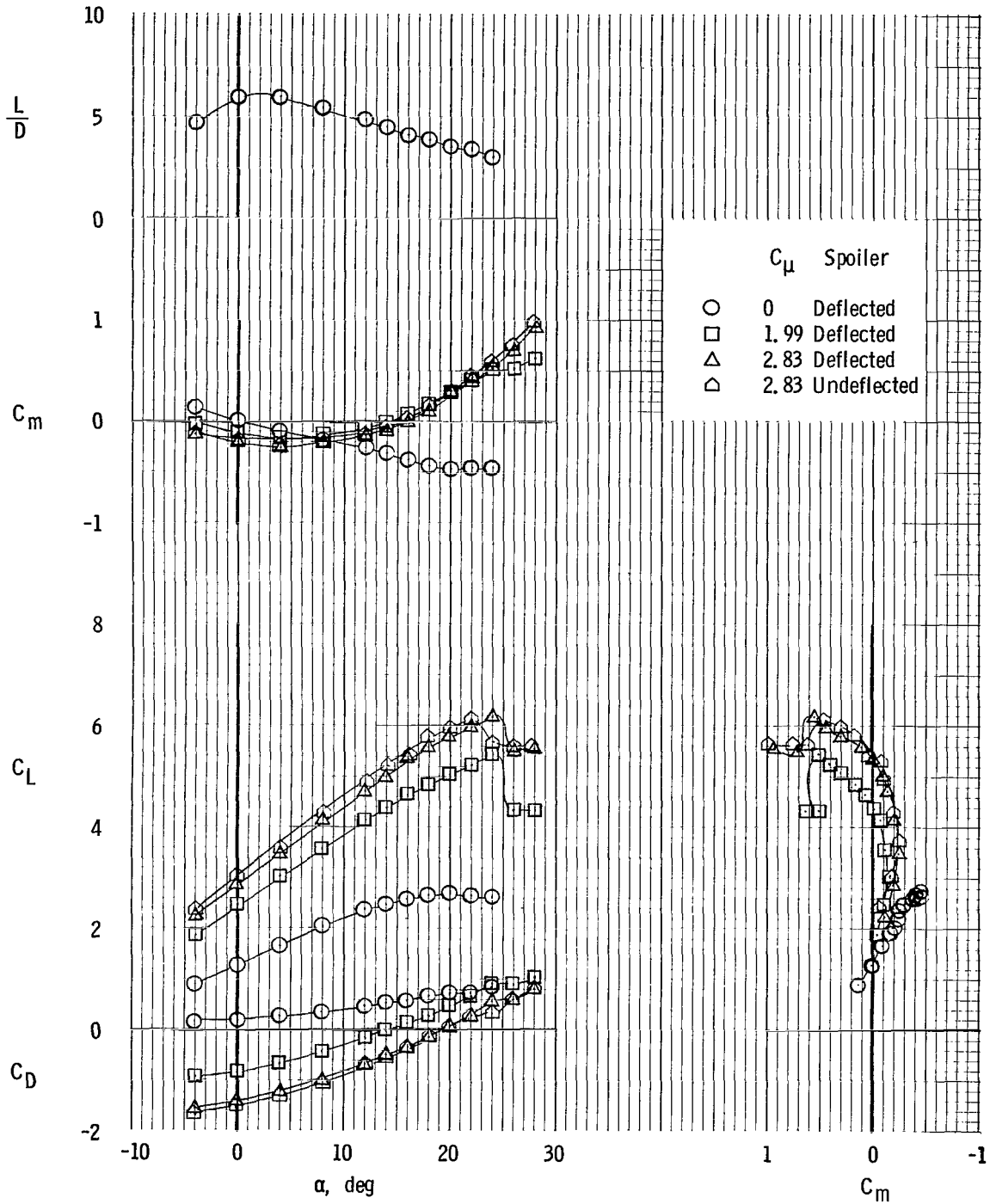


Figure 19.- Effect of thrust deflectors and drooped ailerons on longitudinal characteristics. Take-off flap setting T0; aileron deflection, 40°; tail on.



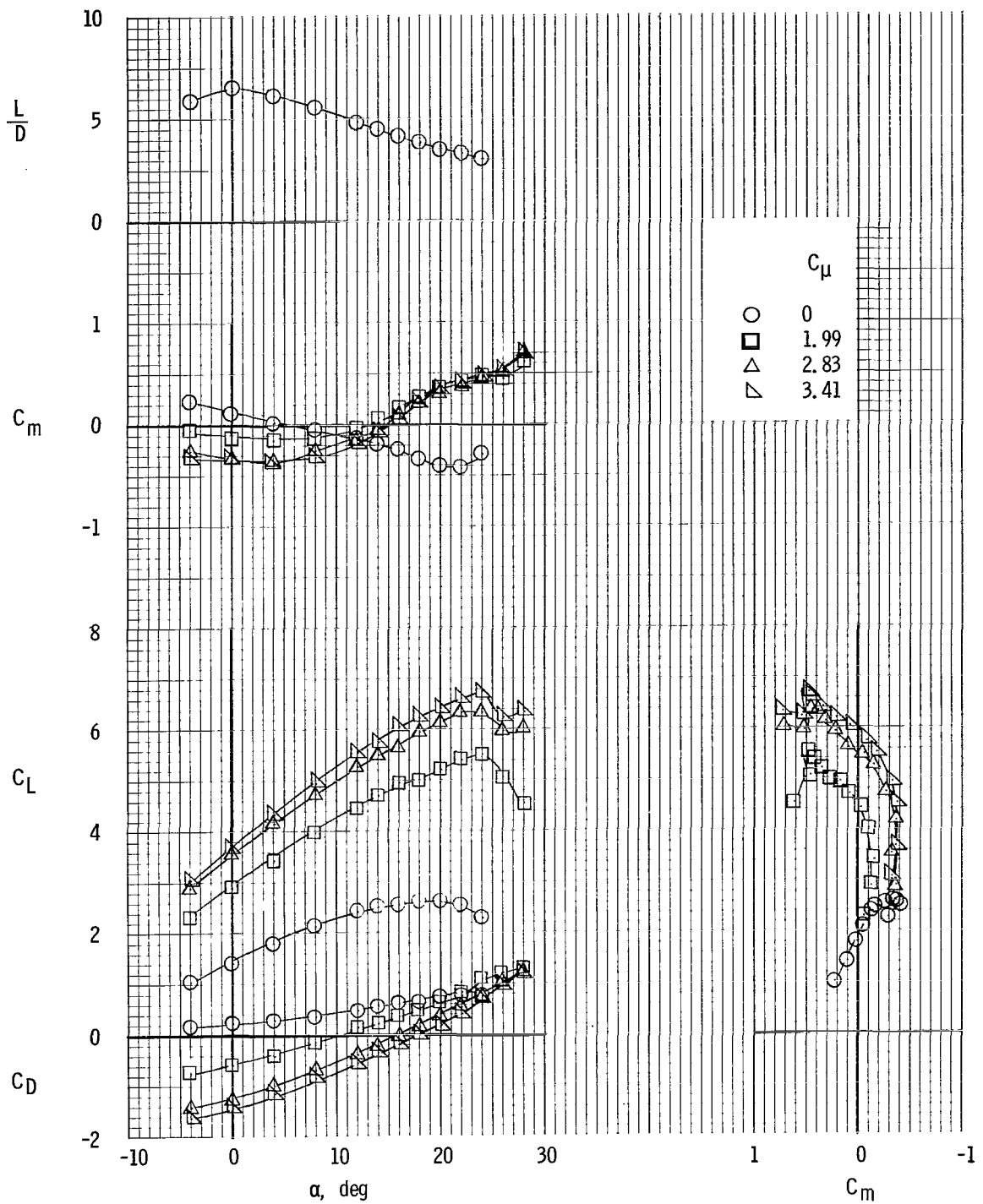
(a) Spoiler deflection,  $10^0$ .

Figure 20.- Effect of symmetric inboard spoiler deflection on longitudinal characteristics. Take-off flap setting TO; tail on.



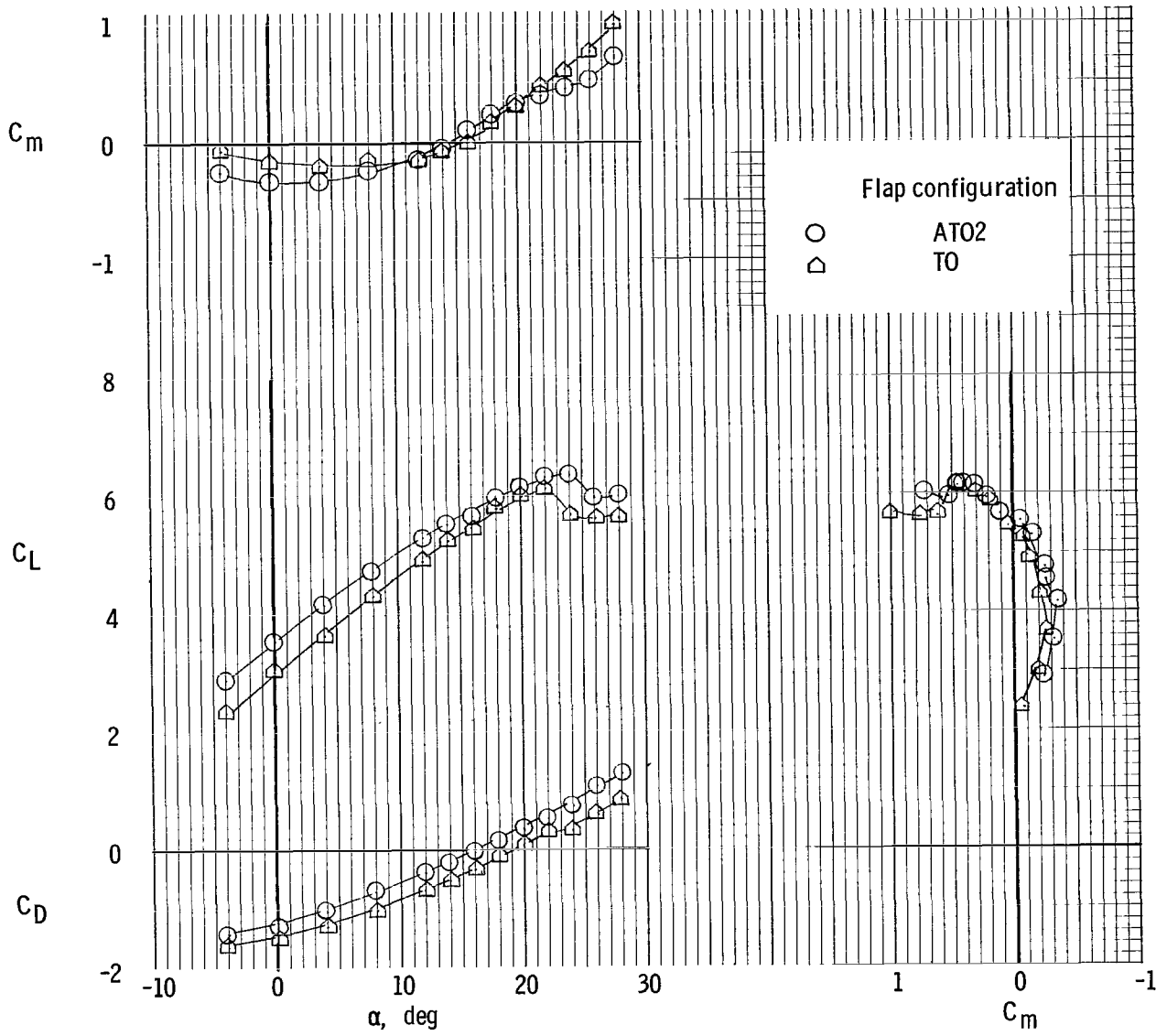
(b) Spoiler deflection,  $60^\circ$ .

Figure 20.- Concluded.



(a) Alternate take-off configuration AT02.

Figure 2L- Longitudinal characteristics of an alternate take-off flap setting. Tail on.



(b) Comparison with basic take-off flap deflection at  $C_\mu = 2.83$ .

Figure 21.- Concluded.

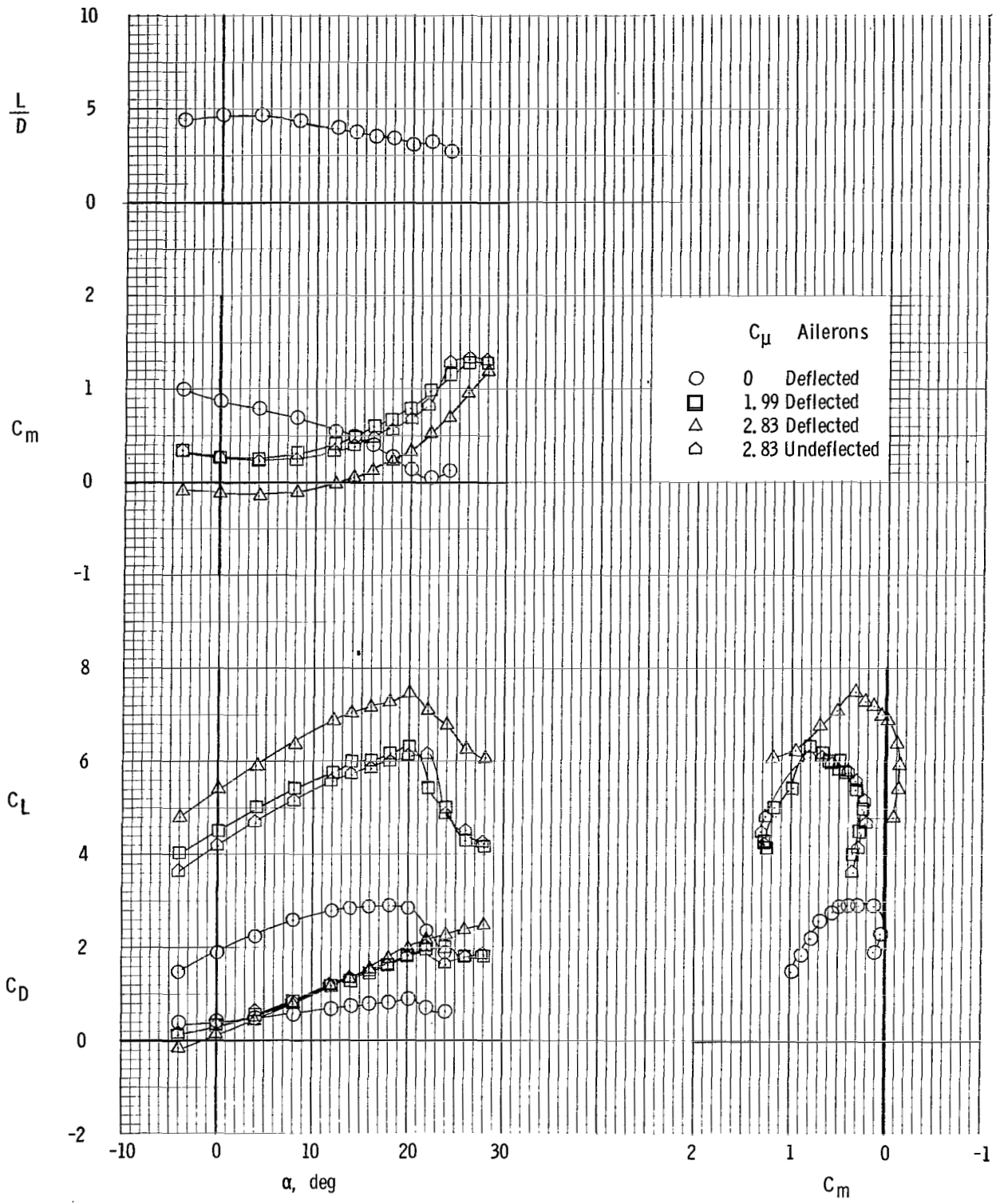


Figure 22.- Effect of aileron droop on longitudinal characteristics. Landing flap setting LDG. Aileron deflection, 40° (each); tail on.

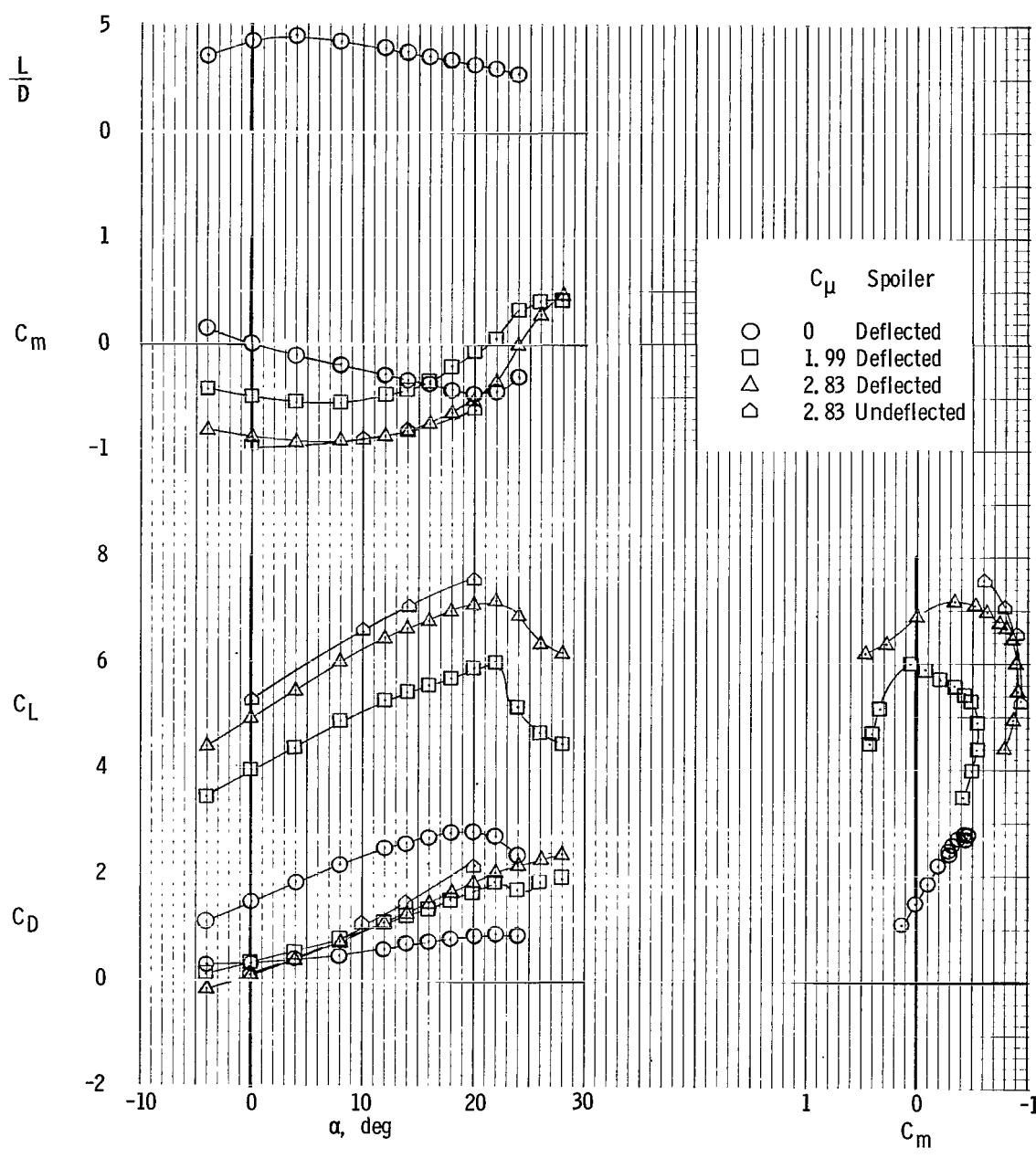
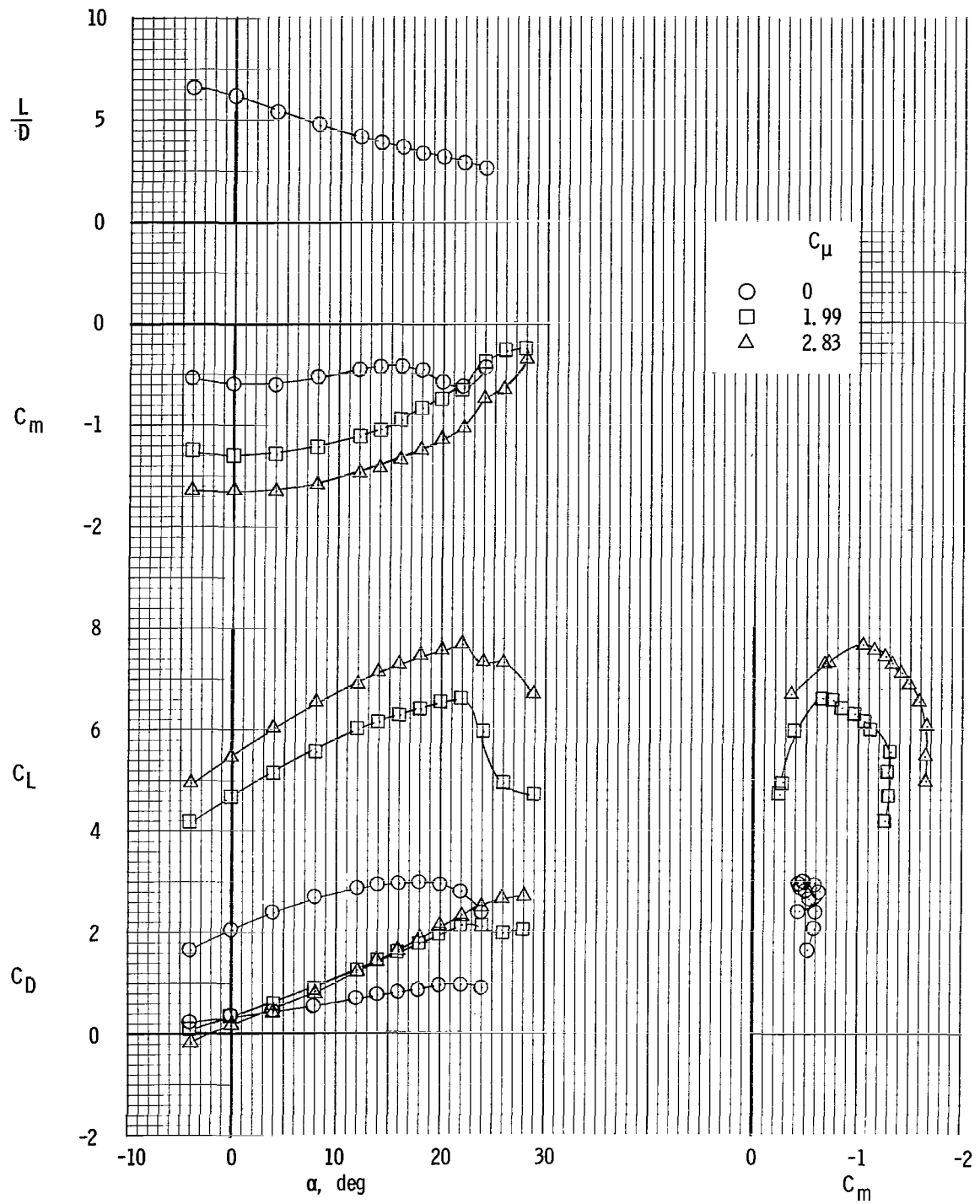
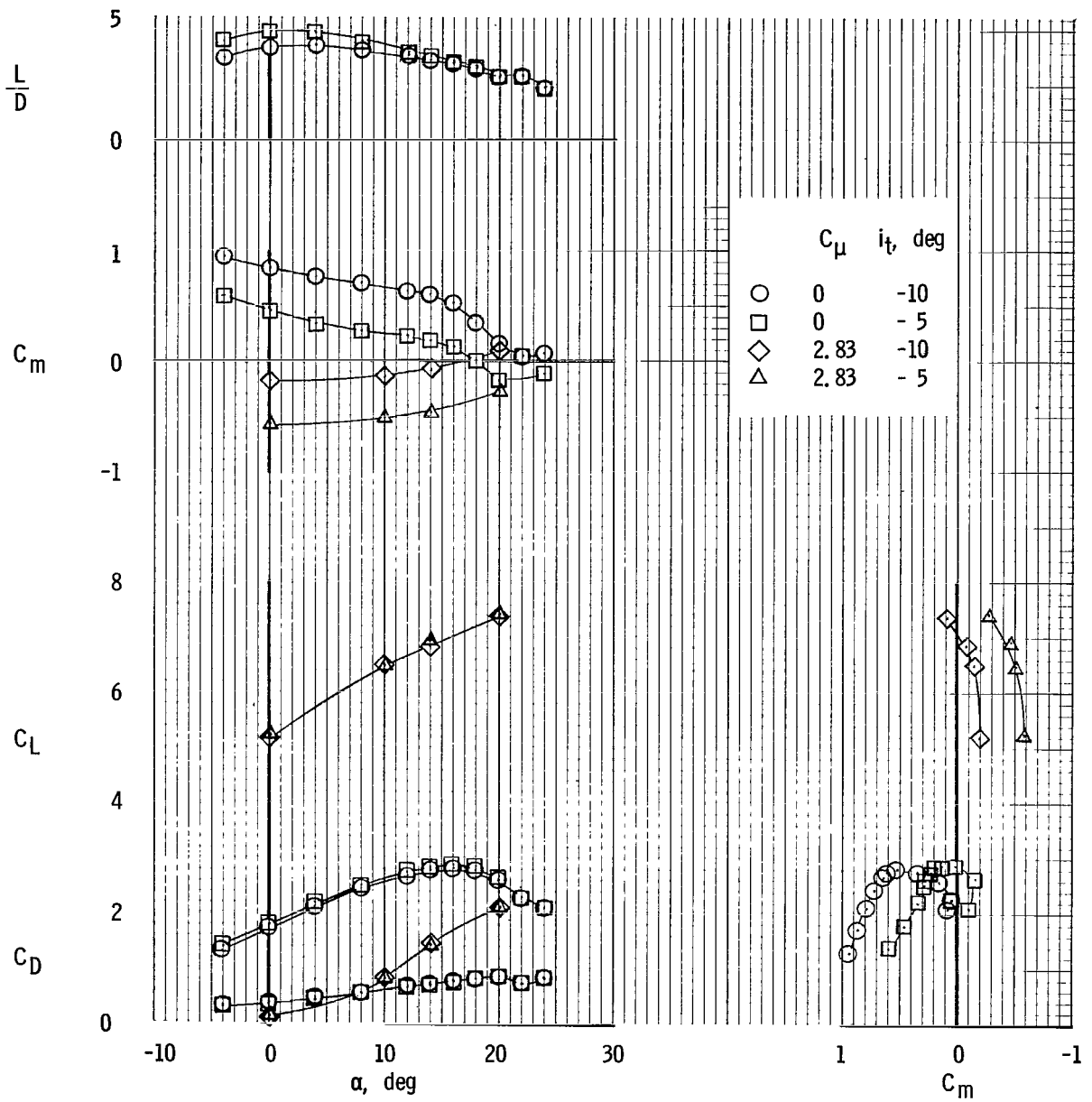


Figure 23.- Effect of symmetric inboard-spoiler deflection on longitudinal characteristics. Landing flap setting LDG; spoiler deflection,  $60^\circ$ ; tail on.



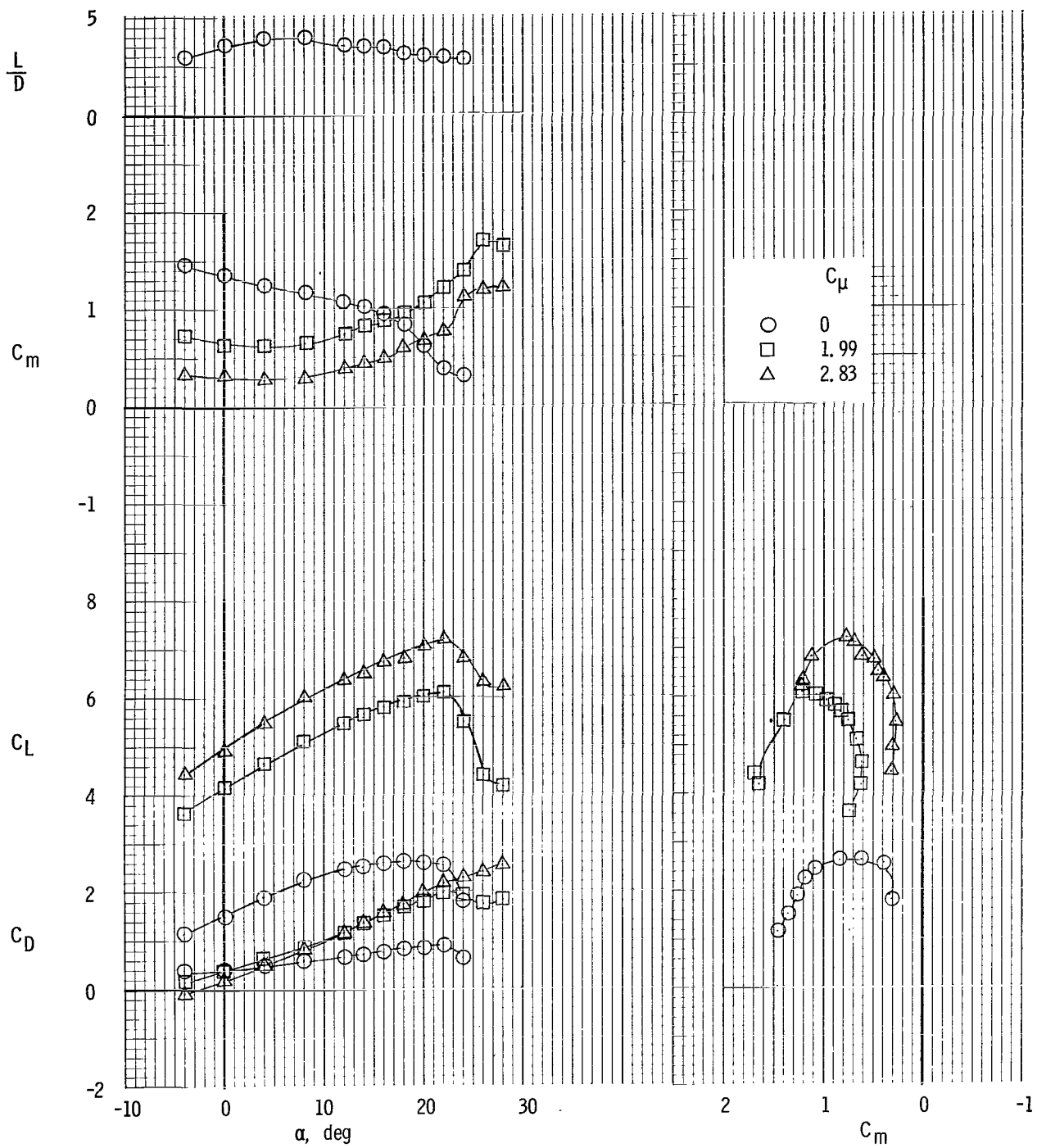
(a) Horizontal-tail incidence,  $10^\circ$ .

Figure 24.- Effect of varying tail incidence on longitudinal characteristics. Landing flap setting LDG.



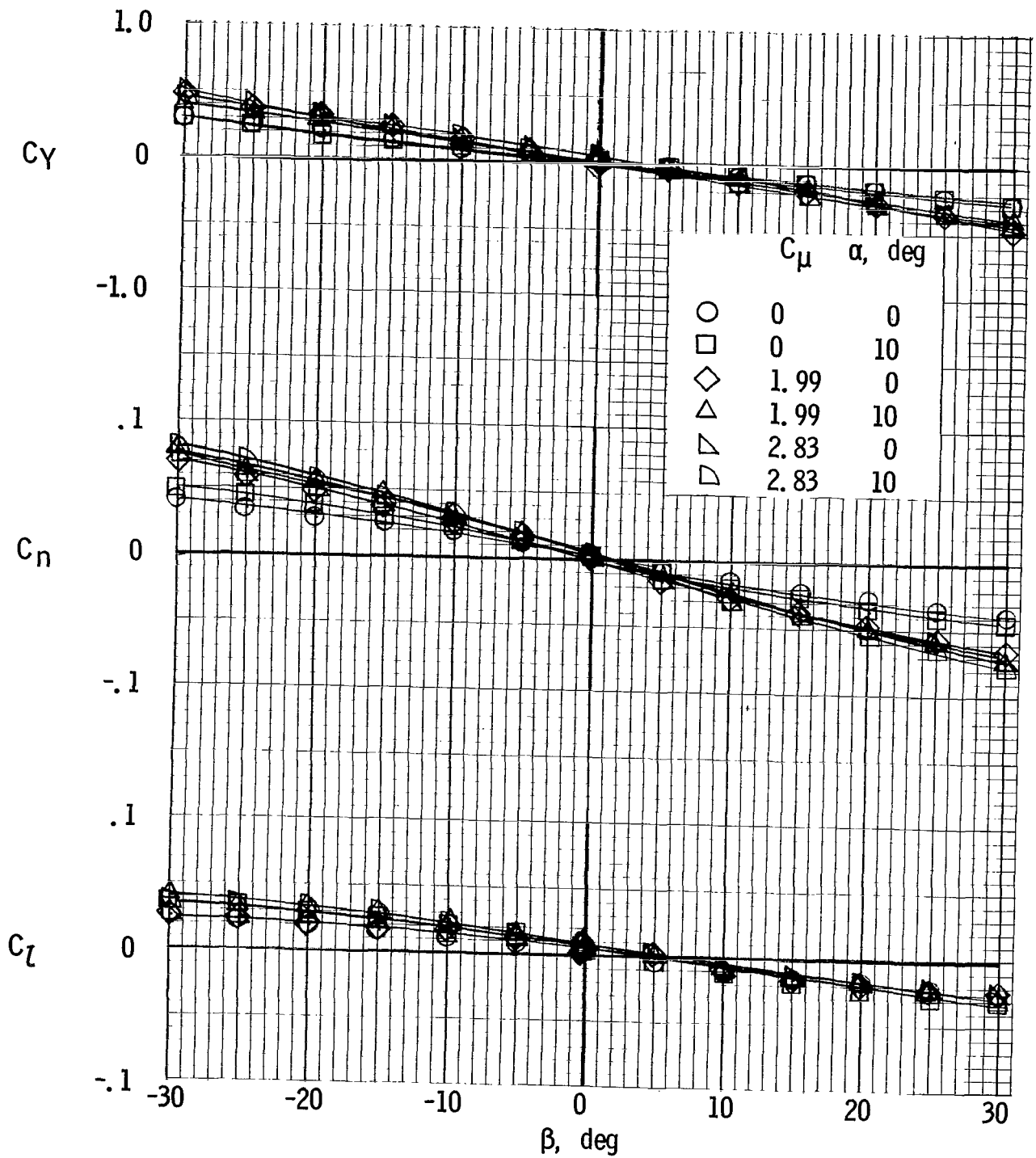
(b) Horizontal-tail incidence,  $-5^\circ$ ,  $-10^\circ$ .

Figure 24.- Continued.



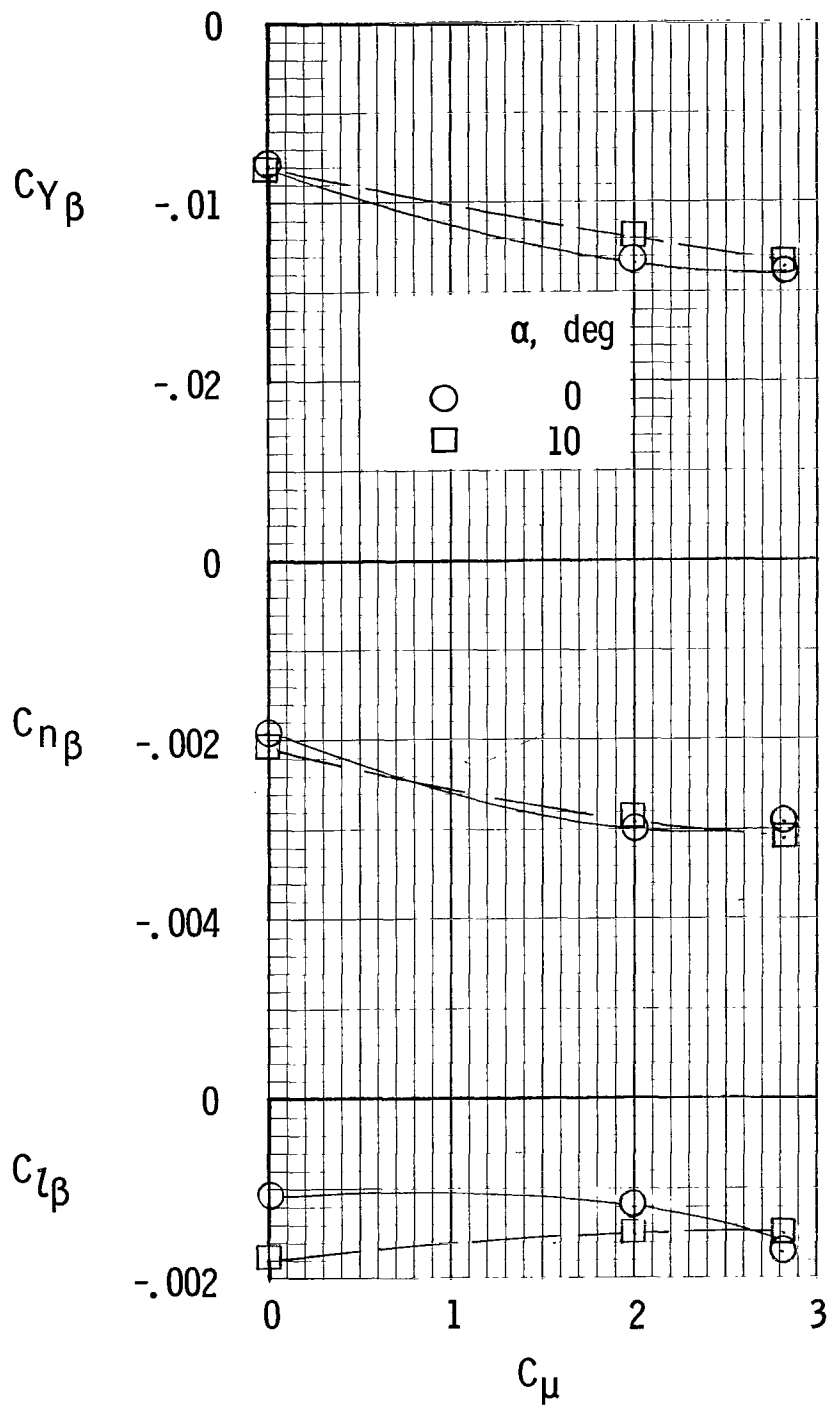
(c) Horizontal-tail incidence,  $-15^\circ$ .

Figure 24.- Concluded.



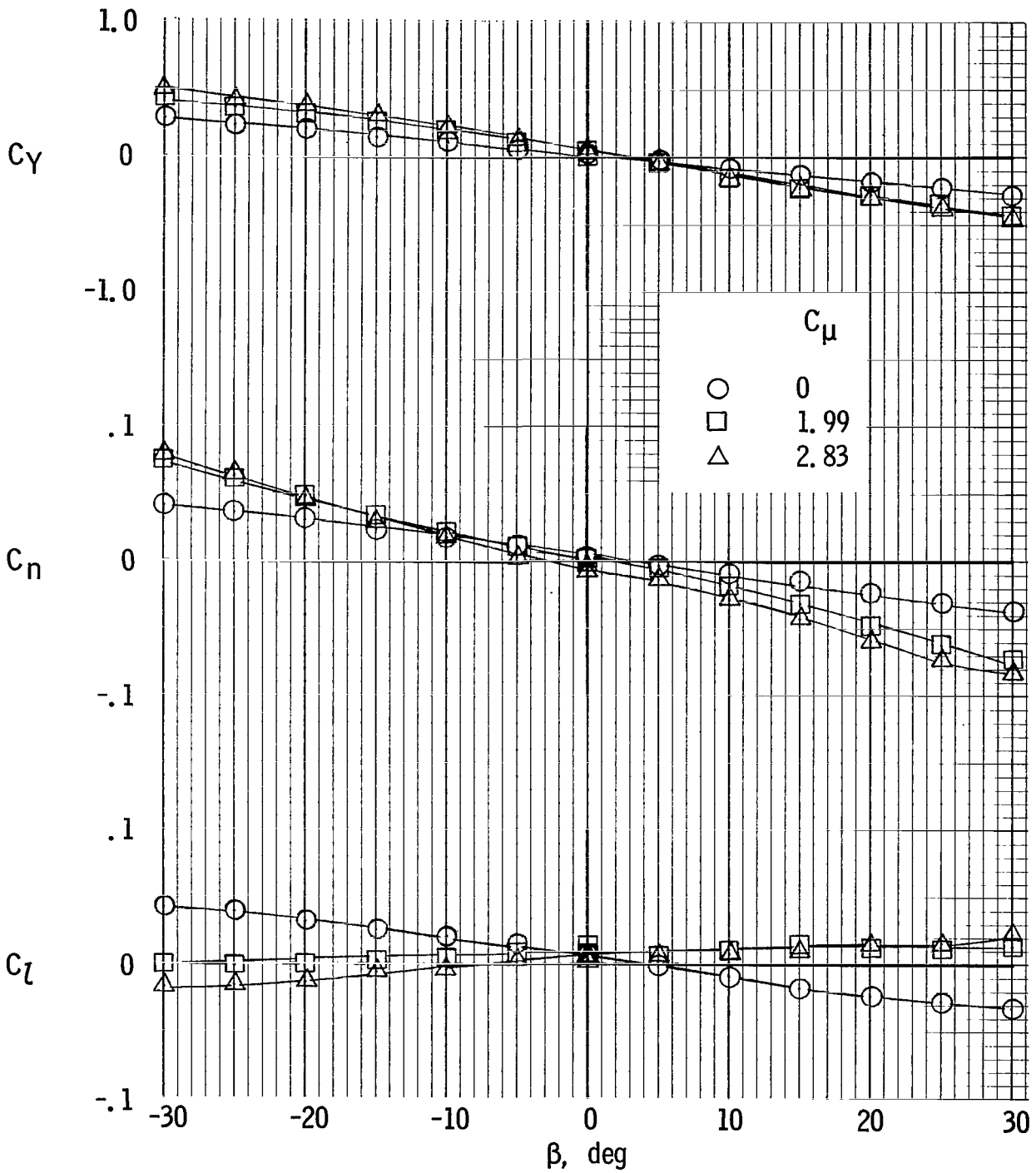
(a) Basic data.

Figure 25.- Tail-off lateral characteristics for cruise flap setting CR.



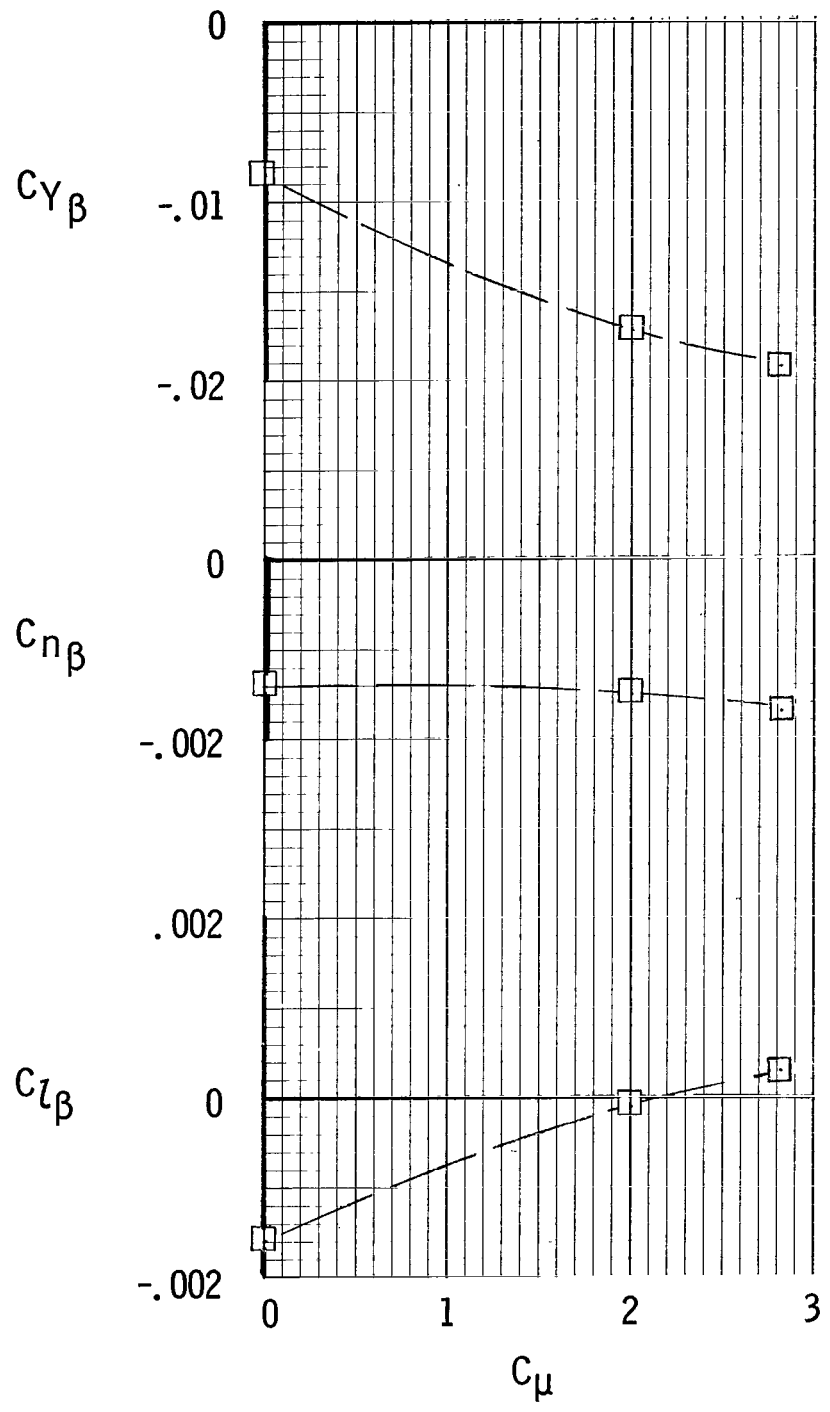
(b) Static stability derivatives.

Figure 25.- Concluded.



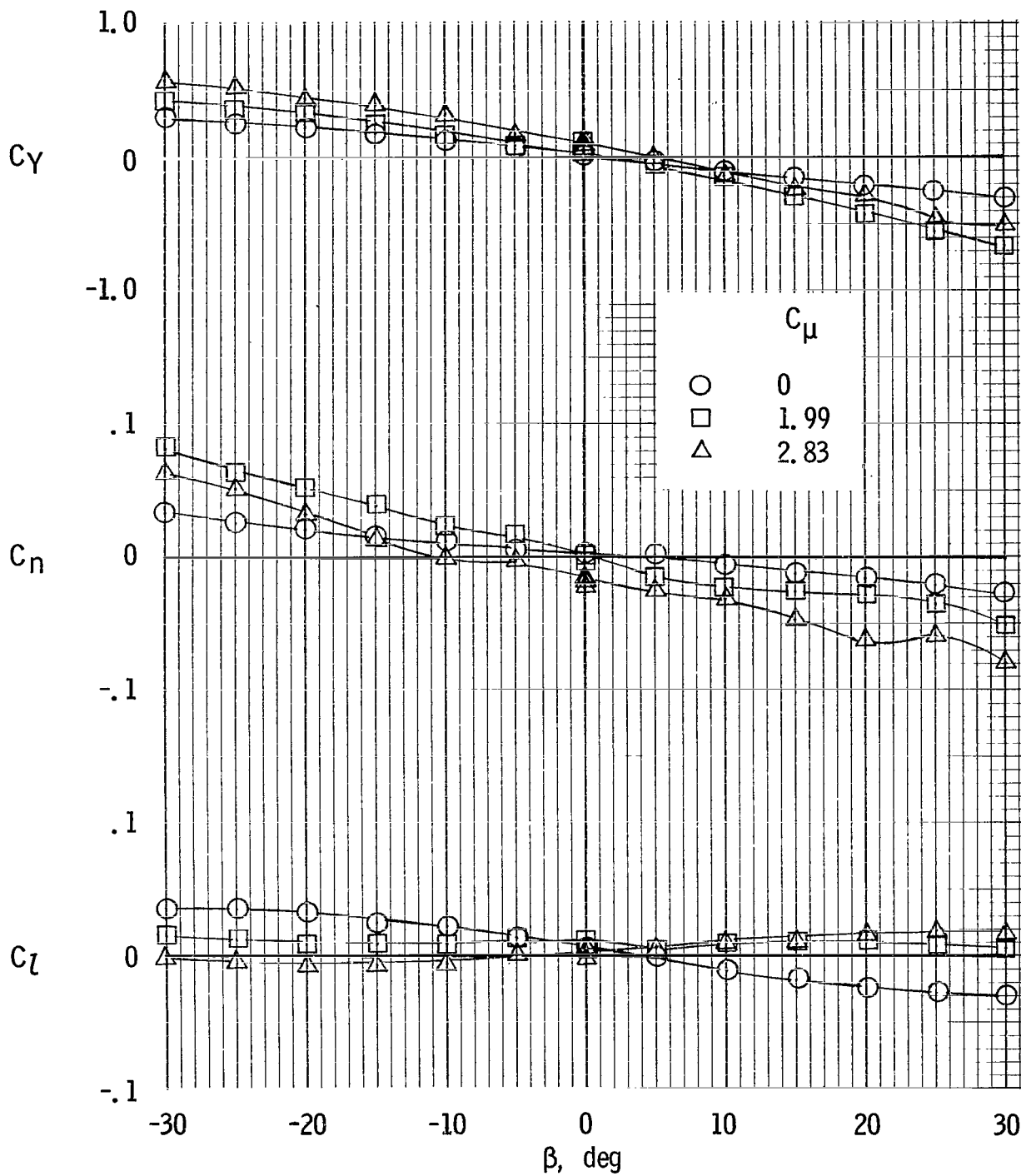
(a) Basic data.

Figure 26.- Tail-off lateral characteristics for take-off flap setting T0.  $\alpha = 10^\circ$ .



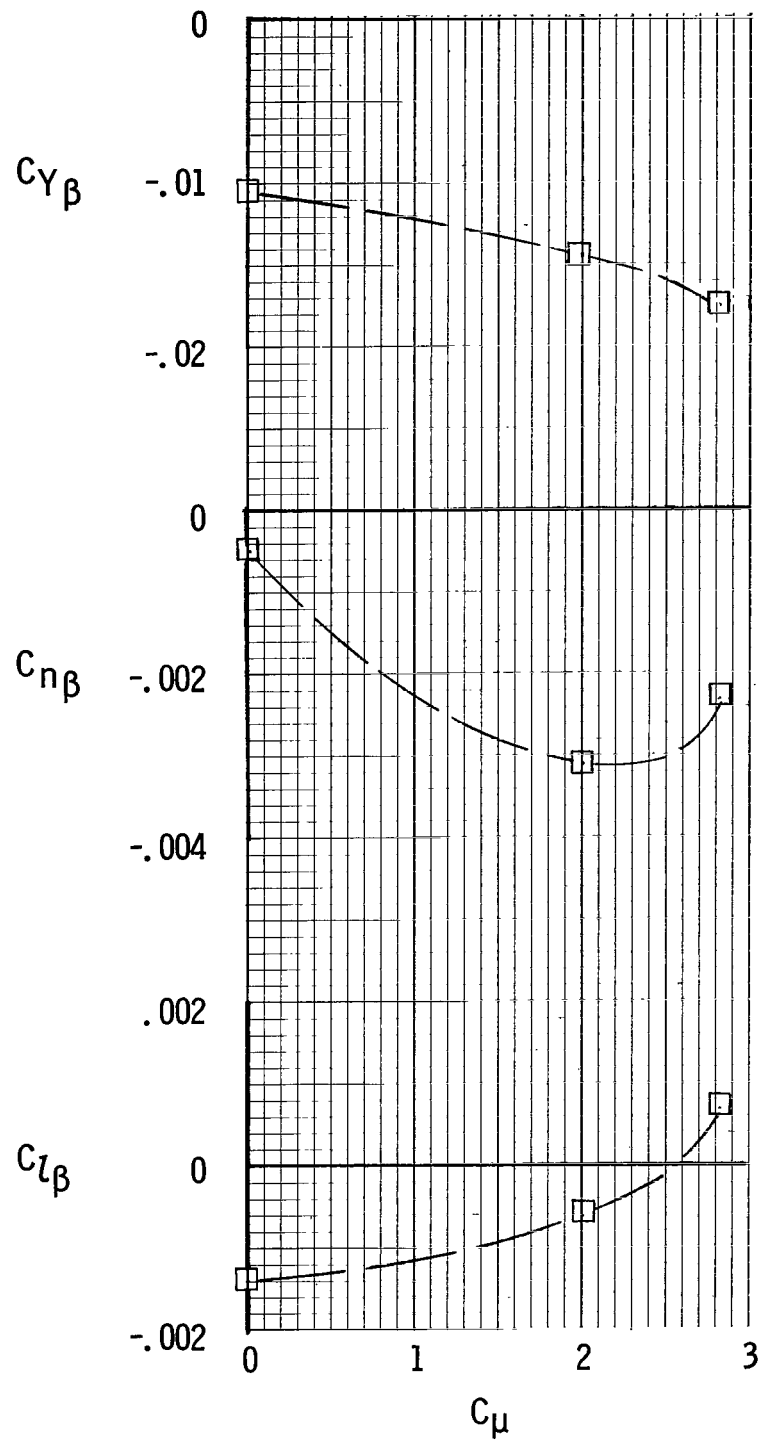
(b) Static stability derivatives.

Figure 26.- Concluded.



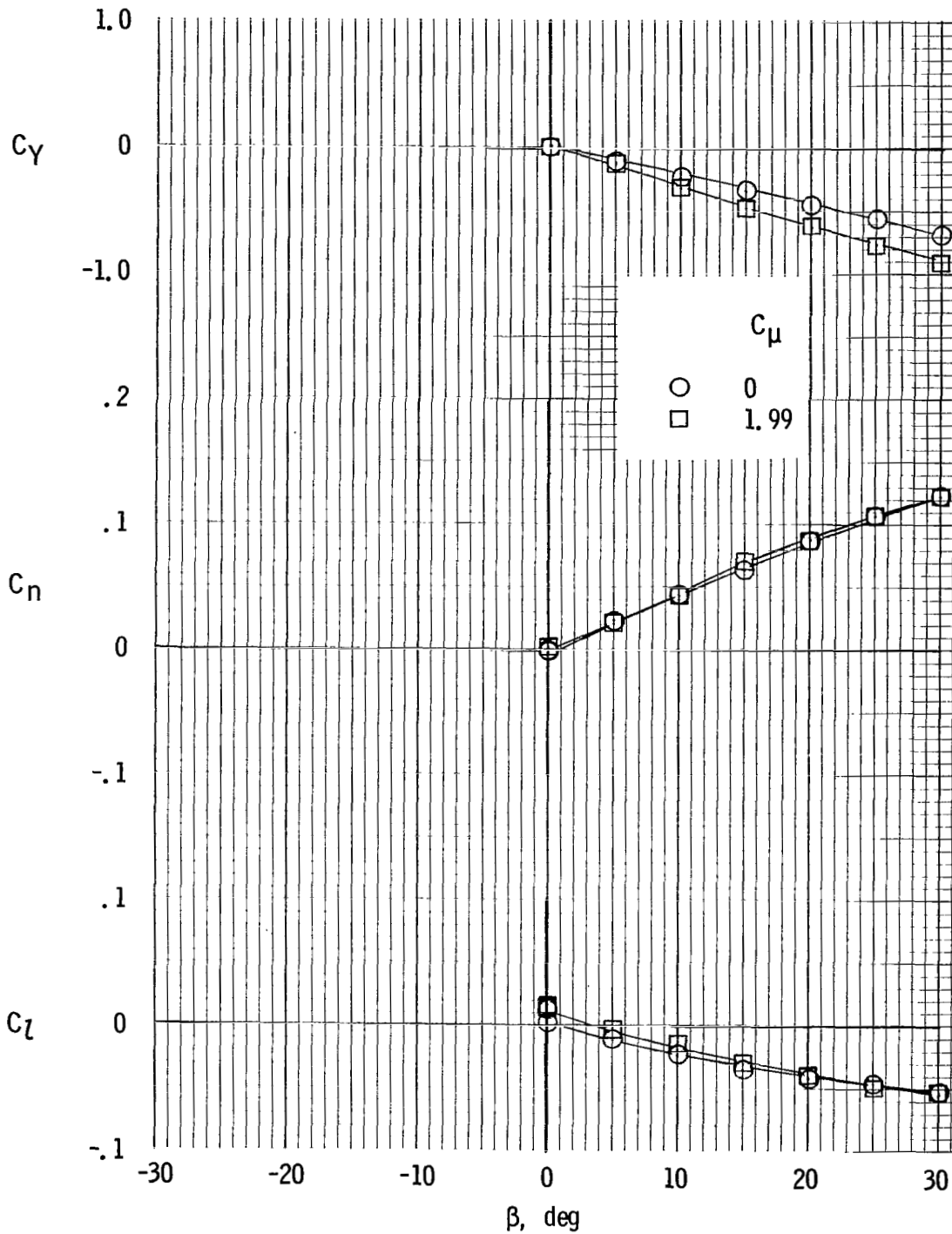
(a) Basic data.

Figure 27.- Tail-off lateral characteristics for landing flap setting LDG.  $\alpha = 10^\circ$ .



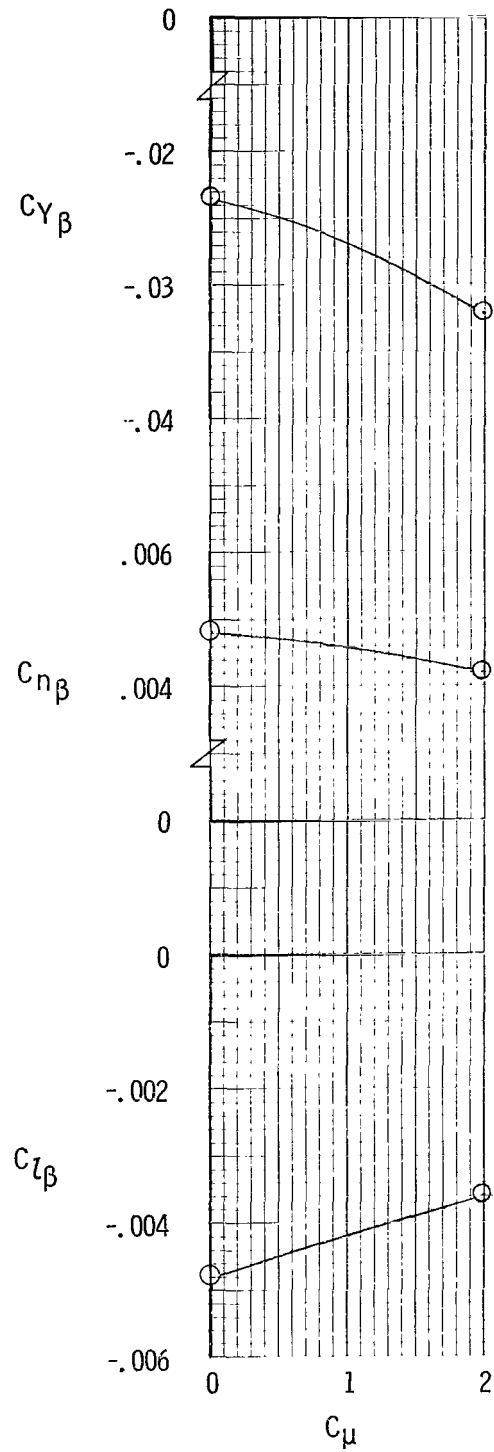
(b) Static stability derivatives.

Figure 27.- Concluded.



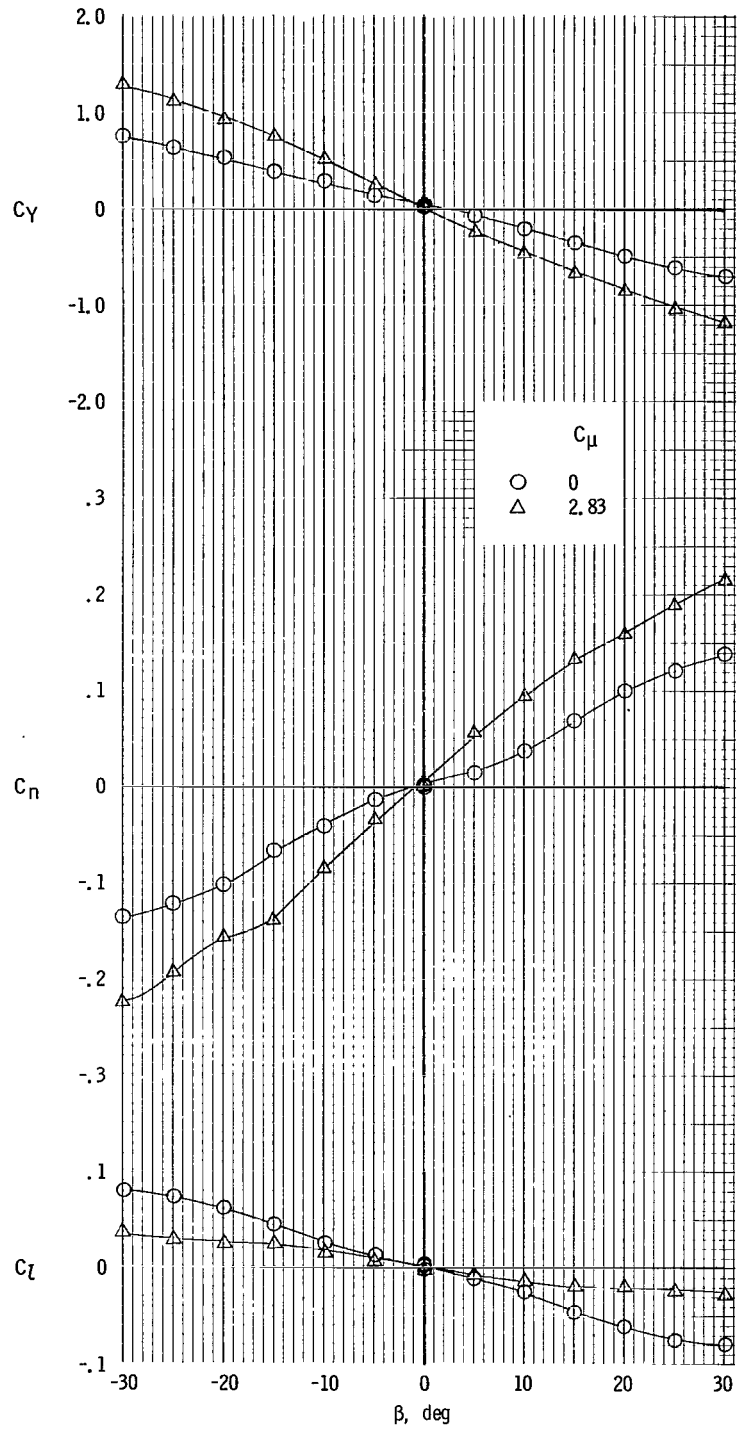
(a) Basic data.

Figure 28.- Tail-on lateral characteristics for cruise flap setting CR.  $\alpha = 0^\circ$ .



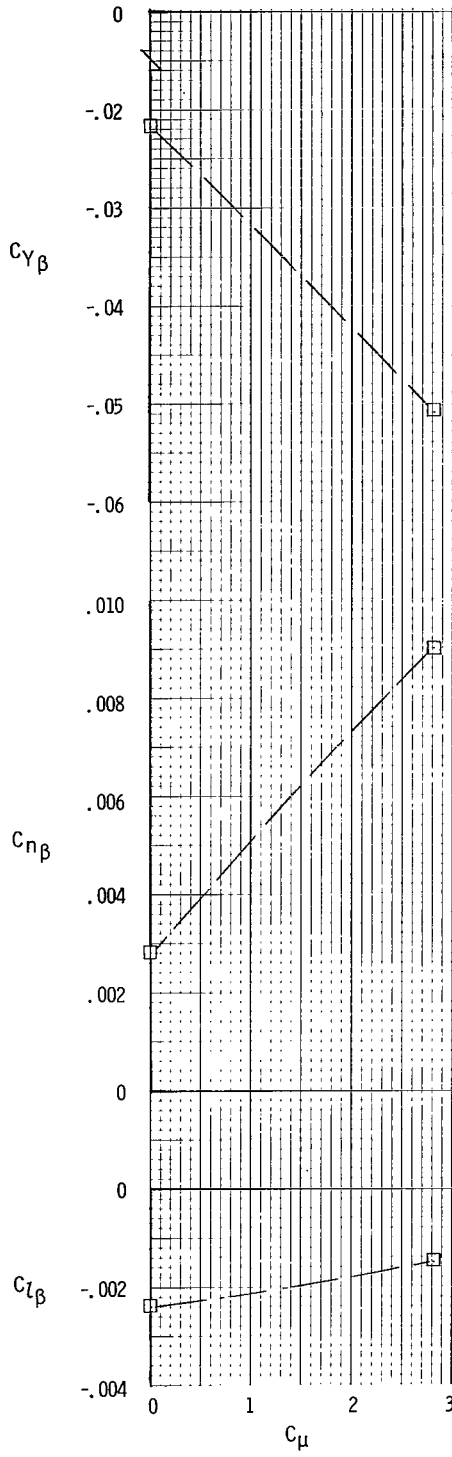
(b) Static stability derivatives.

Figure 28.- Concluded.



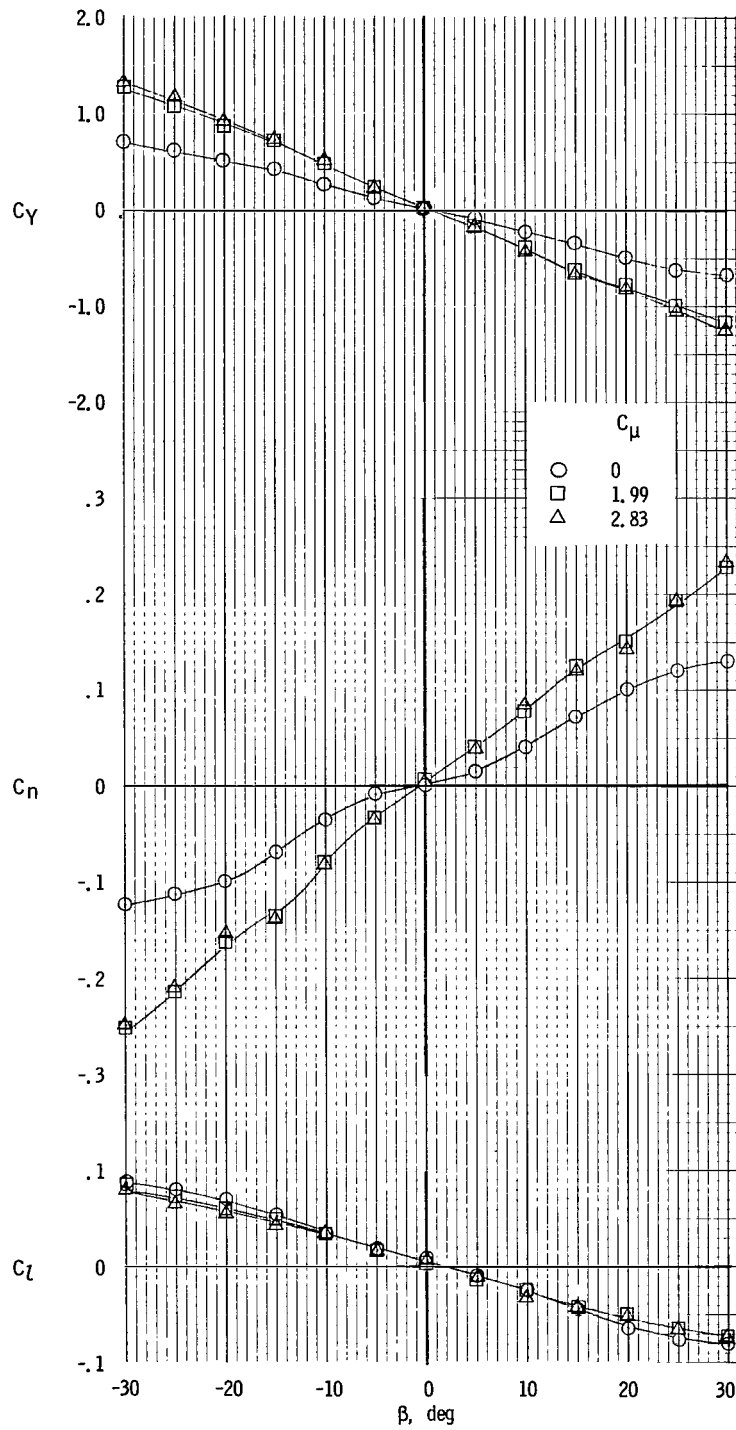
(a) Basic data.

Figure 29.- Tail-on lateral characteristics for take-off flap setting T0.  $\alpha = 10^\circ$ .



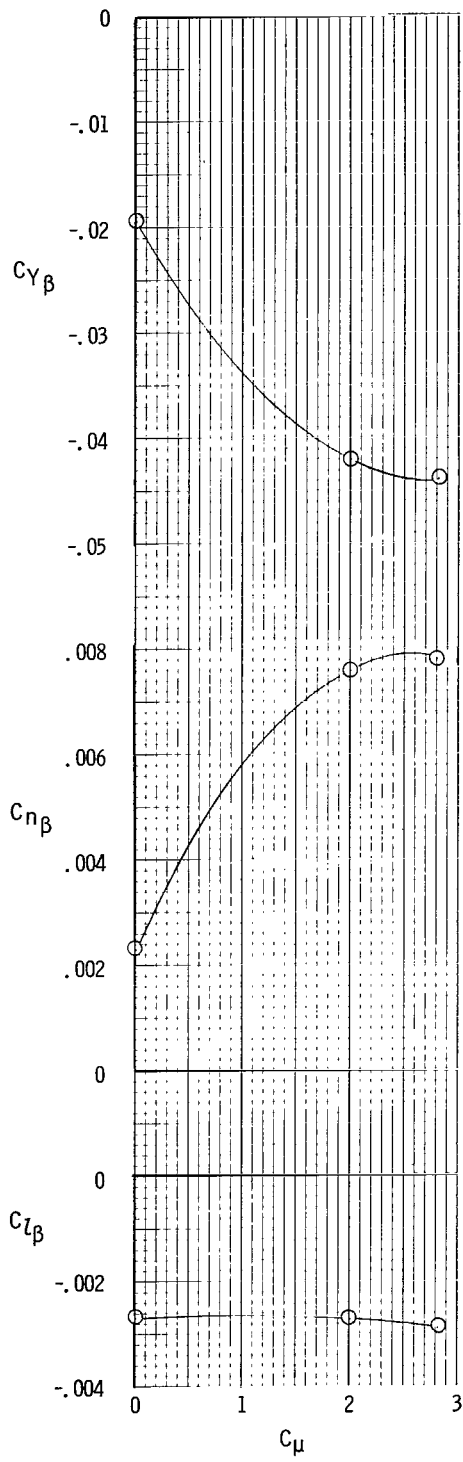
(b) Static stability derivatives.

Figure 29.- Concluded.



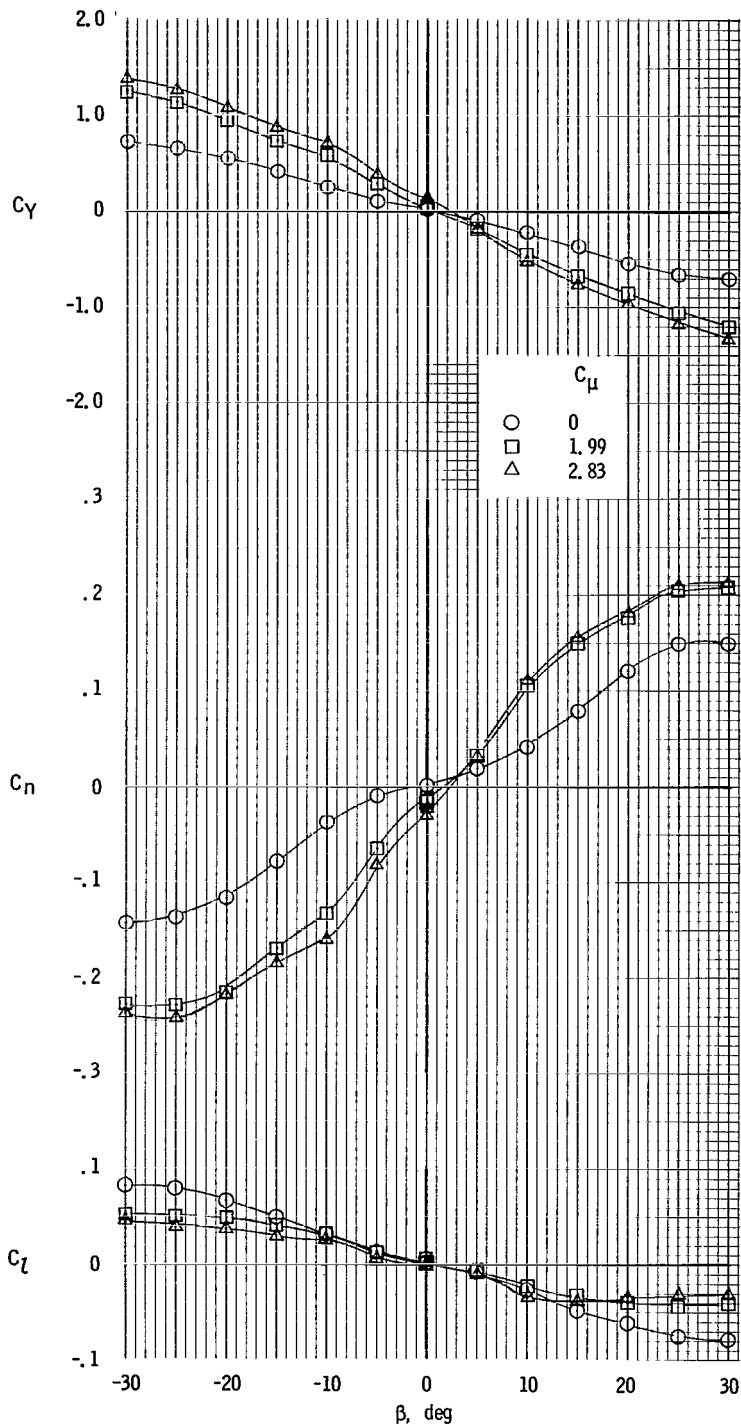
(a) Basic data.

Figure 30.- Tail-on lateral characteristics for an alternate take-off flap setting ATO2.  $\alpha = 10^\circ$ .



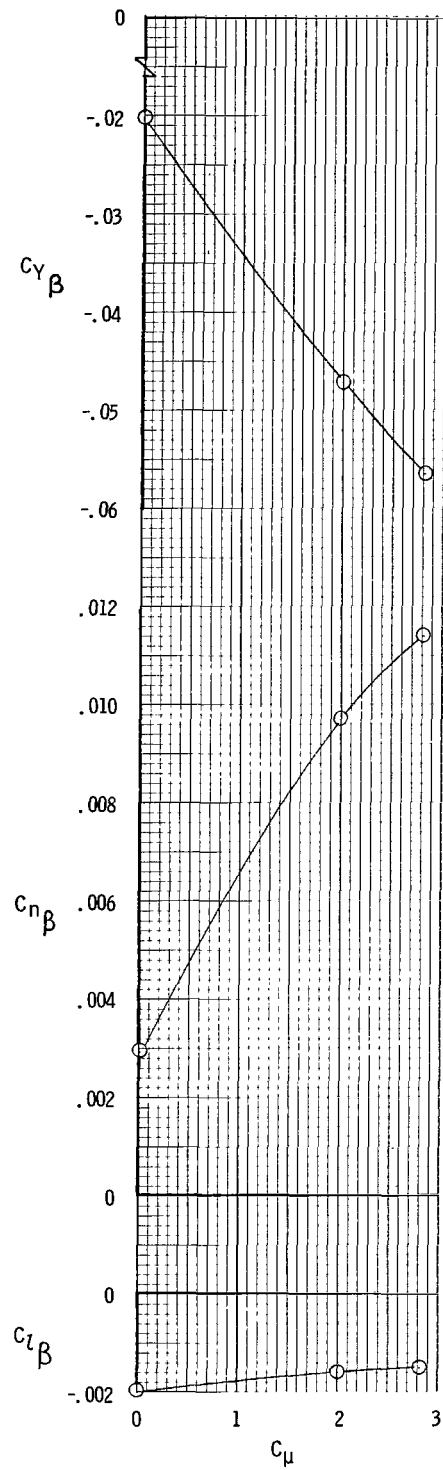
(b) Static stability derivatives.

Figure 30.- Concluded.



(a) Basic data.

Figure 31.- Tail-on lateral characteristics for landing flap setting LDC.  $\alpha = 10^\circ$ ;  $i_t = -10^\circ$ .



(b) Static stability derivatives.

Figure 3L.- Concluded.

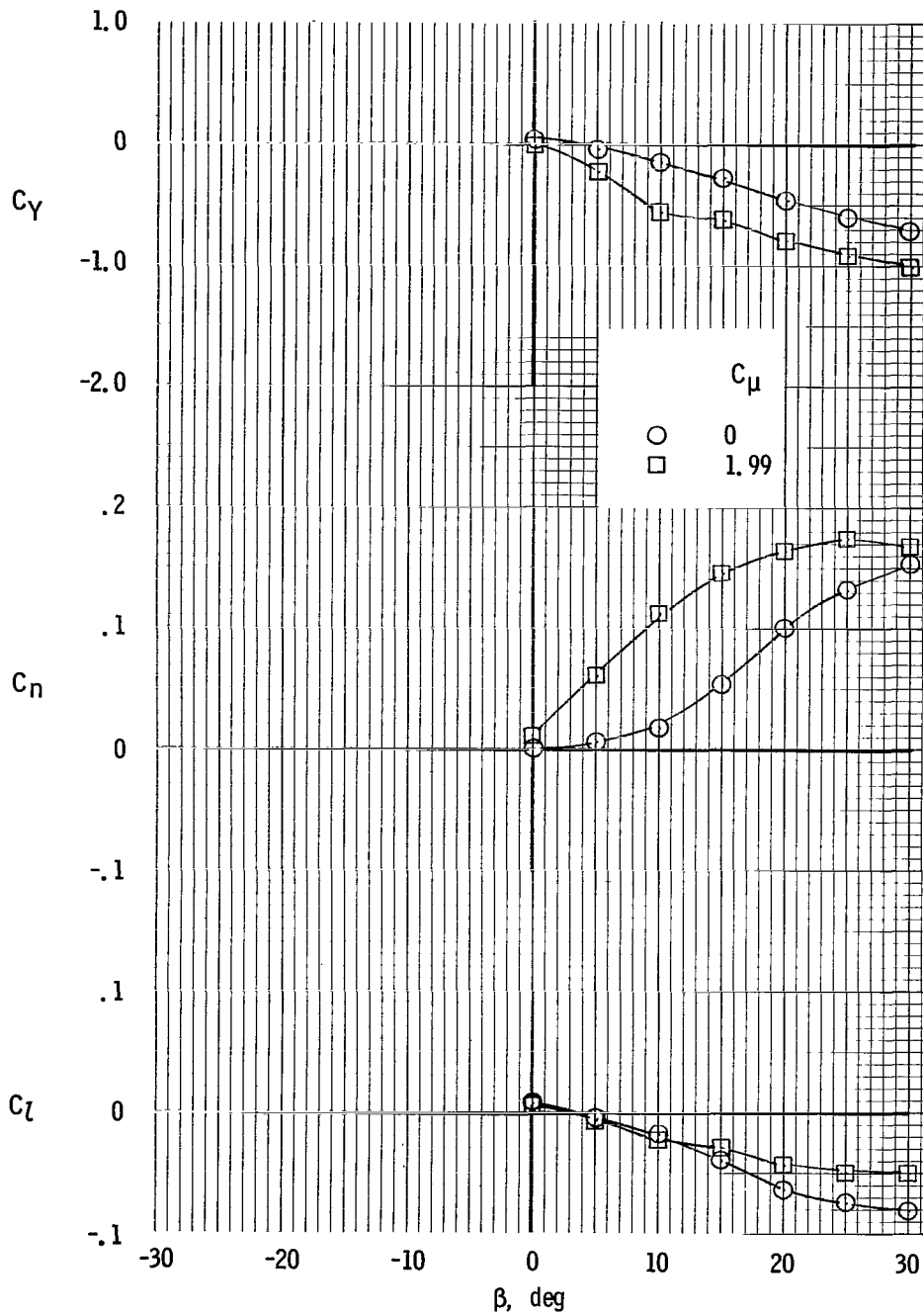
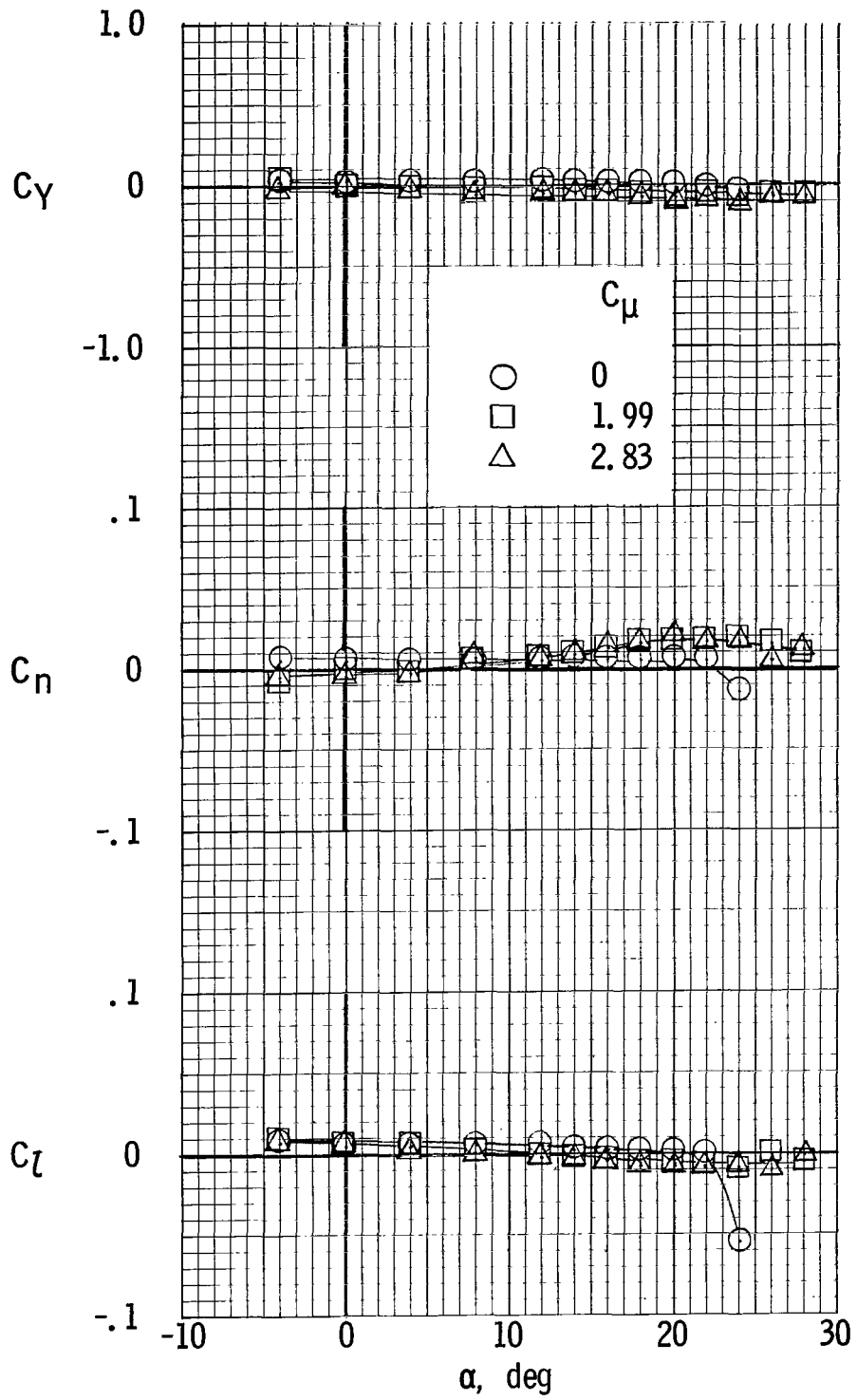
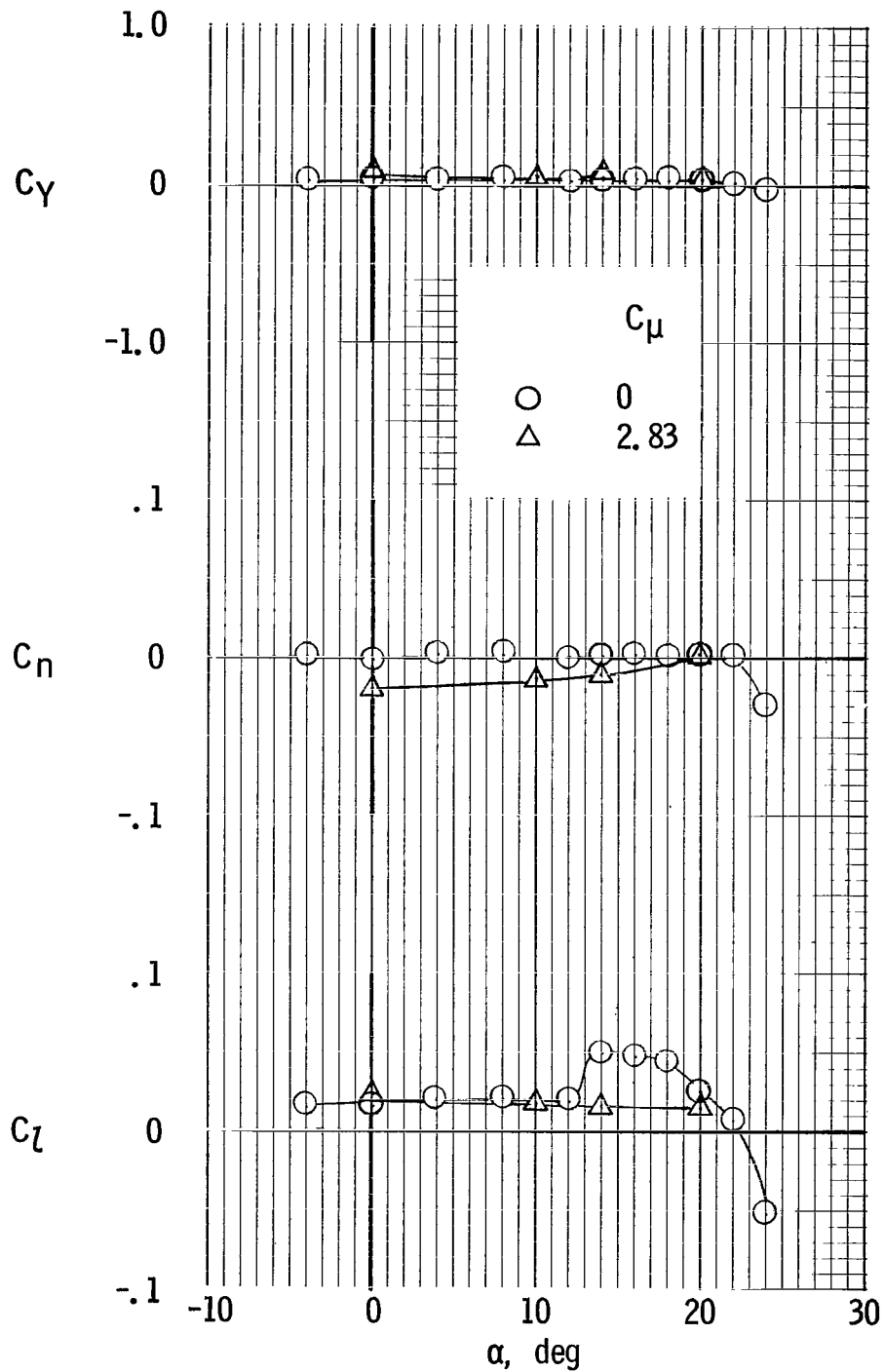


Figure 32.- Lateral characteristics with inboard spoilers deflected. Landing flap setting LDG. Spoiler deflection,  $60^\circ$ ;  $\alpha = 10^\circ$ ;  $i_t = 0^\circ$ ; tail on.



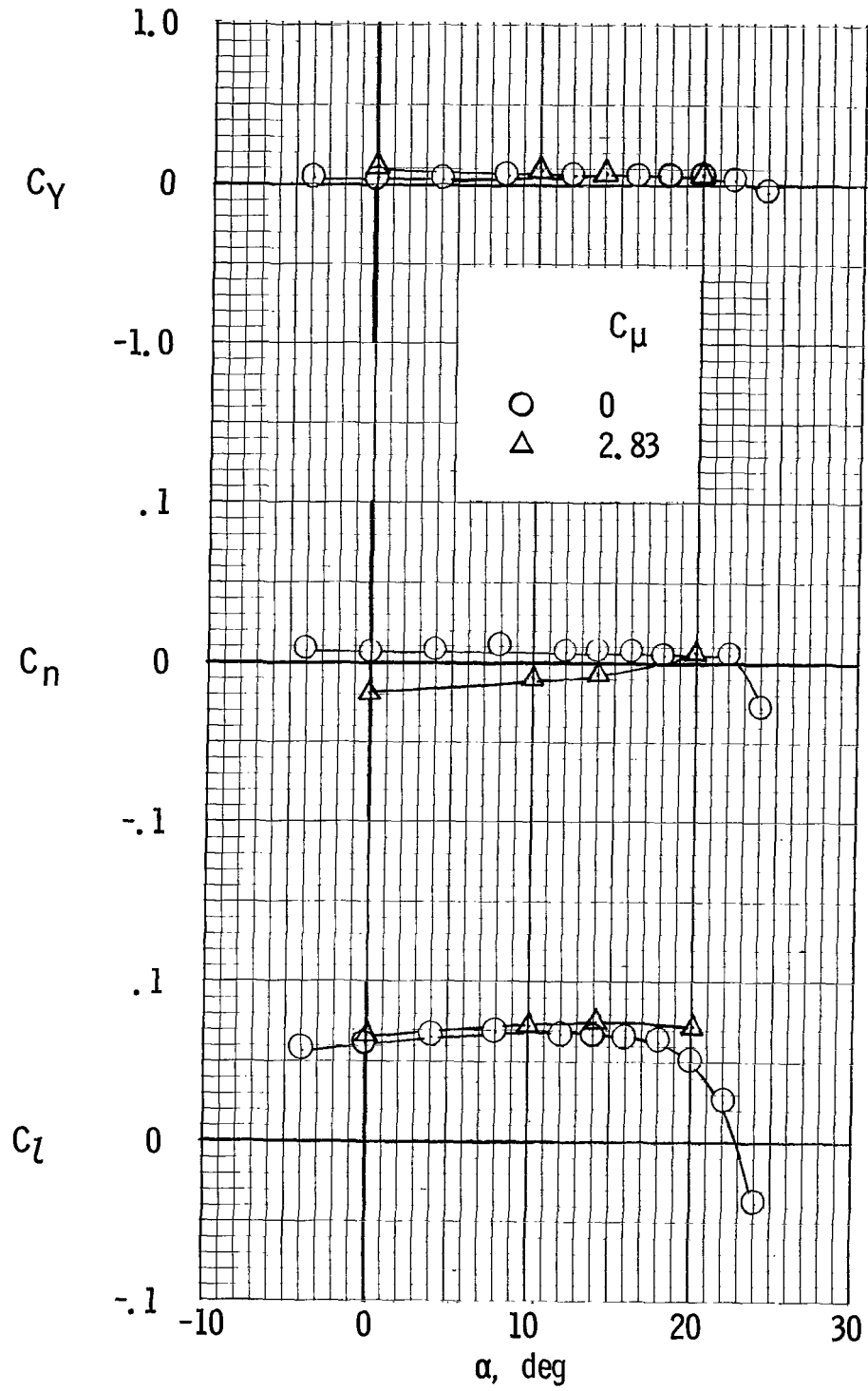
(a) Inboard-spoiler deflection,  $10^\circ$ .

Figure 33.- Lateral characteristics with right spoilers deflected. Take-off flap setting T0.



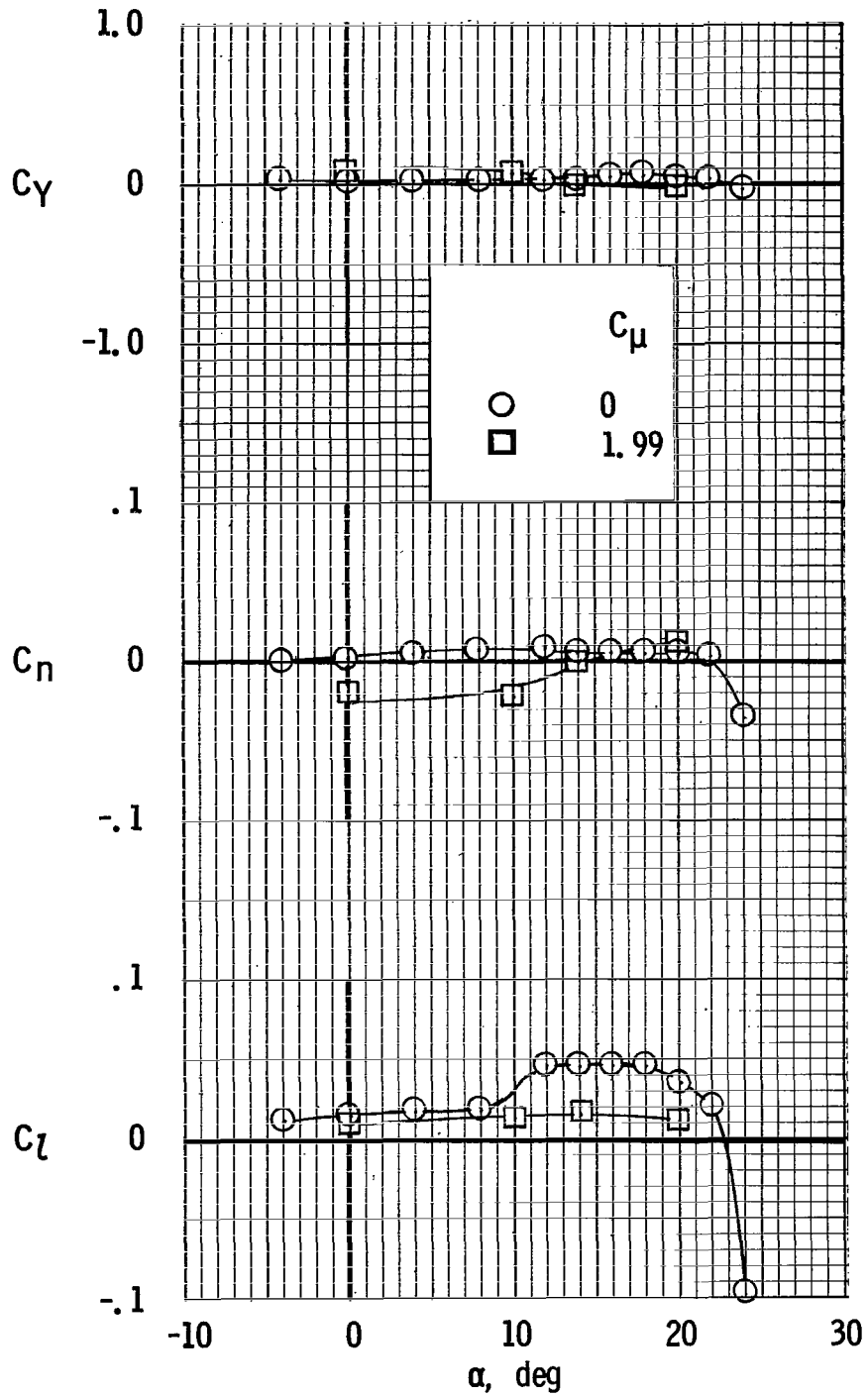
(b) Outboard-spoiler deflection,  $10^\circ$ .

Figure 33.- Continued.



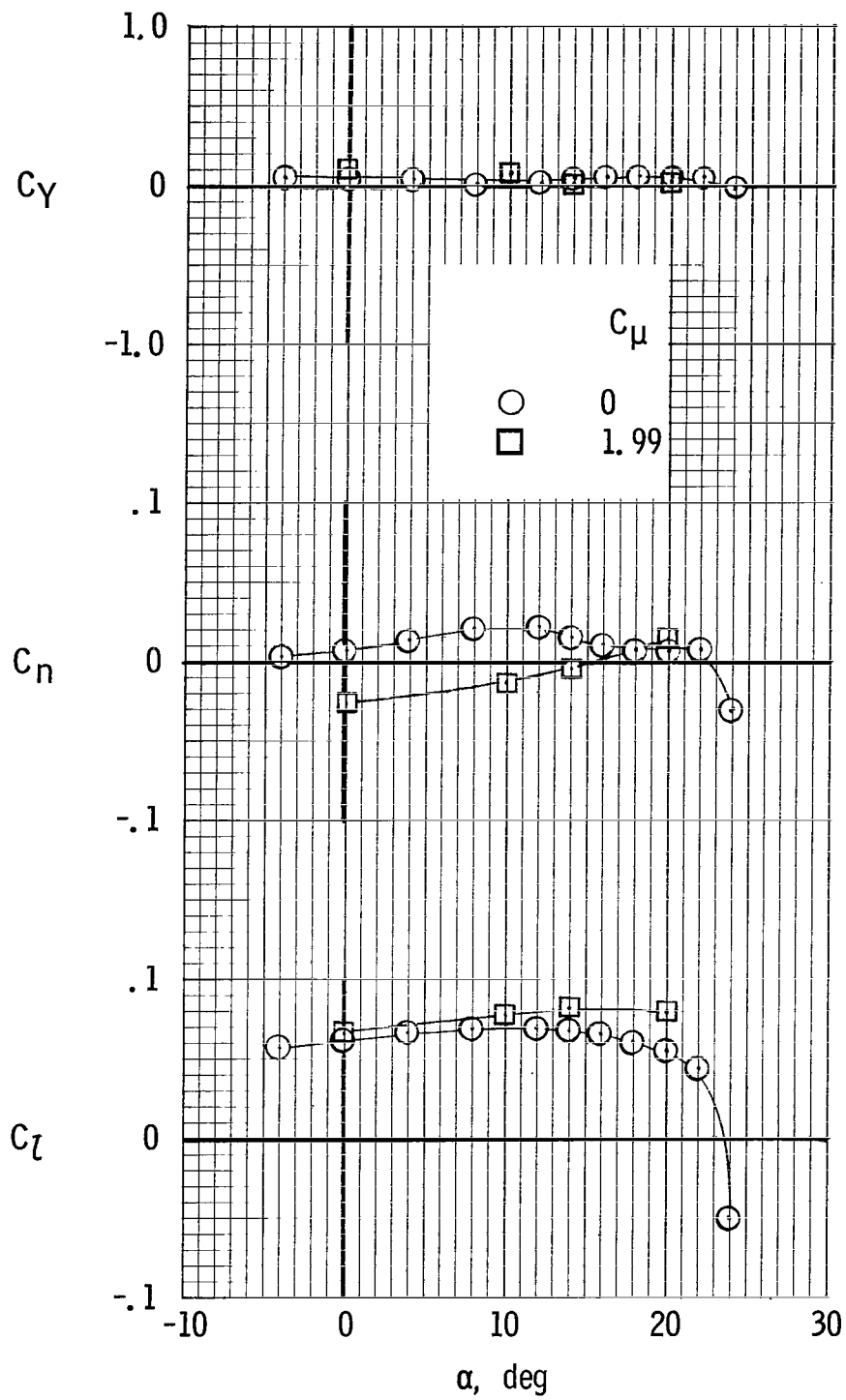
(c) Outboard-spoiler deflection, 30°.

Figure 33.- Concluded.



(a) Outboard-spoiler deflection,  $10^\circ$ .

Figure 34.- Lateral characteristics with right spoiler deflected. Landing flap setting LDG; tail on.



(b) Outboard-spoiler deflection, 30°.

Figure 34.- Concluded.

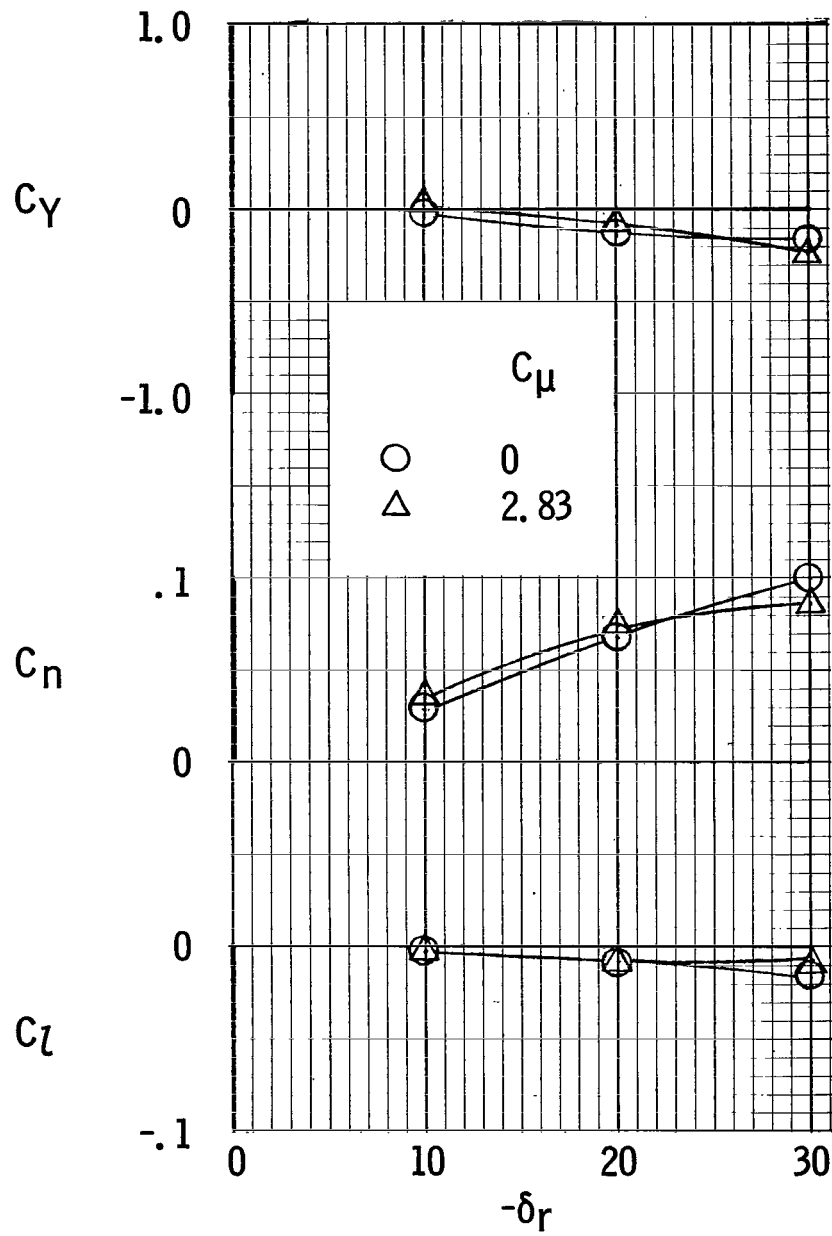
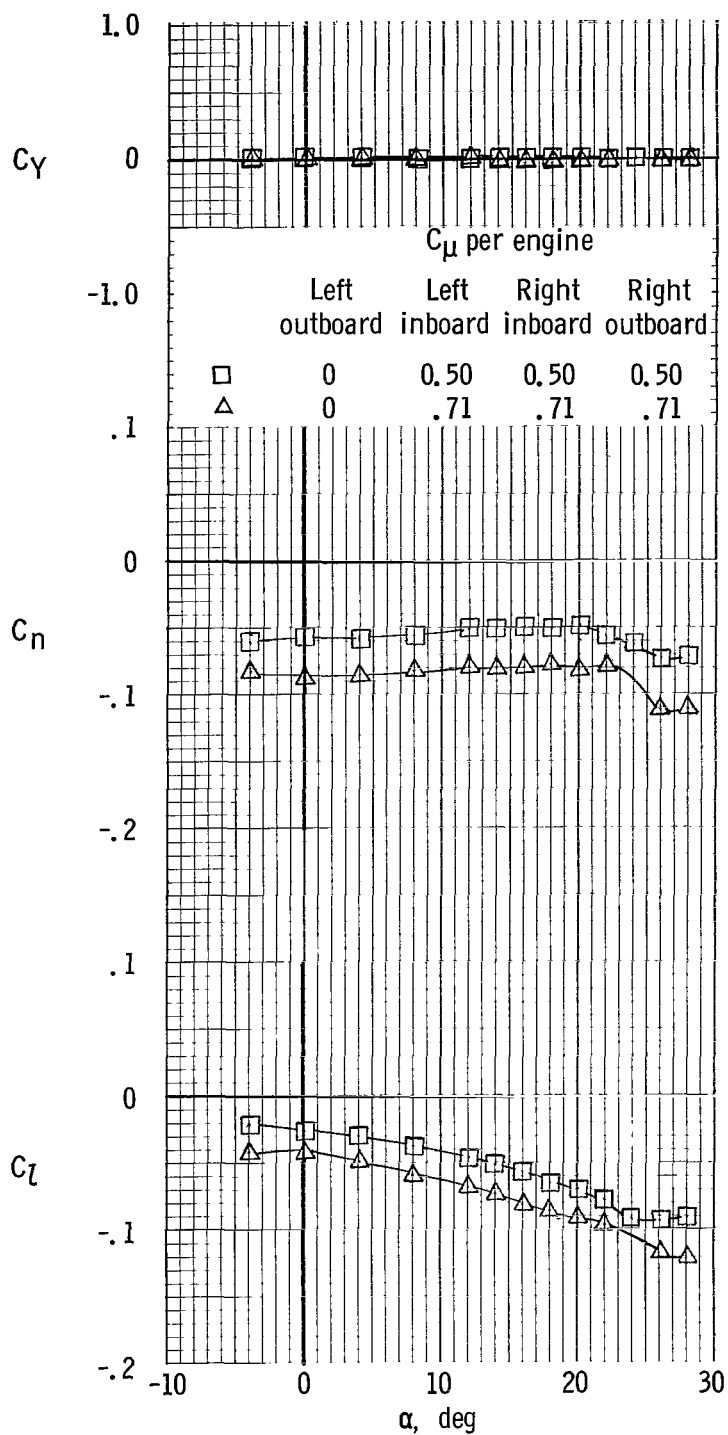
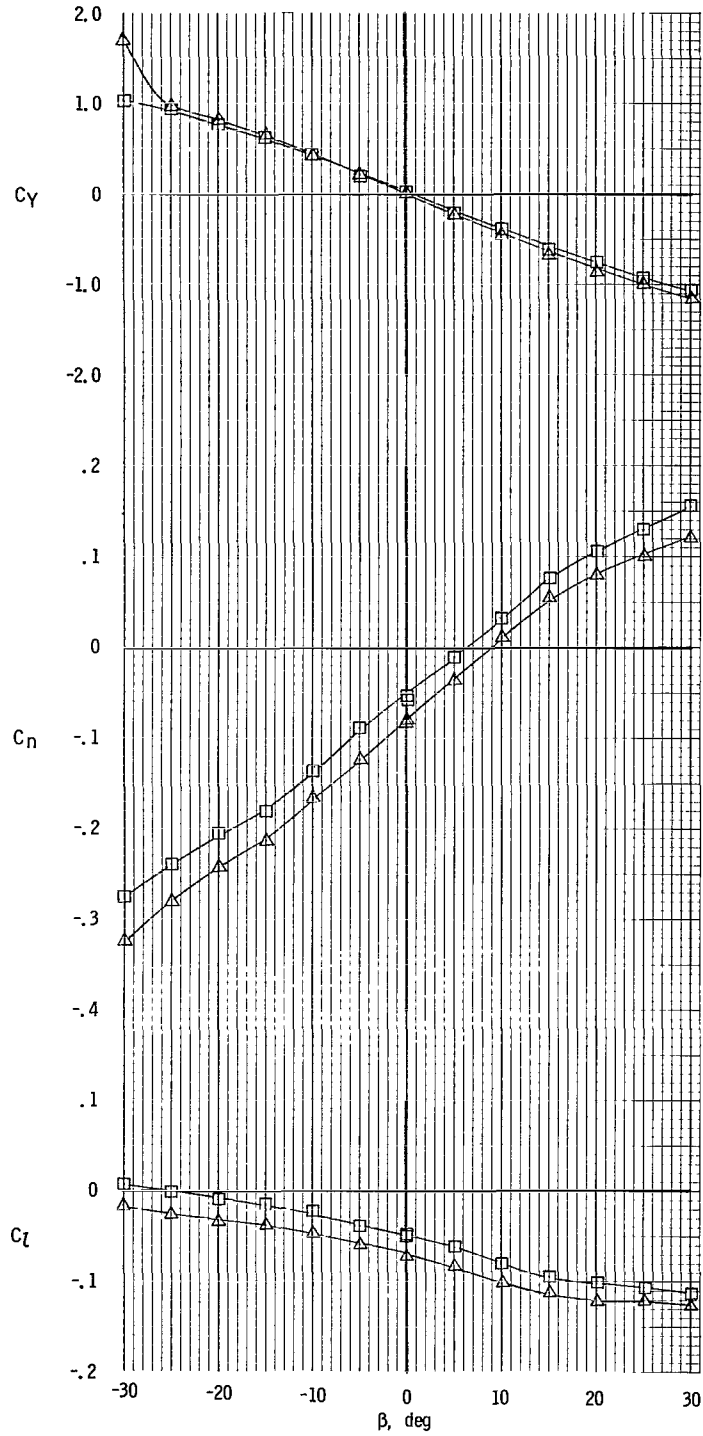


Figure 35.- Rudder effectiveness, take-off flap setting T0;  $\alpha = 10^\circ$ .



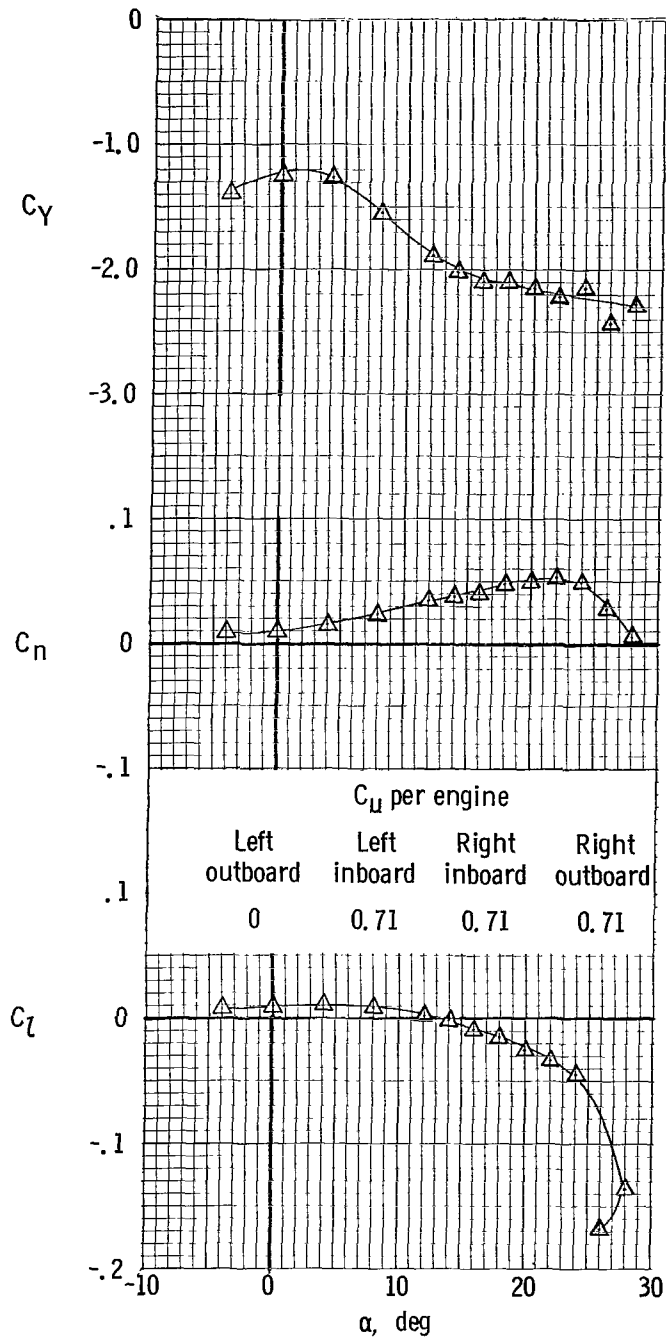
(a) Effect of varying angle of attack.

Figure 36.- Lateral characteristics with left outboard engine not operating. Take-off flap setting T0; tail on.



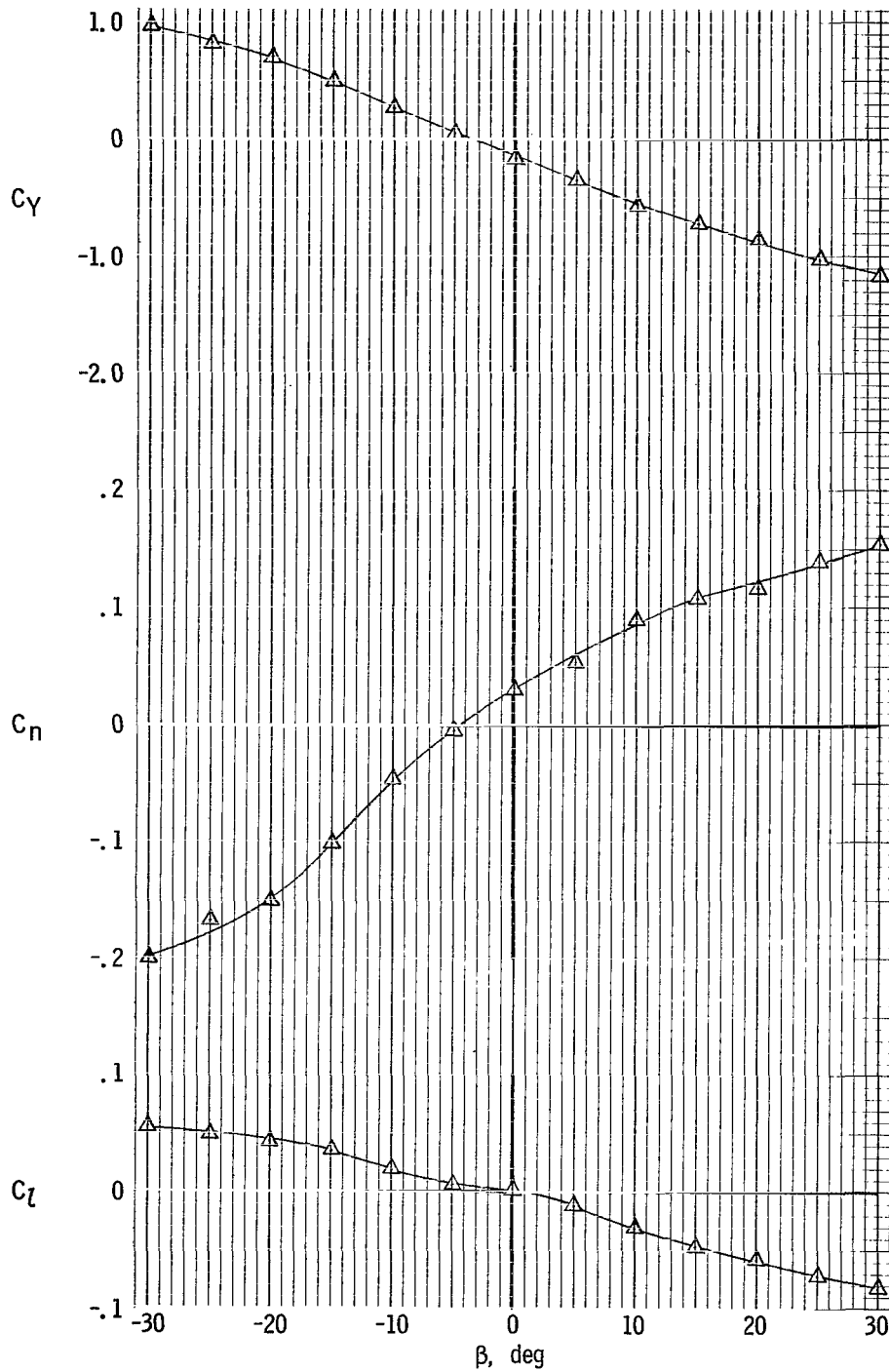
(b) Effect of varying angle of sideslip;  $\alpha = 10^\circ$ .

Figure 36.- Concluded.



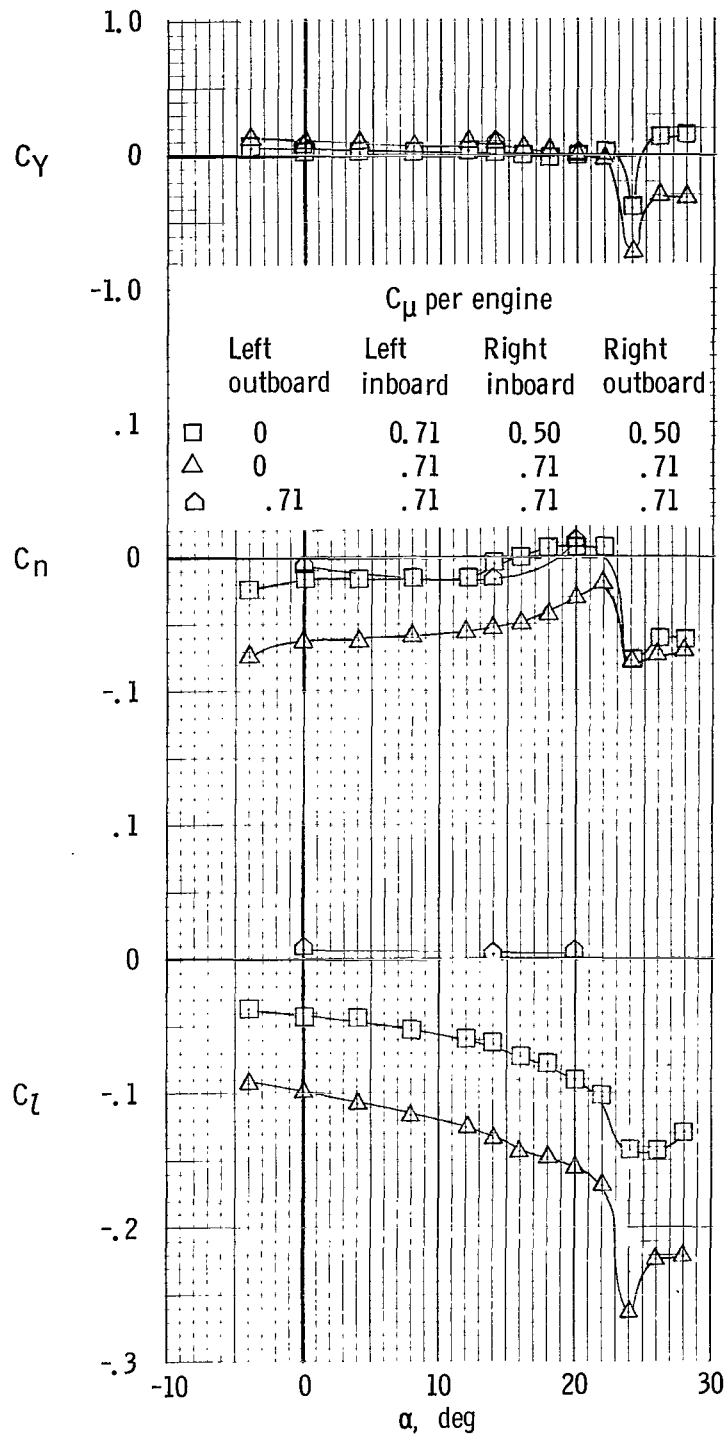
(a) Variation with angle of attack.

Figure 37.- Lateral characteristics with left outboard engine not operating. Take-off flap setting T0; aileron deflection,  $20^\circ$  (each); spoiler deflection (right outboard),  $30^\circ$ ; rudder deflection,  $-30^\circ$ .



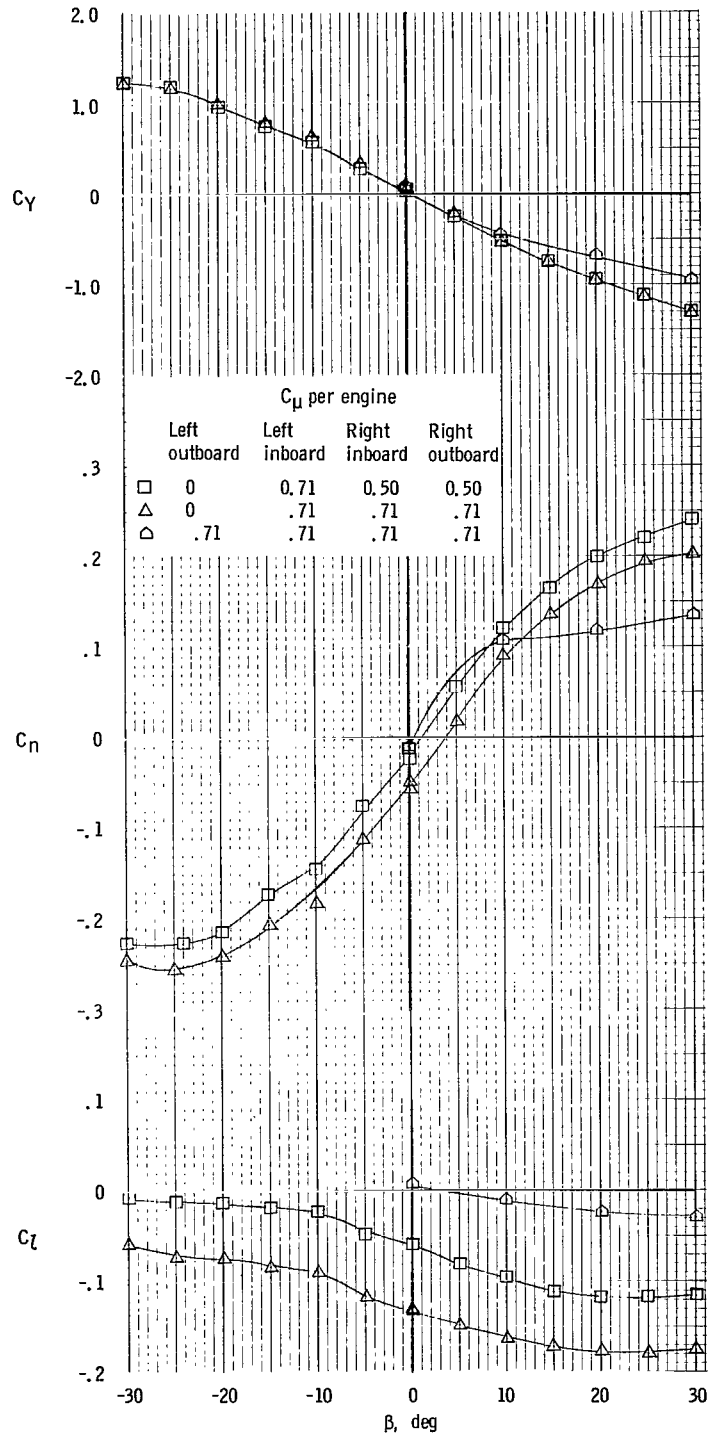
(b) Variation with angle of sideslip;  $\alpha = 10^\circ$ .

Figure 37.- Concluded.



(a) Variation with angle of attack.

Figure 38.- Lateral characteristics with left outboard engine not operating. Landing flap setting LDG.



(b) Variation with angle of sideslip,  $\alpha = 10^\circ$ .

Figure 38.- Concluded.

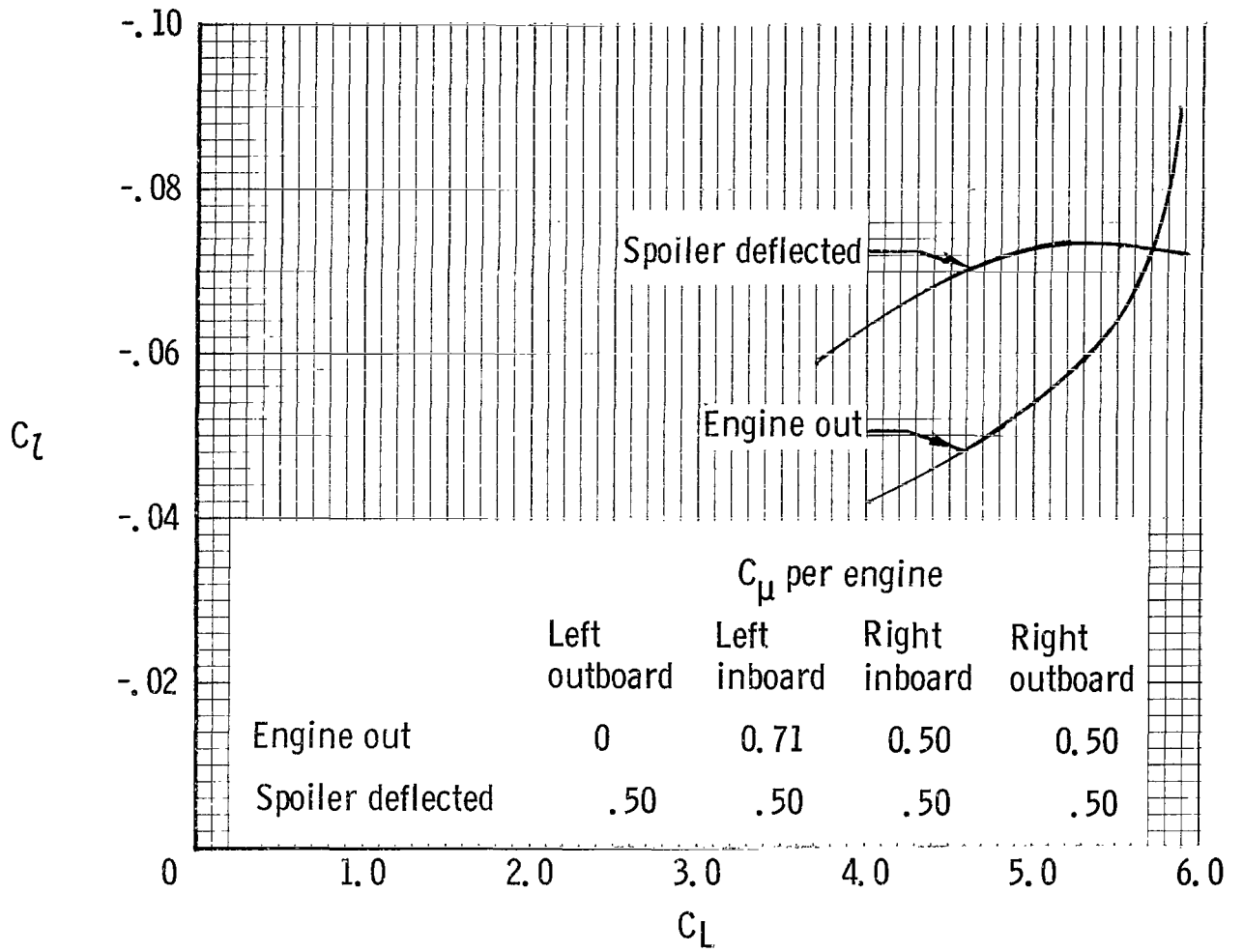


Figure 39.- Rolling moment trim capability of outboard spoiler, one outboard engine not operating. Landing flap setting LDG.

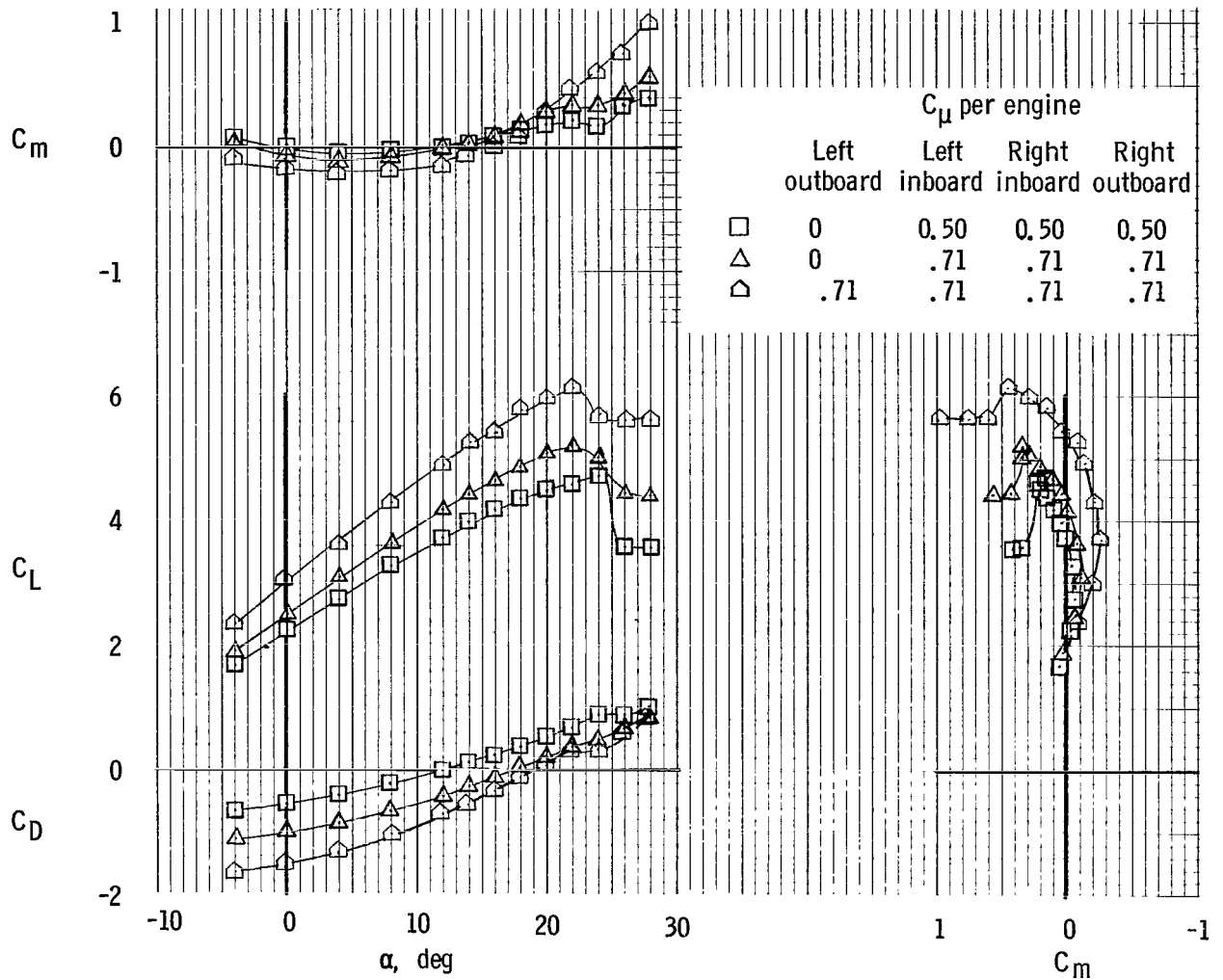


Figure 40.- Longitudinal characteristics with left outboard engine not operating. Take-off flap setting T0.

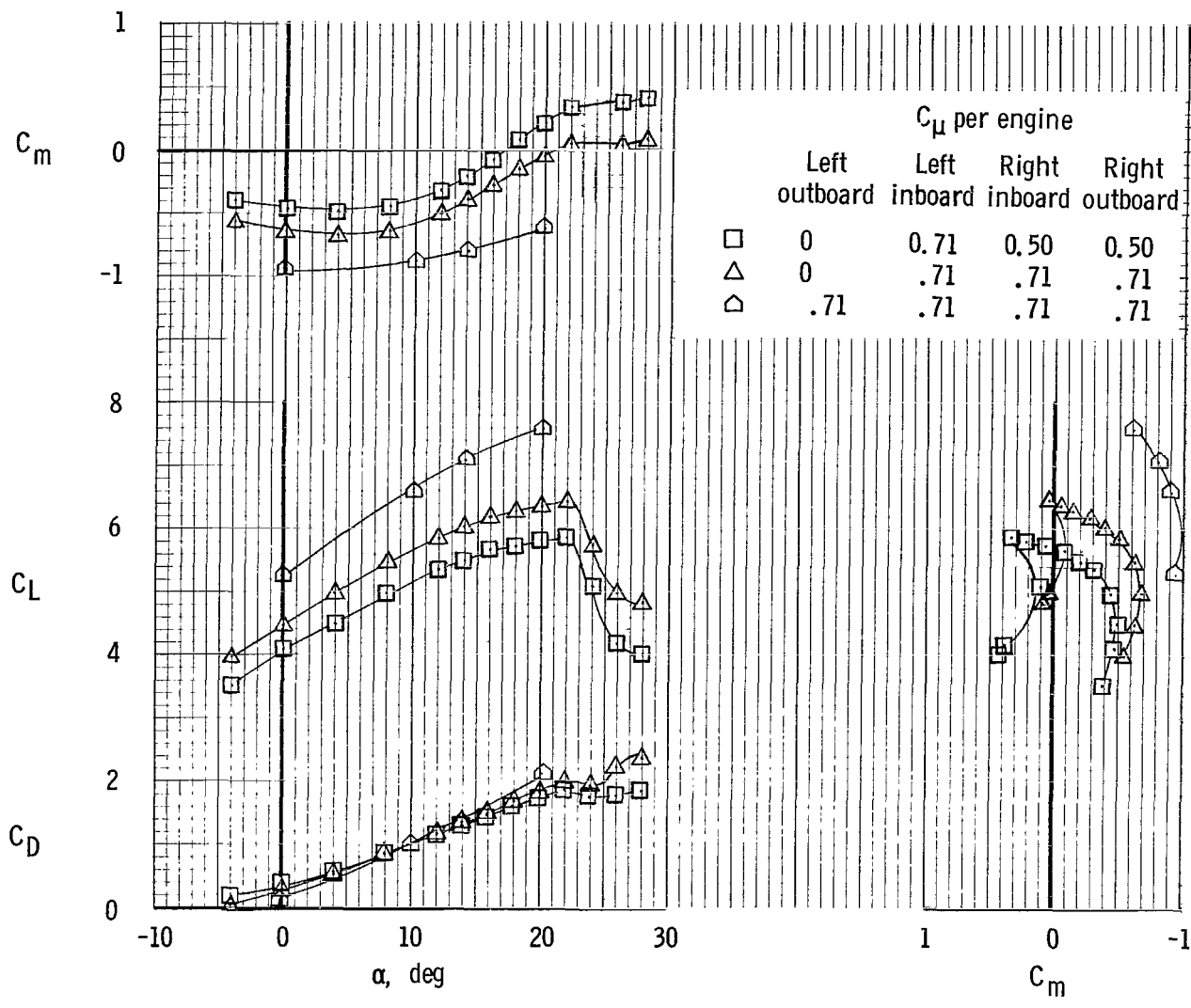


Figure 4L- Longitudinal characteristics with left outboard engine not operating. Landing flap setting LDG.

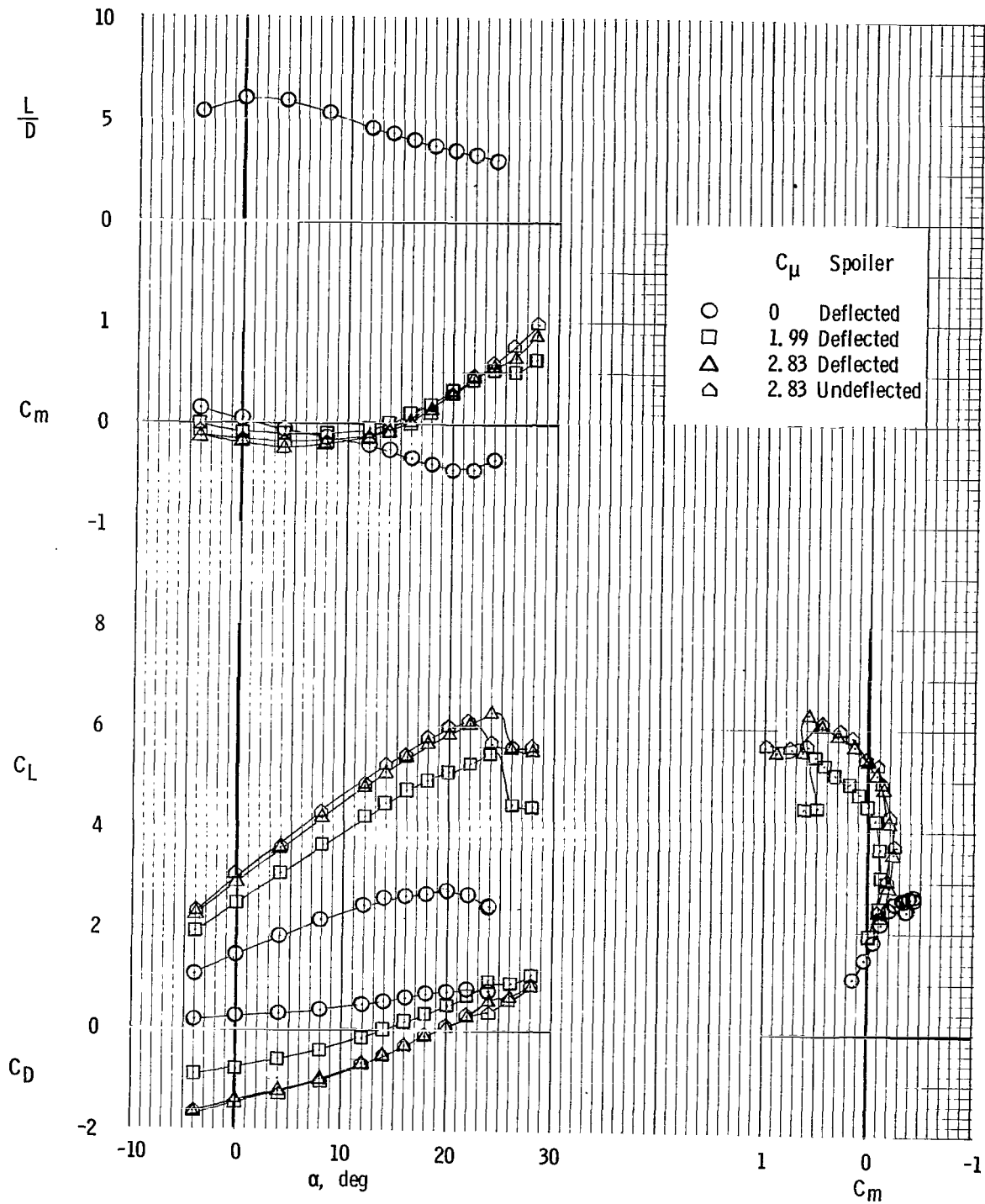
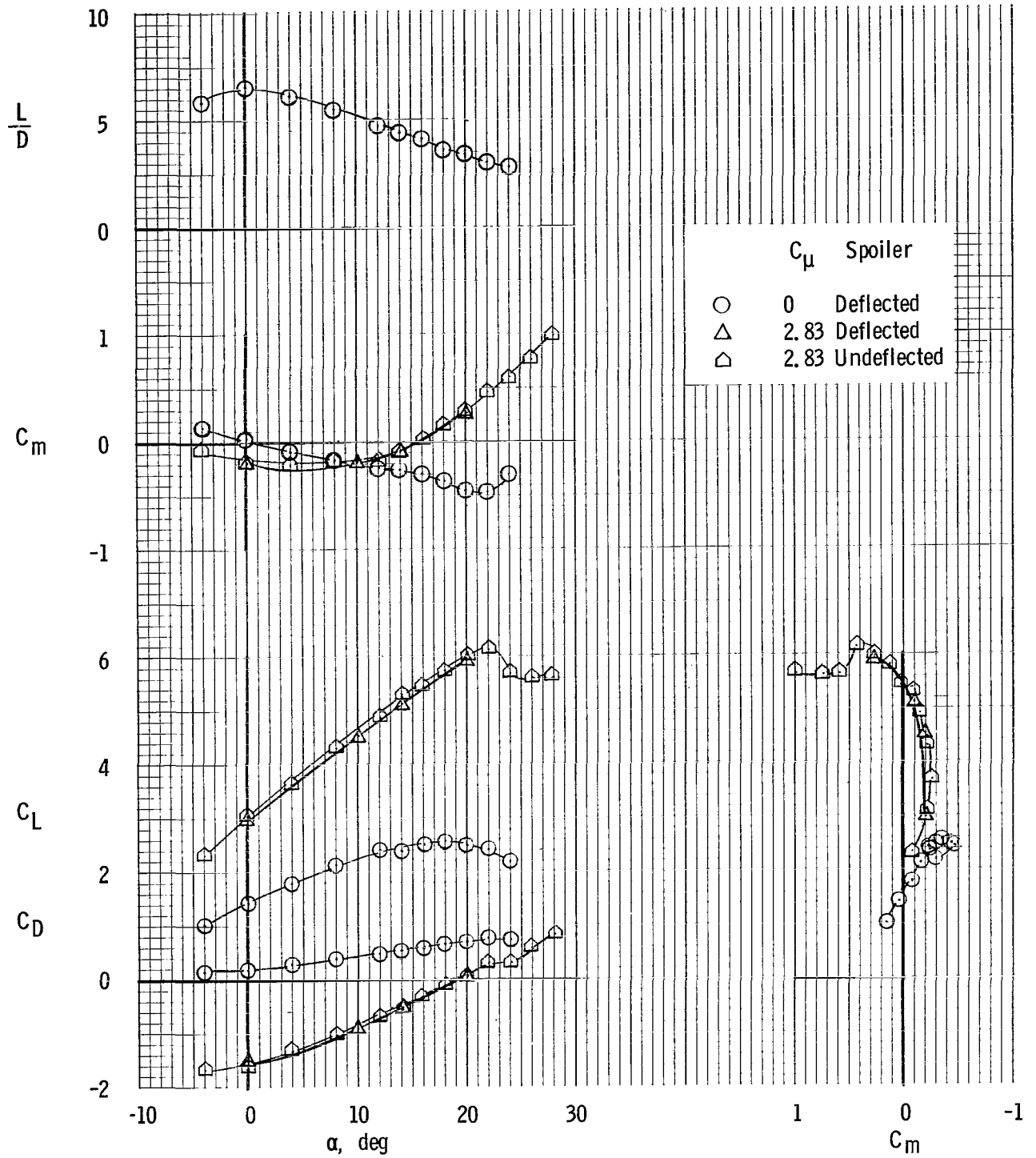
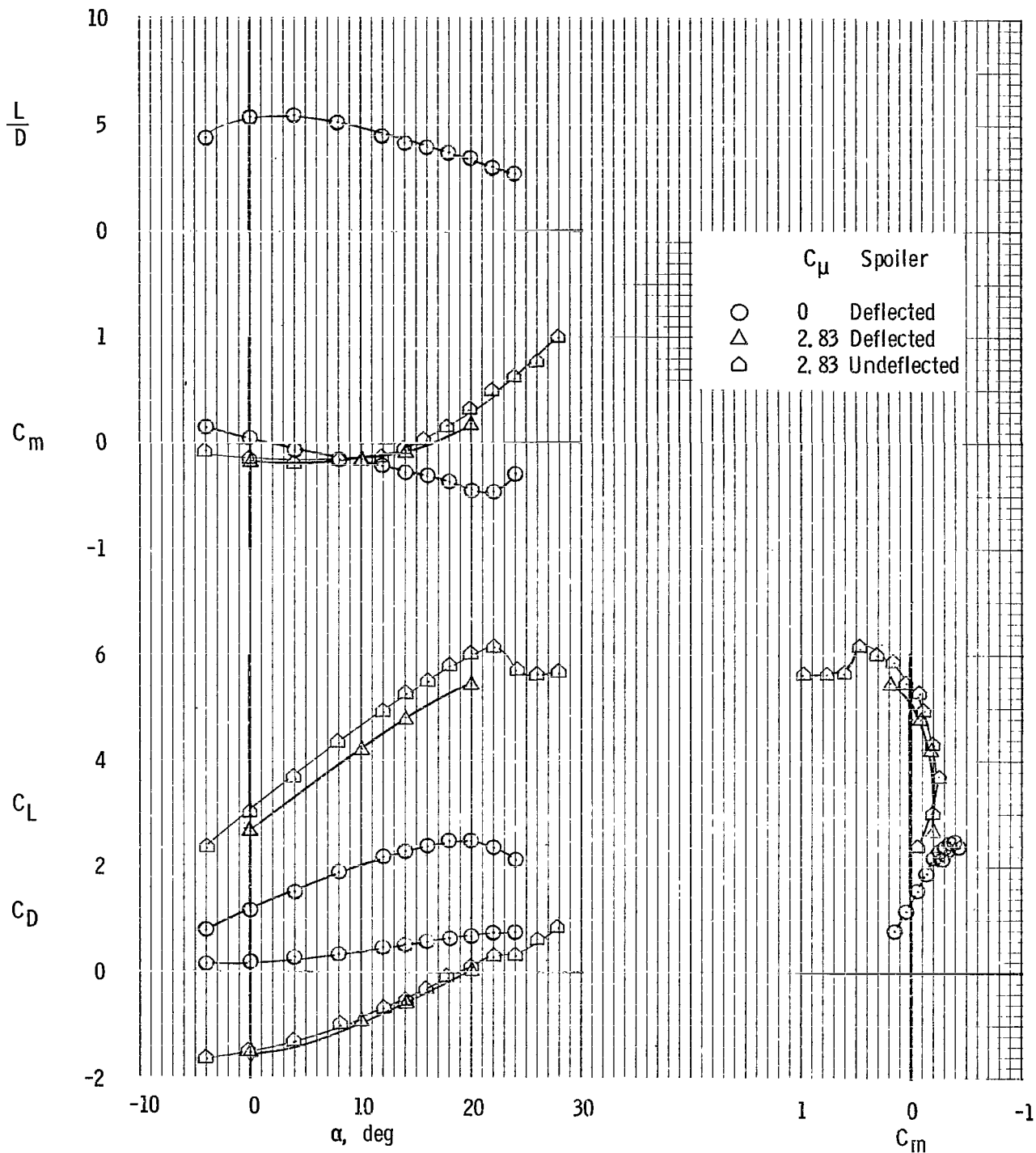


Figure 42.- Longitudinal characteristics with right inboard spoiler deflected  $10^\circ$ . Take-off flap setting T0.



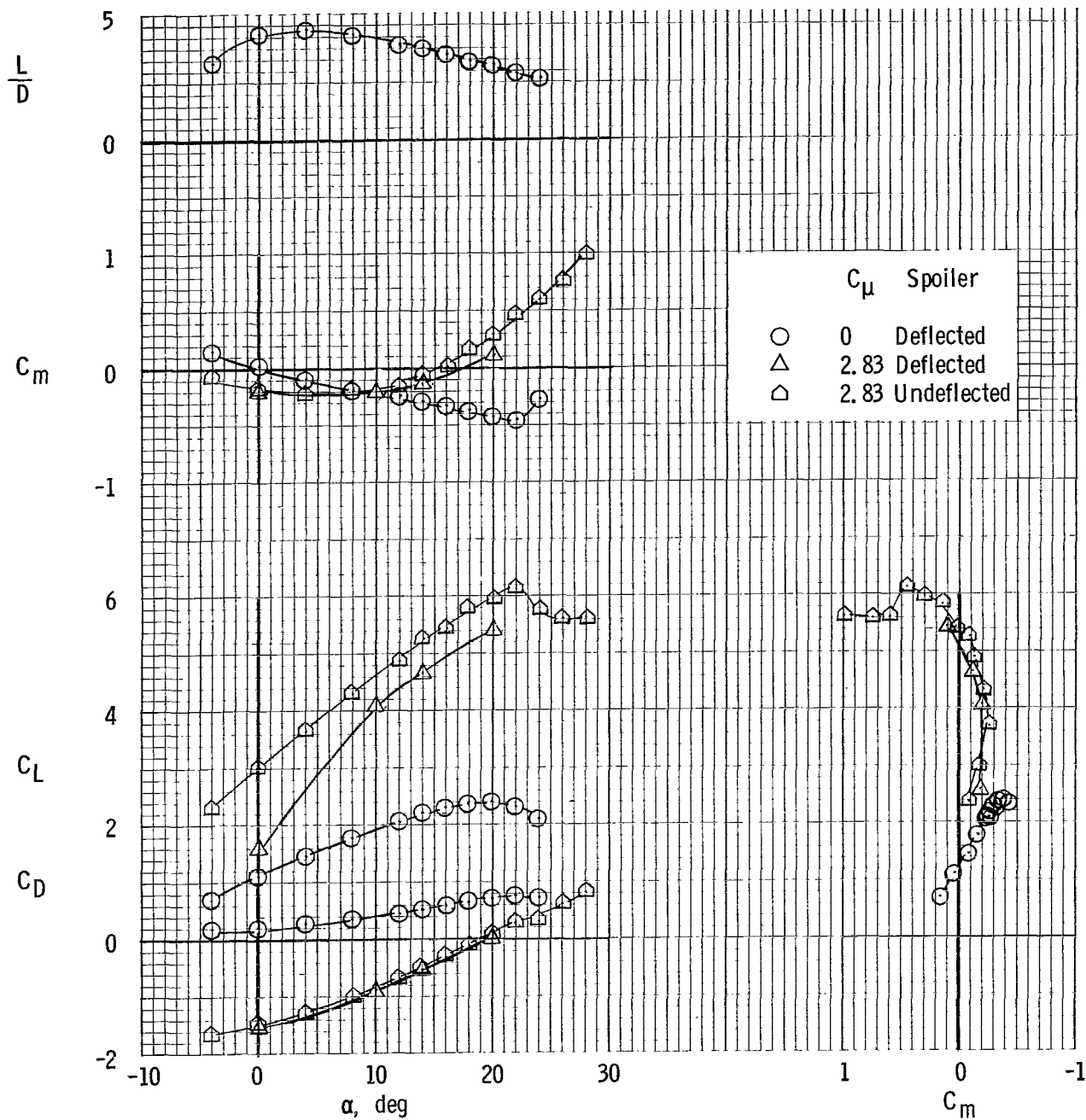
(a) Spoiler deflection, 10°.

Figure 43.- Longitudinal characteristics with right outboard spoiler deflected. Take-off flap setting T0.



(b) Spoiler deflection, 30°.

Figure 43.- Continued.



(c) Spoiler deflection, 60°.

Figure 43.- Concluded.

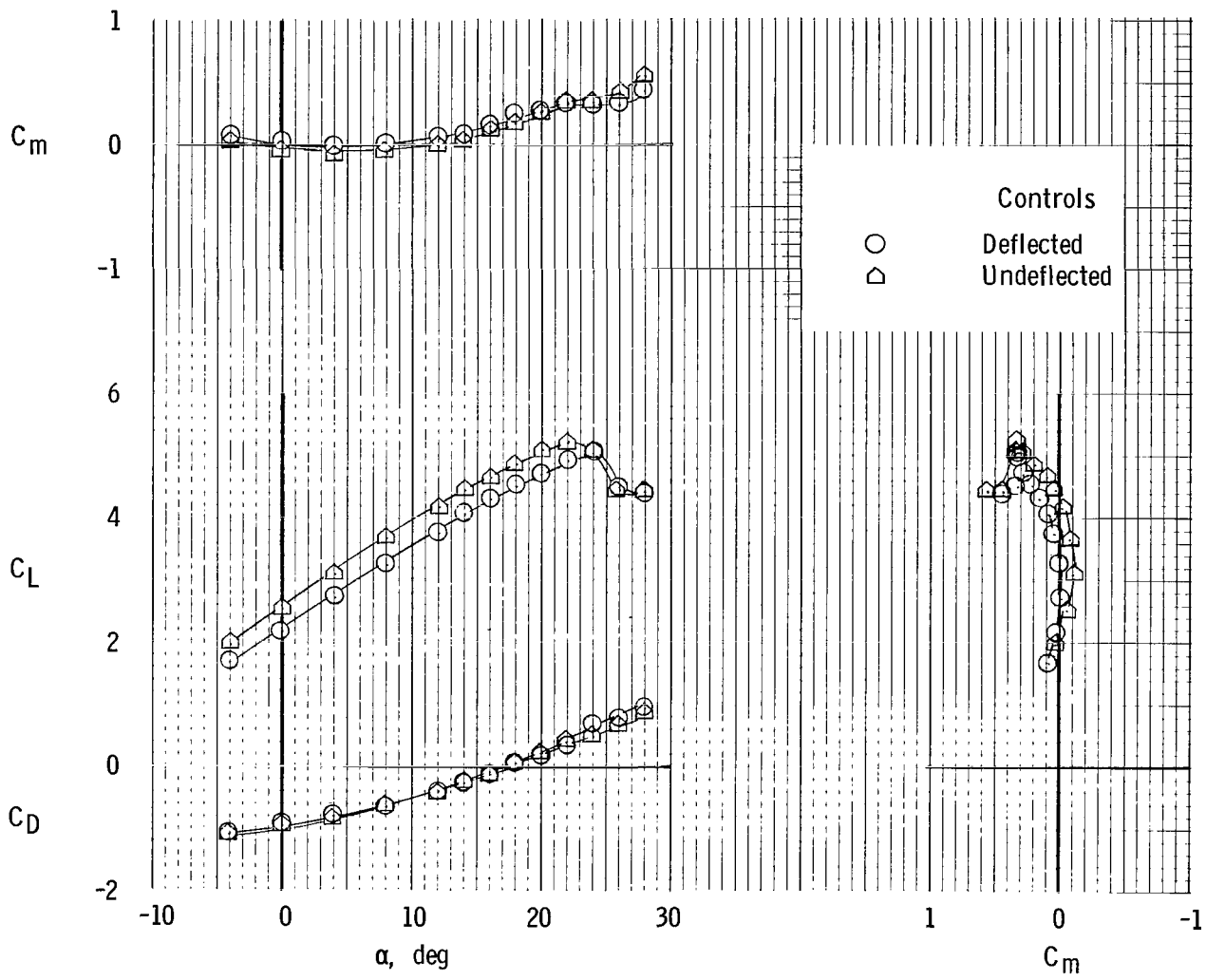


Figure 44.- Longitudinal characteristics with left outboard engine not operating. Take-off flap setting,  $T_0$ ; aileron deflection,  $20^\circ$  (each); spoiler deflection (right outboard),  $30^\circ$ ; rudder deflection,  $-30^\circ$ ;  $C_{\mu} = 2.83$ .

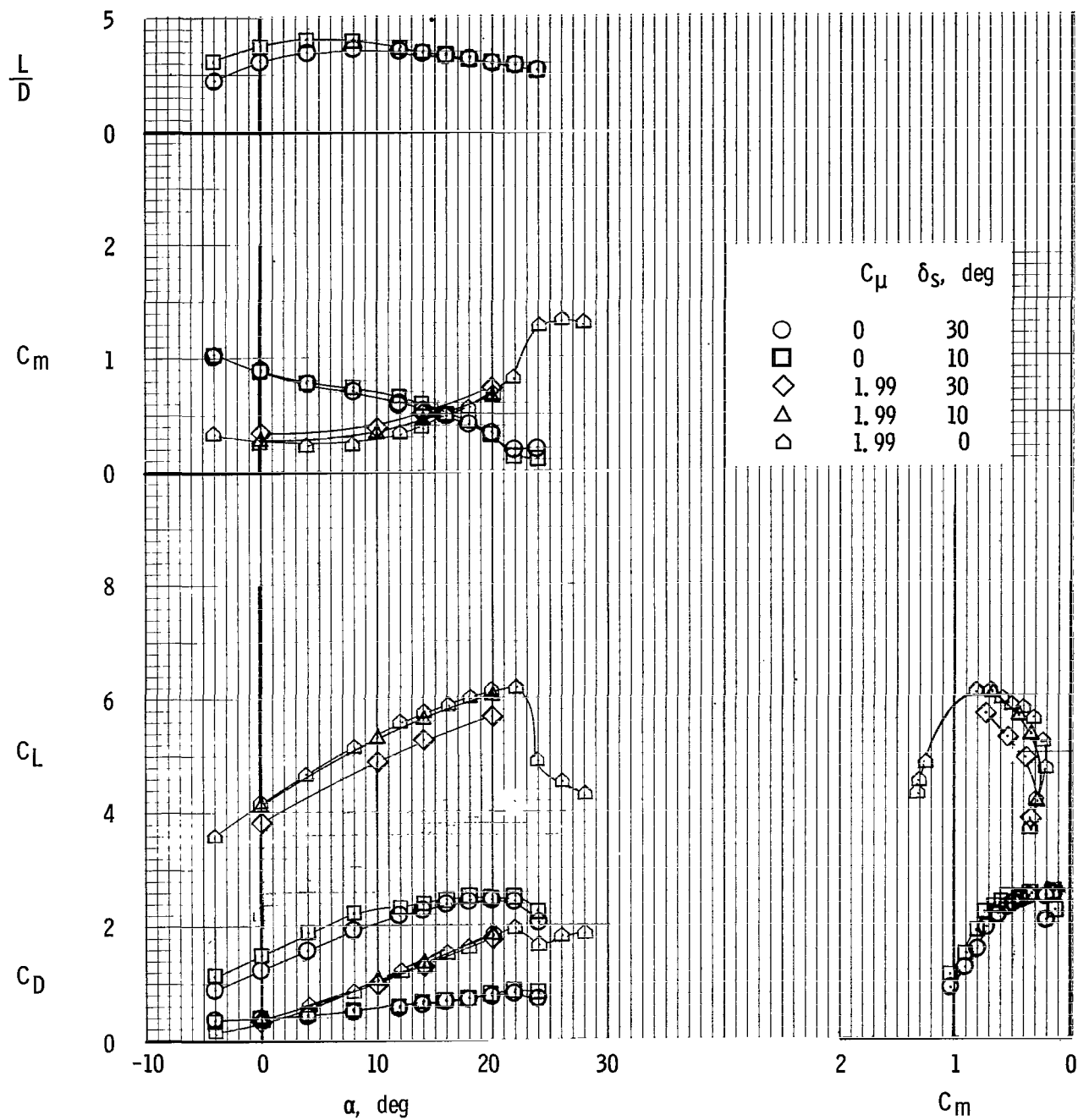


Figure 45.- Effect of right outboard spoiler deflection on longitudinal characteristics. Landing flap setting LDG.

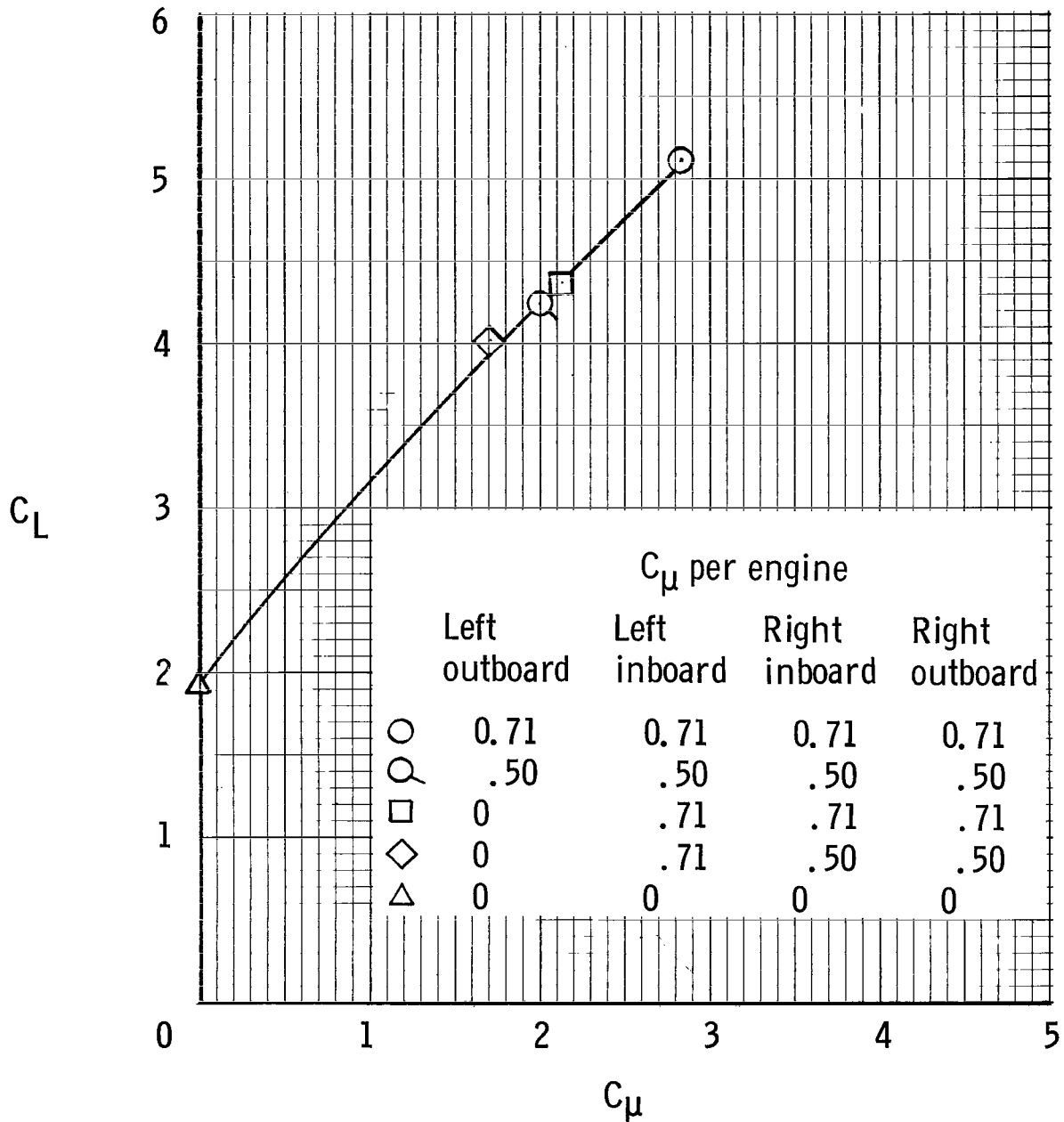


Figure 46.- Effect of thrust distribution on lift. Landing flap setting LDG;  $\alpha = 0^\circ$ .

FIRST CLASS MAIL



POSTAGE AND FEES PAID  
NATIONAL AERONAUTICS AND  
SPACE ADMINISTRATION

1958-1959  
NATIONAL AERONAUTICS AND SPACE ADMINISTRATION  
WASHINGTON, D. C. 20546

1958-1959

POSTMASTER: If Undeliverable (Section 158  
Postal Manual) Do Not Return

*"The aeronautical and space activities of the United States shall be conducted so as to contribute . . . to the expansion of human knowledge of phenomena in the atmosphere and space. The Administration shall provide for the widest practicable and appropriate dissemination of information concerning its activities and the results thereof."*

— NATIONAL AERONAUTICS AND SPACE ACT OF 1958

## NASA SCIENTIFIC AND TECHNICAL PUBLICATIONS

**TECHNICAL REPORTS:** Scientific and technical information considered important, complete, and a lasting contribution to existing knowledge.

**TECHNICAL NOTES:** Information less broad in scope but nevertheless of importance as a contribution to existing knowledge.

**TECHNICAL MEMORANDUMS:** Information receiving limited distribution because of preliminary data, security classification, or other reasons.

**CONTRACTOR REPORTS:** Scientific and technical information generated under a NASA contract or grant and considered an important contribution to existing knowledge.

**TECHNICAL TRANSLATIONS:** Information published in a foreign language considered to merit NASA distribution in English.

**SPECIAL PUBLICATIONS:** Information derived from or of value to NASA activities. Publications include conference proceedings, monographs, data compilations, handbooks, sourcebooks, and special bibliographies.

**TECHNOLOGY UTILIZATION PUBLICATIONS:** Information on technology used by NASA that may be of particular interest in commercial and other non-aerospace applications. Publications include Tech Briefs, Technology Utilization Reports and Notes, and Technology Surveys.

Details on the availability of these publications may be obtained from:

SCIENTIFIC AND TECHNICAL INFORMATION DIVISION  
NATIONAL AERONAUTICS AND SPACE ADMINISTRATION  
Washington, D.C. 20546